Optimal Planning of Energy Storage Systems in Power Transmission Networks Considering Wind Farms

Ahmad Alahmad

Submitted to the
Institute of Graduate Studies and Research
in partial fulfillment of the requirements for the degree of

Doctor of Philosophy
in
Electrical and Electronic Engineering

Eastern Mediterranean University
June 2021
Gazimağusa, North Cyprus

Approval of the Institute of Graduate Studies and Research

Prof. Dr. Ali Hakan Ulusoy
Director

I certify that this thesis satisfies all the requirements as a thesis for the degree of Doctor of Philosophy in Electrical and Electronic Engineering.

Assoc. Prof. Dr. Rasime Uyguroğlu
Chair, Department of Electrical and Electronic Engineering

We certify that we have read this thesis and that in our opinion it is fully adequate in scope and quality as a thesis for the degree of Doctor of Philosophy in Electrical and Electronic Engineering.

Assoc. Prof. Dr. Reza Sirjani
Supervisor

Examining Committee

1. Prof. Dr. Osman Kükrer
2. Prof. Dr. Aydoğan Özdemir
3. Prof. Dr. Belgin Emre Türkay
4. Assoc. Prof. Dr. Sahand Daneshvar
5. Assoc. Prof. Dr. Reza Sirjani

ABSTRACT

This thesis is composed of two sections. In the first section, a probabilistic discretising method is derived and developed to discretise the continuous joint power distribution of correlated wind farms. Combining the probabilistic discretizing method with a multi-objective hybrid particle swarm optimisation (MOPSO) and non-dominated sorting genetic algorithm (NSGAII), a new hybrid probabilistic optimisation algorithm is proposed. The proposed hybrid algorithm aims to search for the best location and size of energy storage system (ESSs) and considers the power uncertainties of multi-correlated wind farms. The objective functions to be minimised include a system's total expected cost restricted by investment budget, total expected voltage deviation and total expected carbon emission. IEEE 30-bus and IEEE 57-bus systems are adopted to perform the case studies using the proposed hybrid probabilistic optimisation algorithm. The simulation results demonstrate the effectiveness of the proposed hybrid method in solving the optimal allocation problem of ESSs and considering the uncertainties of wind farms' output power and the correlation among them. The expected cost, emission, voltage deviation and power losses reduced by 66.99%, 60.54%, 71.13% and 33.03%, respectively, in the case study of IEEE 30-bus system and decreased by 36.12%, 88.90%, 81.74% and 68.49%, respectively, in the case study of IEEE 57-bus system, compared to the cases without considering ESSs.

In the second section, bi-level mixed integer non-linear optimisation planning and operation model is formulated for the optimal configuration (location, capacity and power ratings) of compressed air energy storage system (CAES) in power transmission networks. The model was formulated with consideration for independent and

correlated wind farms. The single objective function in the inner layer of the bi-level model includes the difference between the total daily expected operational cost of conventional generators and the energy arbitrage benefits derived when considering the operational strategies of ESSs. The outer layer is a multi-objective function composed of three objective functions to be minimised. The objective functions encompass the total daily expected planning and operational cost, total daily expected emission and the maximum expected voltage deviation. Wind power uncertainties in independent and correlated wind farms were also examined. A hybrid non-dominating sorted genetic algorithm and multi-objective particle swarm optimisation were used to minimise the outer layer objective function, whilst fast tabu search algorithm that considers the probabilistic load flow represented by wind power uncertainties and the operational strategies of ESSs was adopted to minimise the inner layer objective function. An IEEE 57-bus system was subjected to a case study using the proposed two-stage model. The simulation results confirmed the advantage of considering the benefits of a peak shaving operational strategy from economic, technical and environmental points of view. The total daily expected cost, emission and maximum voltage deviation were reduced by 1.077%, 14.756% and 21.055%, respectively, after considering the peak shaving operation strategy considering independent wind farms

Keywords: Energy Storage System (ESS); Correlated Wind Farms; Probabilistic Load Flow (PLF); Operational Strategy; Two-Stage Optimization Problem; Non-Dominated Sorting Genetic Algorithm (NSGAII); Multi-Objective Particle Swarm Optimization (MOPSO); Tabu Search Algorithm (TSA)

ÖZ

Bu tez iki bölümden oluşmaktadır. İlk bölümde, ilintili rüzgar çiftliklerinin sürekli ortak güç dağılımını ayrıklaştırmak için olasılıksal bir ayrıklaştırma yöntemi türetilmiş ve geliştirilmiştir. Olasılıksal ayrıklaştırma yöntemini çok hedefli bir hibrit parçacık sürüsü optimizasyonu (MOPSO) ve baskın olmayan sıralamalı genetik algoritması (NSGAII) ile birleştiren yeni bir hibrit olasılıklı optimizasyon algoritması önerilmiştir. Önerilen hibrit algoritma, enerji depolama sisteminin (ESS'ler) en iyi konumunu ve boyutunu aramayı amaçlamaktadır ve çoklu-ilintili rüzgar çiftliklerinin güç belirsizliklerini dikkate almaktadır. En aza indirilecek hedef işlevler, bir sistemin yatırım bütçesi, toplam beklenen gerilim sapması ve toplam beklenen karbon salınımı ile sınırlandırılmış toplam beklenen maliyetini içerir. IEEE 30-bara ve IEEE 57-bara sistemleri, önerilen hibrit olasılık optimizasyon algoritmasını kullanarak vaka çalışmaları gerçekleştirmek için seçilmiştir. Benzetim sonuçları, ESS'lerin en iyi tahsis problemini çözmede ve rüzgar çiftliklerinin çıktı gücünün belirsizliklerini ve bunlar arasındaki ilintiyi dikkate alarak önerilen hibrit yöntemin etkinliğini göstermektedir. IEEE 30-bara sisteminin vaka çalışmasında beklenen maliyet, salınım, gerilim sapması ve güç kayıpları ESS'ler dikkate alınmayan durumlara kıyasla sırasıyla 66,99%, 60,54%, 71,13% ve 33,03%, ve IEEE 57-bara sistemi vaka çalışmasında sırasıyla 36,12%, 88,90%, 81,74% ve 68,49% azaltılmıştır.

İkinci bölümde, güç iletim şebekelerinde basınçlı hava enerji depolama sisteminin (CAES) en iyi düzenleşimi (konum, kapasite ve güç seviyeleri) için iki seviyeli karışık tamsayı doğrusal olmayan optimizasyon planlaması ve işletim modeli formüle edilmiştir. Model, bağımsız ve ilintili rüzgar çiftlikleri dikkate alınarak formüle edildi.

İki seviyeli modelin iç katmanındaki tek hedef işlevi, geleneksel üreteçlerin toplam günlük beklenen işletim maliyeti ile ESS'lerin işletim stratejileri dikkate alındığında elde edilen enerji arbitraj faydaları arasındaki farkı içerir. Dış katman, en aza indirilmesi gereken üç hedef işlevinden oluşan çok hedefli bir işlevdir. Hedef işlevleri, toplam günlük beklenen planlama ve işletim maliyetini, toplam günlük beklenen salınımı ve beklenen en büyük gerilim sapmasını kapsar. Bağımsız ve ilintili rüzgar çiftliklerindeki rüzgar gücü belirsizlikleri de incelendi. Dış katman hedef işlevini en aza indirmek için hibrit baskın olmayan sıralamalı genetik algoritma ve çok hedefli parçacık sürüsü optimizasyonu kullanılırken, iç katman hedef işlevini en aza indirmek için ise rüzgar gücü belirsizlikleri ve ESS'lerin işletimsel stratejileri tarafından temsil edilen olasılıklı yük akışını dikkate alan hızlı tabu arama algoritması benimsenmiştir. IEEE 57-bara sistemi, önerilen iki aşamalı model kullanılarak bir vaka çalışmasına tabi tutuldu. Benzetim sonuçları, ekonomik, teknik ve çevresel bakış açılarından, tepe tıraşlama işletim stratejisinin faydalarını değerlendirmenin üstünlüğünü doğruladı. Bağımsız rüzgar çiftlikleri dikkate alınarak tepe tıraşlama işletim stratejisi değerlendirildikten sonra, toplam günlük beklenen maliyet, salınım ve en büyük gerilim sapması sırasıyla 1.077%, 14.756% ve 21.055% azaltıldı.

Anahtar Kelimeler: Enerji Depolama Sistemi (ESS); İlintili Rüzgar Çiftlikleri; Olasılıklı Vük Akışı (PLF); İşletimsel Strateji; İki Aşamalı Optimizasyon Problemi; Baskın Olmayan Sıralamalı Genetik Algoritması (NSGAII); Çok Hedefli Parçacık Sürüsü Optimizasyonu (MOPSO); Tabu Arama Algoritması (TSA).

To:

My Beloved Family

ACKNOWLEDGMENT

I would like to thank my supervisor, Assoc. Prof. Dr. Reza Sirjani, for his encouragement and support during my PhD degree's period. I gratefully acknowledge the invaluable guidance and advise he has provided me throughout this process. I appreciate the opportunities he has given me and cannot say enough about my gratitude to him.

I would like to thank the Chair of the Electrical and Electronic Department Assoc. Dr. Rasime Uyguroğlu for her support and friendship.

Special thanks also go to all my friends for providing invaluable support. Their support has been invaluable on personal level, for which I am very grateful

Last but not least, I would like to express my deepest gratitude to my lovely family; they gave me a chance for completing my higher education in Cyprus. Without their support, both in financial and emotional matter, achievement of this level was impossible.

TABLE OF CONTENTS

LIST OF TABLES

LIST OF FIGURES

LIST OF ABBREVIATIONS

BESS	Battery Energy Storage System
CO	Carbon Monoxide
CDF	Cumulative Distribution Function
CAES	Compressed Air Energy Storage System
CPLEX	CPLEX Optimization Studio
DG	Distributed Generation
DESS	Distributed Energy Storage System
ESS	Energy Storage System
EMS	Energy Management System
ERCOT	Electric Reliability Council of Texas
FACTS	Flexible Alternating Current Transmission System
GA	Genetic Algorithm
GCM	Grid-Connected Mode
GAMS	General Algebraic Modelling System
ICOA	Improved Coyote Optimisation Algorithm
ISPO	Intelligent Single-Particle Optimizer
IGWO	Improved Grey Wolf Optimisation
IC	Total Daily Investment Cost
MOPSO	Multi-Objective Particle Swarm Optimization
MCS	Monet Carlo Simulation
MILP	Mixed Integer Linear Programming
MINLP	Mixed Integer Non-Linear Programming
MIQCP	Mixed Integer Quadratic Constrained Programming

MISOCP	Mixed Integer Second-Order Cone Programming
NSGAII	Non-Dominating Sorting Genetic Algorithm
NAA	Natural Aggregation Algorithm
OPF	Optimal Power Flow
OPS	Operational Strategy
PEM	Point Estimation Method
PDF	Probability Density Function
PLF	Probabilistic Load Flow
POPF	Probabilistic Optimal Power Flow
PHS	Pumped Hydro Storage
RD	Radial Distribution
SAM	Stand-Alone Mode
TSA	Tabu Search Algorithm
TOPSIS	Technique for Order of Preference by Similarity To Ideal Solution
TEOCG	Total Daily Expected Variable Operation Cost Of Thermal Generating Units
TEVOCS	Total Daily Expected Variable Operational Cost Of Storage Devices
TFOMCS	Total Daily Fixed Operation and Maintenance Cost Of Allocated Storage Device

Chapter 1

INTRODUCTION

1.1 Research background and motivation

Power networks have become increasingly complex systems due to the alarming increase in load demand, which have significant effects on transmission lines. During operation, they are often either overloaded or underloaded [1]. Existing transmission systems in most countries are outdated. For example, in the United States, the 345 KV bulk transmission system and associated sub-stations, cables and wires are 40 years old and above [2]. Moreover, due to the high cost of the construction and development of new power networks, the exacerbation of some existing challenging issues, such as excessive power losses, voltage profile problems, instability problems and reliability problems, is inevitable [3]. According to the Energy Information Administration (EIA) report, the residential, commercial and industrial sectors are expected to increase by 0.5%, 0.8% and 0.9% annually from 2013 through 2040, respectively [4]. On the other hand, the same report states that about 1134.6 GW of power generation capacity would be required by 2040 to meet the growing demand of electricity [4]; however, the system's capability to meet the demand and to transfer the generated power from centralised power generation to the distribution system is not expected. This could result in a bottleneck in the transmission system [5]. Thus, the best solution is the optimal utilisation of the existing generation and transmission networks.

On the other hand, due to the global climate change associated with serious environmental pollution problems and reduction in fossil energy, interest in renewable energy sources such as wind power has increased dramatically. For example, in USA,

the following states/groups including MISO, Illinois, Indiana, Michigan, Minnesota, Missouri, North Dakota, South Dakota and Wisconsin have a wind power capacity of 27924.68MW, 4861.05 MW, 2415.10 MW, 8786.84 MW, 2120.35 MW, 3871.65 MW, 959.41 MW, 3154.71 MW, 1018.77 MW and 736.79 MW [6] as shown in Figure 1.1.

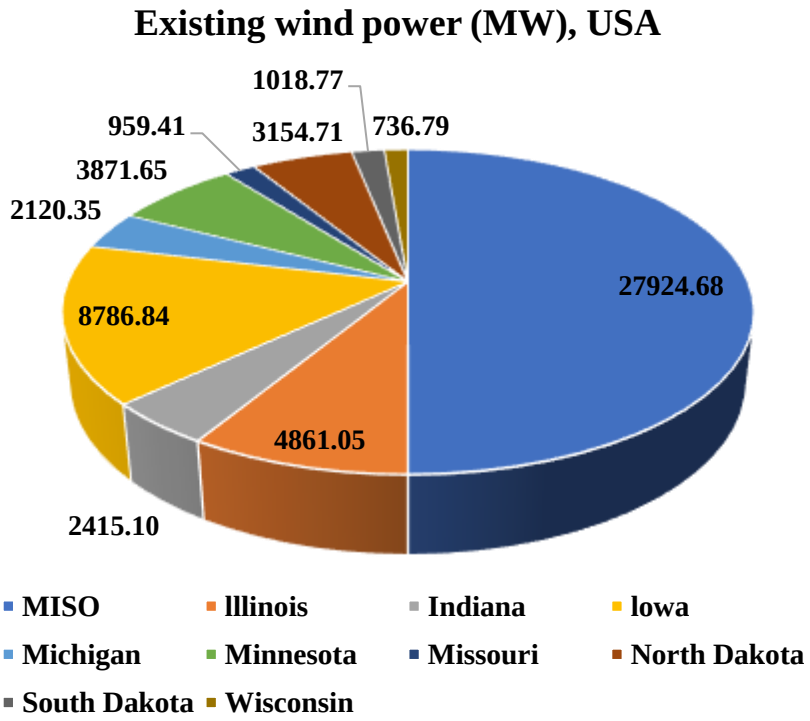

Figure 1.1: Existing wind power (MW) in USA

Moreover, these parts of USA have even a project under construction to increase wind power penetration as shown in Figure 1.2 and table 1.1.

However, wind power integration, especially with high level, raises the power system instability problems, including oscillations in the voltage and frequency, due to its natural variability and unpredictability, which increases system uncertainties [7].

Table 1.1: The existing and planned wind energy in USA

USA States/groups	Existing wind power capacity (MW)	Project under construction (MW)
MISO	27924.68	7203.46
Illinois	4861.05	1087.50
Indiana	2415.10	130.00
lowa	8786.84	1893.88
Michigan	2120.35	779.48
Minnesota	3871.65	750.20
Missouri	959.41	478.50
North Dakota	3154.71	706.00
South Dakota	1018.77	1377.90
Wisconsin	736.79	0.00
Total (MW)	55849.36	14406.92
	70256.28	

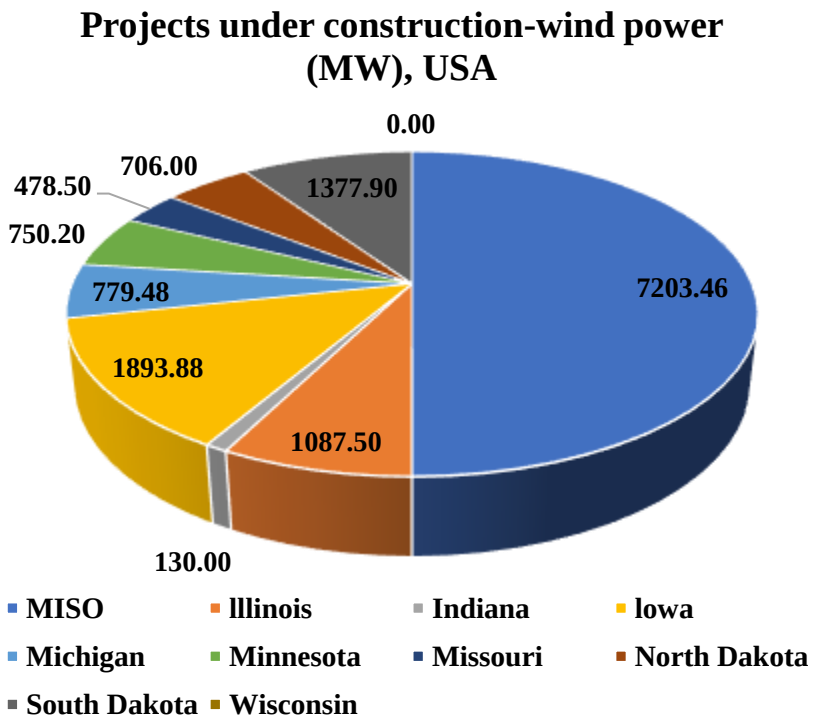

Figure 1.2: The projects under construction for wind power (MW) in USA

One of the best solutions for facilitating the wind power integration is the installation of an energy storage system (ESS). ESS could be optimally allocated to achieve the maximum benefits: 1) smoothing out the fluctuation, and improving supply continuity, which enhances the reliability and power quality; 2) time shifting by storing energy

during low- demand periods and dispatch it during peak demand period; 3) minimize power loss, mitigate transmission congestion and improve power factor and voltage profile; 4) energy arbitrage by managing high-cost energy imbalance charges; and 5) availability of extra reserves for emergency support [8, 9, 10, 11, 12, 13, 14, 15]. Because of these benefits, the deployment of ESS worldwide increased dramatically as presented in Figure 1.3 [16].

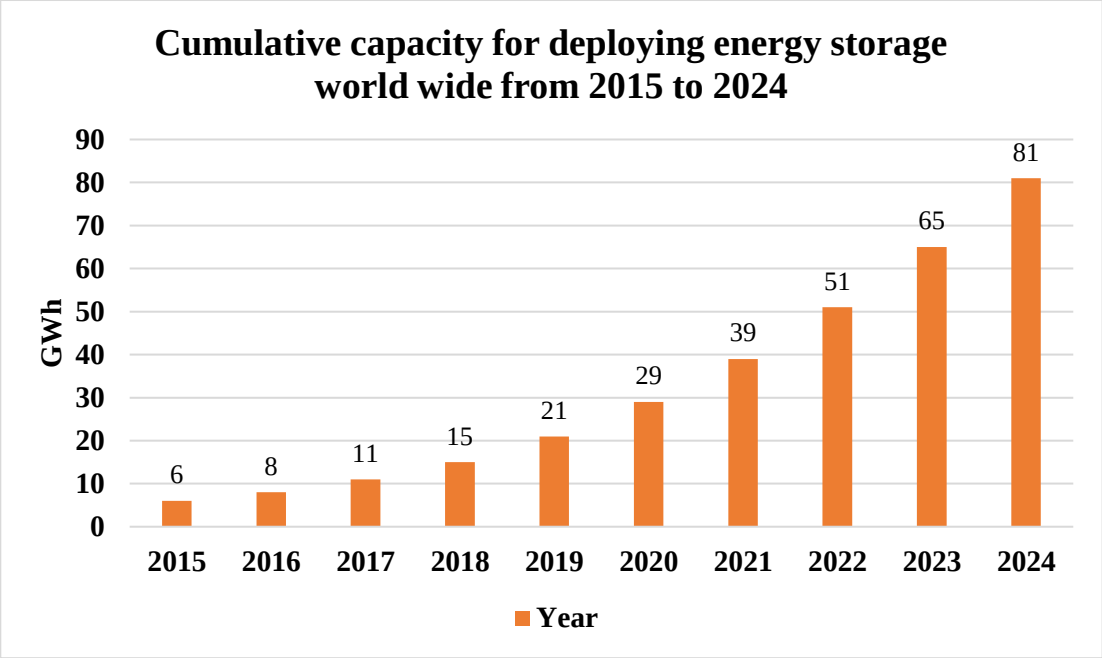

Figure 1.3: The cumulative deployment of energy storage in the world from 2015 to 2024

In addition, the prices of battery energy storage system in USA as an example is decreasing from to year to year as shown in Figure1.4 [17]. So, the capability of energy storage system to achieve multiple services together with renewable energy sources in an efficient manner from technical point of view and the decrease in its prices from economic point of view are a real motivation to move up for wide deployment of energy storage system as proved in Figure 1.3.

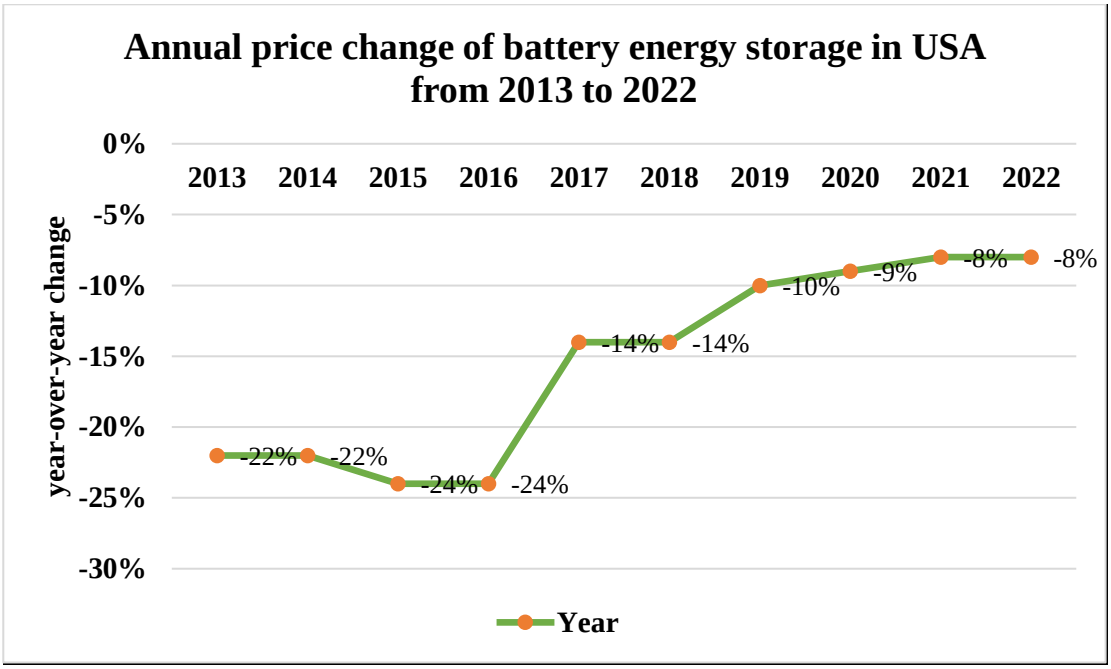

Figure 1.4: The annual price change of battery storage system in USA from year 2013 to 2022

1.2 Problem statement

Due to the increase of demand on energy and the rise of environmental problems, integration of renewable resources such as wind and solar in power systems is indispensable. The contribution of renewable energy resources in power systems can help in covering the gap in required energy and provides an environmental support. However, variability and unpredictability of output power of these resources due to their intermittent nature (excess of energy at a certain time and lack of energy at another time) affects power system's performance and reliability and limits their level of penetration.

One of the best solutions for facilitating the wind power integration is the installation of an energy storage system (ESS). However, the location and sizing of ESSs should be optimally allocated and planned to achieve maximum benefits such as minimizing

total cost, time shifting, reliability and power quality enhancement, minimizing power loss and providing environmental support.

Several methods have been developed for optimal planning and operation of different types and technologies of ESSs in power networks. Solutions can be divided into four categories: analytic methods, conventional optimisation algorithms, evolutionary and meta-heuristic optimisation algorithms, and hybrid methods [18] and [19]. Hybridisation of analytic methods, such as sensitivity approaches and meta-heuristic optimisation, can reduce search space and, hence, simulation time, but this combination was rarely utilised in the literature. Such hybrid methods could be used to obtain a solution very close to a global one with less computational effort.

A common drawback in most of the previous research works is the lack of consideration of uncertainties in renewable sources. Very limited number of research works that were presented the optimal planning of ESSs and considered the uncertainties, have not handled the effect of the correlation between the utilised distributed renewable generations on power system performance [20].

The effect of including the correlation between two wind farms on the optimal allocation problem of energy storage system was considered in [21], however the mathematical derivations of the discretising method need to be revised in terms of formulation. Moreover, authors in [21] utilised a single stage optimization method to minimize three simple objective functions simultaneously without considering any operational strategy for ESS charging/discharging modes. The aforementioned work, lacks comparison between the values of the objective functions in the cases of independent and correlated wind farms and considers only the peak load.

On the other hand, research works in the literature are often used a single weighted objective function rather than a decision-making technique to choose best solution from a set of solutions for multiple objective functions.

1.3 Thesis objectives

The main objectives of this thesis are as follows:

- To investigate an appropriate wind power modelling, including the correlation between wind farms,
- To develop a hybrid probabilistic optimisation algorithm for optimal allocation of energy storage systems in power transmission networks considering correlated wind farms,
- To propose a new optimal planning and operational strategy of energy storage systems in power transmission networks considering the uncertainties of wind farms.

1.4 Thesis contribution

The main contribution of this work in the first section, comprises as following:

- Considering three objective functions as three incompatible, nonlinear and non-convex to be minimized simultaneously: Minimizing the total expected cost in such a way that the total purchasing cost of optimal sizes of ESSs should not exceed the budget of investment, minimizing the total voltage deviation and minimizing carbon emission.
- Developing a new discretisation method based five-point estimation method to discretise the continuous joint power distribution of two correlated wind farms into 25 scenarios.
- Proposing a framework for a hybrid probabilistic multi-objective optimization (PLF-NSGAII-MOPSO) algorithm to solve the optimal allocation problem.

- Determining the optimal solution from a set of non-dominated solutions using decision making algorithm (TOPSIS).

The main contribution of this work in the second section, comprises as following:

- Two-stage mixed integer non-linear optimization planning model is proposed for optimal configuration of energy storage system
- The single objective function in the lower stage includes the difference between the daily expected operation cost of thermal generating units and the arbitrage benefits of ESSs. The upper stage multi-objective function composed of three objective functions including the total daily expected planning and operation cost, total daily expected emission and the maximum expected voltage deviation.
- Multivariate model-based clayton copulas represent joint power distribution of correlated wind farms is adopted to be discretized by a developed discretizing method based five-point estimation method to generated wind power scenarios associated with their probabilities.
- Hybrid NSGAII-MOPSO is utilized to minimize the outer multi-objective function while the fast Tabu-search algorithm (TS) is adopted for minimizing the inner layer objective function considering probabilistic load flow (PLF) represented by the wind power uncertainties of independent and correlated wind farms.
- An operational strategy for scheduling charging/discharge profiles of ESS in coordination with thermal and wind generating units is considered.
- Decision making algorithm called technique for order of preference by similarity to ideal solution (TOPSIS) is adopted to determine the optimal solution from a set of non-dominated solutions

1.5 Thesis outline

The remainder of the thesis is organized as follows:

- Chapter 2 describes the components of energy storage system (ESS), technical and economic characteristics of different types of ESS and applications in power system. It focuses on compressed air energy storage system (CAES) in terms of construction and role in power systems. Moreover, it introduces the different optimization techniques utilized in the literature to solve different optimization problems.
- Chapter 3 presents the modelling of uncertainties and correlation among wind farms. A discretization method is derived mathematically from scratch to discretise wind power distribution of two independent or correlated wind farms into 25 scenarios
- Chapter 4 explains the utilization of hybrid NSGAII-MOPSO-PLF in solving mixed integer non-linear multi-incompatible objective functions. The three objectives are subjected to some technical and economic constraints and they will be minimized simultaneously. The optimal objective functions can be achieved by optimally allocating the location and power ratings of multiple ESSs.
- Chapter 5 models two stage planning and operational optimization problem to determine the optimal locations, power ratings, capacities, optimal charging/discharging profiles and optimal coordination between allocated CAESs, wind farms and thermal generating units. The objective functions in each optimization layer are to be minimize by the hybrid NSGAII-MOPSO-TS-PLF.
- Chapter 6 discusses system configuration, case of studies and simulation results for the first section. The values of the three objective functions are compared in the case of independent and correlated wind farms. Moreover, simulation results

prove the superiority of hybrid NSGAII-MOPOS compared to MOPSO alone regarding the total operational cost and emission.

- Chapter 7 discusses system configuration, case of studies and simulation results for the second section. Four cases are studied and the simulation results determine the optimal configuration of CAES in each described case. Simulation results prove that the case stated as ‘’Hybrid NSGAII-MOPSO-TS solved the proposed two stage model considering correlated wind farms with operational strategy with considering CAES reactive power’’ is the best in terms of benefits of allocated CAES.
- Chapter 8 summarizes the contents of thesis and presents some conclusion, as well as, discusses the possible scope for future work.

Chapter 2

LITERATURE REVIEW

2.1 Energy storage systems

The recent developments in energy storage systems (ESSs) technologies and their efficient capability to store excess energy provided by renewable resources and discharging it again when required, makes ESSs an irreplaceable solution for hybrid power system operation. In this respect, several state-of-the-art reviews about ESSs performed. Refs in [8, 9, 10, 11, 12, 13, 14, 22, 23] provides an overview about energy storage system (ESS) types and technologies, technical and economic characteristics, modelling, benefits, advantages and disadvantages, optimal planning and configuration (number, location, capacity and power ratings), objective functions and constraints, applications, solution methods, operation and control strategies, uncertainty management, case of studies, recent projects, challenges and future works.

Energy storage system (ESS) stores the electrical energy from the power network in different forms via an external interface. ESS converts the stored energy into electrical energy to be injected to the network when needed via an external interface. The general diagram for any ESS is presented in Figure 2.1 [9].

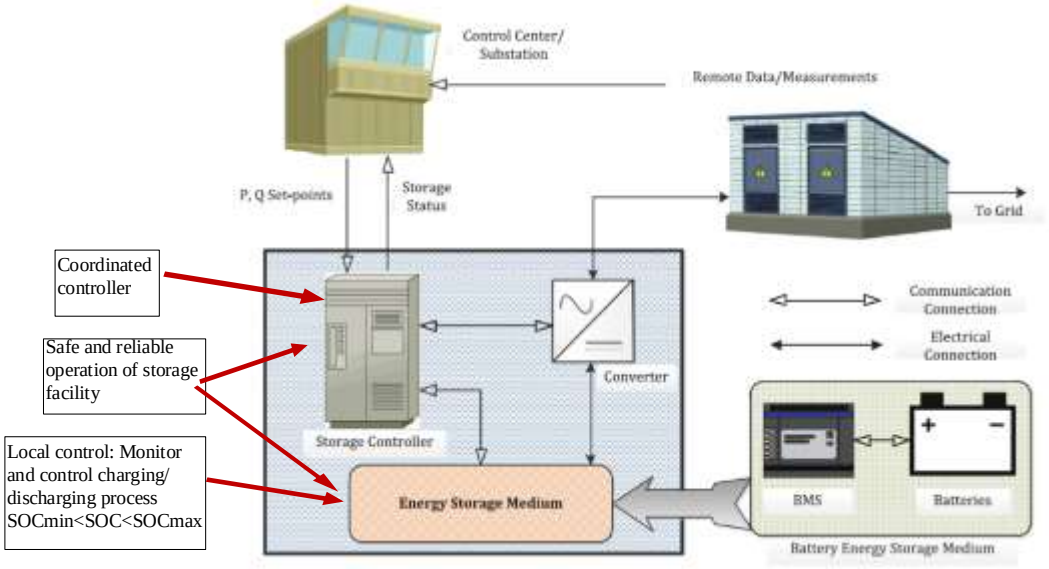

Figure 2.1: Basic diagram of an ESS

ESS composed of energy storage medium with energy management system, storage controller, converter and electrical and communication links. The energy storage medium corresponds to the energy storage technology being utilized such as batter energy storage medium or the compressor, pumps, cavern, turbines and synchronous generator in compressed air energy storage system (CAES) [24]. In Figure 2.1, BESS is taken as an example.

Energy management systems (EMS) corresponds to the local control. The role of EMS is to monitor the state of charge and control the charging and discharging modes. EMS monitors if the state of charge (SOC) of storage device is within limits. After that, it allows the storage device to start either charging or discharging. EMS ensures the safe and reliable operation of energy storage device over life time.

The storage controller corresponds to the coordinated control between ESS, converter and control center (power network). For example, the control center receives the electrical measurements from the power network. After that, the control center

performs power system analysis to check power balance at each bus, system stability, voltage deviation and other objectives. According to the measured values and the objectives required to be improved like voltage profile improvement, wind power curtailment mitigation, peak shaving and others, the control center will determine the required operating set-points (P-Q active and reactive power of storage device) and send it to the coordinated controller via communication link. The coordinated controller will send the required PQ point to the EMS and converter via communication link. EMS will determine if the energy storage device has a sufficient capacity to discharge or charge within limits of state of charge.

The converter has an electrical connection between storge device and the grid. It is responsible for modulating the current and voltage waveforms being transmitted from/to grid as required according to the orders being received from coordinated controller via communication link. Moreover, the inverter has reactive power capability for voltage regulation purposes.

2.2 Energy storage system technologies

As noted, the energy storage medium corresponds to the energy storage technology being utilized. As shown in Figure 2.2 [9, 11] and mentioned in [8, 9, 10, 11, 12, 13, 14, 22, 23]., the converted electrical energy from network can be in the form of :

1 Mechanical ESS: compressed air in compressed air energy storage system (CAES), kinetic energy in flywheels (FA) and gravitational potential energy with water reservoirs in pumped hydro storage (PHS).

2 Electrical ESS: electrical field in capacitors.

3 Magnetic ESS: magnetic field in inductors.

4 Chemical ESS: chemical energy in fuel cell.

5 Electrochemical ESS: electrochemical energy in batteries and flow batteries.

6 Thermal ESS: cryogenic energy storage (CES), high temperature thermal energy storage (HT-TES).

2.3 Energy storage system characteristics

Optimal planning required energy storage technology selection among the list of storage technologies mentioned in Figure 2.2.

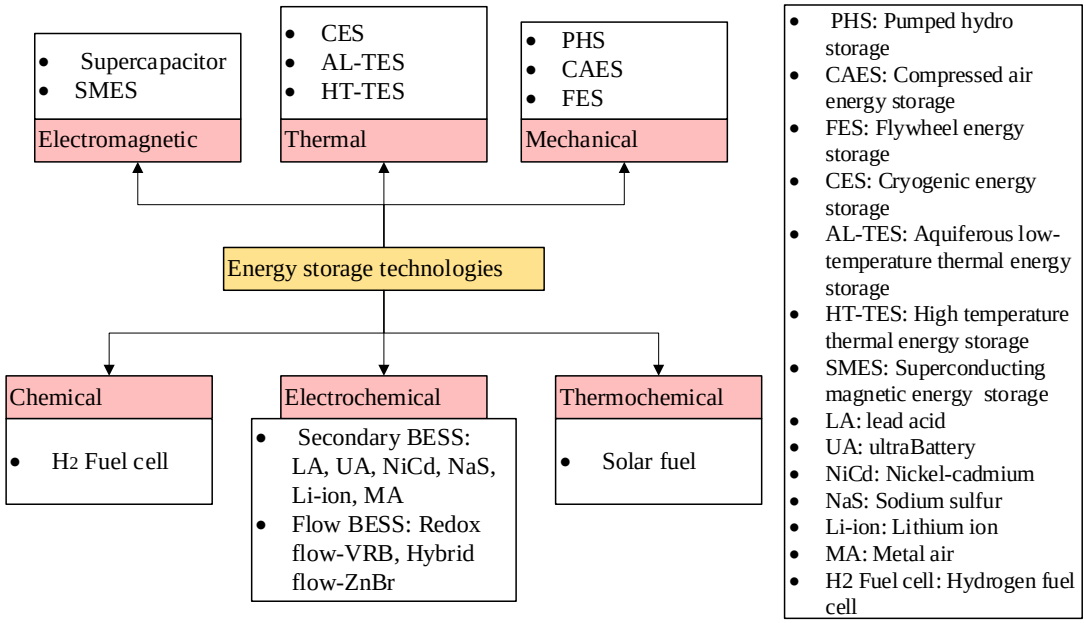

Figure 2.2: Energy storage technologies classifications

The selection process depends on the technical and economic characteristics of each type of ESS from one side and the nature of the application or objectives required for enhancement from the other side. Table 2.1 [9, 11, 25, 22] and Table 2.2 [9, 11, 25] details all the technical and economic characteristic of every type of ESS mentioned in Figure 2.2.

Table 2.1: Technical characteristic for different energy storage technologies

Energy storage system technical characteristics										
ESS technology		Power rating (MW)	Capacity rating (MWh)	efficiency (%)	Response time	Life time		charge time	discharge time	self-discharge per day (%)
						Years	Cycles			
Mechanical ESS	PHS	100-5000	500-8000	75-85	s-min	40-60	>13,000	hr-months	1-24 hr+	very small
	CAES	5-1000	2860	70-89	1-15 min	20-40	>13,000	hr-months	1-24 hr+	very small
	FES	0.1-20	0.025-5	93-95	4ms-s	15+	>100,000	s-min	ms-15min	100
Thermal	CES	0.1-300		40-50		20-40	>13,000	min-days	1-8 hr	
	AL_TES	0-5		50-90		10,20		min-days	1-8 hr	
	HT-TES	0-60		30-60		5_15	>13,000	min-months	1-24 hr+	
Electro-magnetic	Supercapacitor	0-0.3	0.01	90-95	8ms	20+	>100,000	s-hr	ms-60 min	20-40
	SMES	0.1-10	0.015	95-98	<100ms	20+	>100,000	min-hr	ms-8 s	15,15
Thermo-chemical	Solar Fuel	0-10		20-30				hr-months	1-24 hr+	
Chemical	H2 Fuel cell	0-58.8	120	25-58	<1s	5-20+	1000-20,000	hr-months	s-24 hr+	0
Electro-chemical	LA	0-40	0.001-40	70-90	5-10ms	3-15	2000	min-days	s-hr	0.1-0.3
	UA	0-36			5ms	3-15	3000	min-days	s-hr	
	NiCd	0-40	6.75	72	ms	10-20	2000-3500	min-days	s-hr	0.2-0.6
	NaS	0.05-34	0.4-244.8	80-90	1ms	10-15	2500-4500	s-hr	s-hr	20
	Li-ion	100	0.0015-50	85-90	20ms-s	5-15	1000-20,000	min-days	min-hr	0.1-0.3
	MA	0-0.01		50	ms		100-300	hr-months	s-24 h+	
	VRB	0.03-3	120	85	<1ms	5-10	12,000+	hr-months	s-10 hr	small
	ZnBr	0.05-10	0.1-3	75	<1ms	5-10	2000+	hr-months	s-10 hr	small

The mechanical ESS has the highest power rating and energy capacity among all the other types of ESS. PHS and CAES capacities can reach up to 8000 MWh and 5000MWh and power ratings of range [100MW-5000MW] and [5MW-1000MW]. The efficiency, charging time, discharging time and self-discharge for both PHS and CAES are approximately the same. However, PHS has longer life time than CAES reaches up to 60 years for the first one and 40 years for the later. Moreover, PHS is faster in responding to charging or discharging order compared to CAES, where PHS response time is in the range of s-min and CAES ranges up to 15 minutes. Hence, PHS

Table 2.2: Economic characteristic for different energy storage technologies

Energy storage system economic characteristics			
ESS technology		Capital cost	
		$/kW	$/kWh
Mechanical ESS	PHS	2000-4300	5-100
	CAES	400-1000	2-120
	FES	250-350	1000-140,000
Thermal	CES	200-300	3-30
	AL_TES		20-50
	HT-TES		30-60
Electro-magnetic	Supercapacitor	100-450	300-2000
	SMES	200-489	1000-72,000
Thermo-chemical	Solar Fuel	-	-
Chemical	H2 Fuel cell	500-10,000	15
Electro-chemical	LA	300-600	200-400
	UA		200
	NiCd	500-1500	400-2400
	NaS	1000-3000	300-500
	Li-ion	900-4000	600-3800
	MA	100-250	10,60
	VRB	600-1500	150-1000
	ZnBr	700-2500	150-1000

is more suitable than CAES from the technical point of view. From the economic point of view, CAES is more favorable than PHS because the investment cost related to the capacity of PHS is higher than that of CAES. PHS capacity capital cost ranges from 2000$/kW up to 4300$/kW and CAES ranges from 400$/kW up to 1000$/kW. Compared to other storage technologies, PHS and CAES have largest ratings (power and capacity), longest duration, very small self-discharge and the ability to store the energy for a period of time extends from 1 hour to more than 24 hours. Hence PHS and CAES are suitable for high power applications like time shifting [26], [27] and [28], peak shaving [29] and [30], spinning reserve [31] and [32].

BESS like Zn/Br battery has very fast response time < 1ms makes it a promising technology for power quality issues like voltage regulation. Moreover, the maximum ratings of 10MW and 3MWh, life time up to 10 years, ability to discharge up to 10 hours with 75% efficiency provides Zn/Br the ability to improve system reliability and peak shaving in distribution system [20]. On the other hand, lithium-ion BESS which has higher investment cost compared to Zn/Br, has large ratings up to 100MW and 50MWh with higher efficiency reaches 90% and longer life time compared to Zn/Br. Hence lithium ion battery is utilized in [33], [34], [35] , [36] and [37] for different applications including Power loss reduction, peak shaving, voltage regulation and load leveling.

Another BESS as sodium sulfur NaS has ratings of 34MW and 244MWh, life time up to 15 years, high efficiency ranges from 80 to 90%, ability to store energy for some hours makes this storage has capability in reliability enhancement [38]. Moreover, the fast response time 1ms provides NaS the ability to serve in voltage regulation [39]. However, NaS battery technology still has large daily self-discharge reaches up to 20% which is considered a critical case during selection of this type of energy technology.

Other BESS including LA, CAES, NA/S and VR has been selected for reliability enhancement [38]. Lead acid LA battery has a low power and energy cost. Moreover, LA has ratings of 40MW and 40 MWh, very fast response time 10ms, maximum of 15 years of operation and the stored energy lasts for some hours. LA is considered as a good choice from the economic and technical point of view for different application as voltage regulation (high response time) [40] and most of the applications detailed in section 2.4. Other selected energy storage technology for a specific application is detailed in table 2.3.

Table 2.3: Different application of energy storage system types

Refs	ESS application	ESS type
[20]	Peak shaving, voltage regulation and reliability enhancement	Zn/Br batteries
[41]	Voltage profile improvement	Not mentioned
[42]	Voltage profile improvement and environmental support	Not mentioned
[7]	Voltage profile improvement and environmental support	Not mentioned
[27]	Time shift, energy arbitrage and dispatch wind power	CAES
[43]	Network reliability enhancement	Any ESSs has medium duration and quick response
[38]	Reliability enhancement	Candidate storage technologies: LA, CAES, NA/S and VR
[33]	Power loss reduction	lithium-ion BESS
[34]	Power loss reduction	lithium-ion BESS
[36]	Main: Power loss reduction Secondary: peak shaving, voltage regulation and load leveling (flattening of the branch currents)	lithium-ion BESS
[39]	load leveling voltage profile improvement	BESS
[44]	Manage the following: voltage profile, congestion, wind spillage and load curtailment	Not mentioned
[45]	Reliability enhancement	sodium sulfur BESS
[46]	improve profits considering cost benefit analysis	lithium ion and sodium sulfur BESS
[26]	Decrease wind power curtailment by time shifting	Maximum of 270MW/10,000MWh CAES
[35]	mitigate wind power uncertainty	lithium-ion BESS
[37]	1. Network loss reduction 2. Decrease wind power curtailment 3. peak load shifting 4. increase arbitrage benefits	lithium-ion BESS
[40]	Voltage regulation	Lead acid battery
[47]	voltage support Environmental support	Not mentioned
[48]	voltage regulation Manage congestion and load curtailment loss reduction	Not mentioned

2.4 Compressed air energy storage (CAES)

For large energy storage applications, the mechanical energy storage systems including PHS and CAES are a promising technology for facilitating the integration of high penetration level of renewable energy sources especially wind farms. However, the specific geographical limitation of PHS renders CAES as an alternative energy

storage [24]. On the hand, the technical and economic characteristics of CAES listed in table 2.2 and table 2.3 proves the feasibility and reliability of CAES as a promising method for energy storage.

CAES has three operation modes as presented in Figure 2.3 [49] and they are described as follows:

Charging mode: The electrical grid or RES provides electricity to the motor. The motor drives the compressor to compress the air and pumps it into a reservoir tank at a high pressure or into an underground cavern which act as the medium of CAES. As the air pumped to be stored in the storage medium, the pressure and energy inside the medium increases. However, multiple compression stages are performed to ensure an efficient way in storing air inside the medium and this can be done using cooling before and after pumping the air into the cavern. This mode often occurred during off-peak periods.

Discharging mode: The stored air (energy stored) in the medium is to be used whenever required to dispatch RESs output power or performing time shifting for peak shaving purposes [27], reliability improvement [38] and wind power curtailment reduction [26]. In this mode, the stored air is to be heated, mixed with natural gases and burnt together (recuperator) before it is being pumped and expanded in the turbine which is considered as the prime mover of the synchronous generator. The synchronous generator injects the stored wind energy into the electricity grid.

Floating mode: The energy storage is neither charging (compression) nor discharging (expanding). It is in the idle mode.

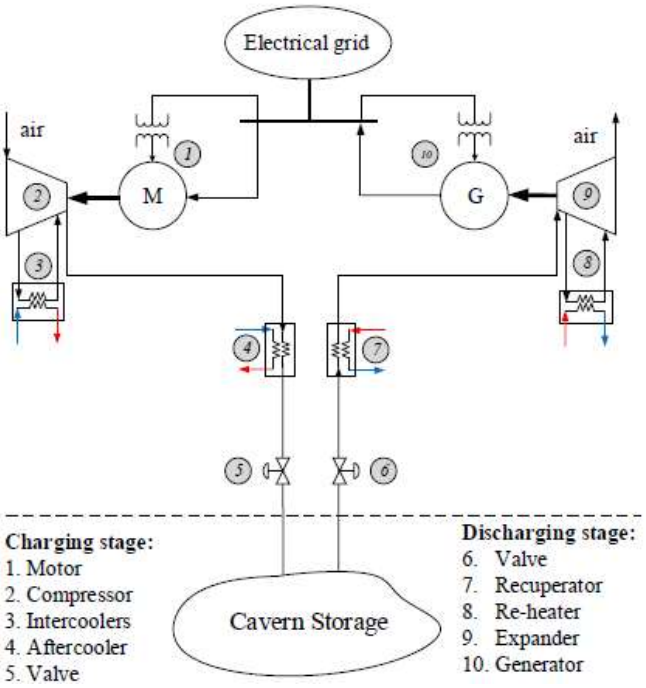

Figure 2.3: CAES general system

2.5 Energy storage system applications

2.5.1 Time shift

Due to the intermittent nature of wind power, it is sometimes available during valley load, but low or lacking during peak load, which is called the anti-peak feature; hence, ESSs are used to store wind energy during times of valley or low demand and distribute the stored wind energy during high and peak load periods. This is called time-shifting (between storage and distribution in some periods). For successful and efficient time shifting, an ESS should have the capability to store energy for long periods (hours or days). Seasonal energy storage involves long-term time-shifting, for which an ESS should have the capability to store energy for up to a few months [27], [26], [37] and [28].

2.5.2 Smoothing of supply output

The variable nature of wind speed results in variable wind power. Sudden changes in wind speed (sometimes within 1 min) result in wind power fluctuations, which cause

variations in network frequency and voltage and, consequently, power quality issues. To mitigate power fluctuation, ESSs are used. The features of ESSs responsible for power quality improvement (fluctuation mitigation) include fast response times, high ramping power rates, and high cycling capability. In [50], a supercapacitor ESS (SCESS) was utilised and placed in the DC link of the back-to-back converter of a wind turbine driving a doubly fed induction generator (DFIG). FESs, SCESSs, or BESSs can be combined in a hybrid system composed of PV wind generation and diesel units for power quality enhancement [51]. More details can be found in [11, 22].

2.5.3 Defer transmission expansion

Injecting wind power into a network in the case of high wind power generation and a low demand period would cause transmission congestion, voltage drop along transmission lines (TLs; voltage deviation), power losses, and network insecurity. In this case, wind power spilling is the only option other than upgrading the transmission line (so-called transmission expansion planning). Controllable ESS charging/discharging modes can absorb excess wind energy and reinject it according to the capacity of TLs [44, 52]. This ESS strategy would definitely defer transmission upgrading or expansion [48].

2.5.4 Voltage regulation

As mentioned previously, ESSs can smooth supply output power, resulting in voltage profile improvement. Moreover, the induction generators of wind turbines require reactive power support, which can be compensated using ESSs. The reactive power capability curve of ESSs contributes to minimising voltage deviation in networks. Also, a sudden change in load results in voltage sags and swells. In this case, an ESS with rapid response and high ramping power capability is required to mitigate voltage

quality problems. BESSs are utilised for voltage regulation [48], [44], [36], [41], [42], [20], [7], [39], [47], [40], [53], [54], [55].

2.5.5 Load leveling

Flattening the current profile in the TLs (load levelling) by eliminating peaks during the charging mode of ESSs can help to decrease voltage drops along lines, resulting in better voltage profiles and power loss mitigation. Also, reducing overcurrent helps in managing congestion along TLs and defers plans for upgrading or expansion [36], [39], [56].

2.5.6 Peak shaving

ESSs store wind energy during off-peak (overnight) periods and distribute it during peak demand; hence, they can improve the typical peak–valley load curve. Peak shaving can use wind energy alone or a combination of wind and diesel units, resulting in decreased operational costs [36], [20], [57], [58], [59], [60].

2.5.7 Energy arbitrage

ESS operators buy wind energy at low prices (off-peak) and sell it at high prices (during peak demand) [27] , [46] and [37].

2.5.8 Reliability enhancement

A system is reliable when the supplies meet demand within security constraints; otherwise, heavy-load industries would lose their production due to insufficient power from grid or because of the system's low power quality and instability problems leading to shutdown of electrical appliances. Customers cannot rely on such a system. Also, faults, such as transmission lines outages, which are quite likely, can decrease the reliability of the network unless a solution is presented. ESSs, for end users, can act as a backup for power supply systems during short outages by providing

uninterruptible power supplies (UPSs) for household appliances and industrial loads, enhancing supply reliability [43], [38], [45], [61], [62].

2.5.9 Black start

Another term for black start is emergency power supply. In the case of a cascaded outage due to catastrophic failure, ESSs can energise power systems without any provocation from the grid [63].

2.5.10 Power loss mitigation

Power loss determination depends on measuring the current passing through TLs. Injecting wind power into TLs during off-peak hours without using ESSs would increase the current passing through TLs, resulting in significant power losses. The ESS load-levelling feature can mitigate current peaks in TLs by consuming some or all wind energy during off-peak periods; hence, load levelling can mitigate power losses [33], [34], [36], [48] and [37].

2.5.11 Wind power curtailment reduction

In the case of high wind power generation during off-peak hours, wind generators are disconnected from the system to maintain security; wind power is then generated and spilled or curtailed unused. ESSs can decrease wind power curtailment by consuming excess wind energy, increasing wind power utilisation and penetration, and reducing curtailment [26], [44] and [37].

2.5.12 Emission reduction

Due to the seriousness of environmental pollution and global warming, interest in renewable energy resources, including wind power, has increased markedly. However, wind power integration causes power system instability problems. The ESS features mentioned above facilitate wind power integration even at a high penetration level.

With ESSs, the wide integration of clean energy (PV and wind power) would decrease carbon emissions, supporting the environment [7], [42] and [47].

2.6 Techniques and algorithm-based ESS optimal configuration

The optimal configuration or allocation of ESSs involves determining the optimal numbers, locations, power ratings, capacities, hourly schedules, and types of utilised ESSs. Such optimisation is complex and greatly limited by the multiple objective functions to be minimised, subject to many technical and economic linear and non-linear constraints. Solutions can be divided into four categories: analytic methods (mainly sensitivity approaches), conventional optimisation algorithms (called arithmetic programming), evolutionary and meta-heuristic optimisation algorithms, and hybrid methods [18] and [19]. This section briefly discusses these categories, except analytic methods, which are mentioned in the hybrid techniques section.

2.6.1 Conventional optimisation algorithms

Although efficient convergence characteristics can be achieved with conventional optimisation algorithms, they are still ineffective for managing optimisation problems with multiple objective functions that are subject to high numbers of non-linear constraints [64].

In [26], a mixed-integer programming model was implemented in GAMS and solved by CPLEX to obtain the optimisation of a CAES for different operating limits [0, 270, 540, 810, 1080 and 1350 MW]. The candidate locations of CAESs are considered to have significant operational charging/discharging efficiency for wind generation buses, since they are installed in ERCOT transmission systems to decrease wind power curtailment.

In [36], a lithium-ion BESS was installed in a distribution network to obtain two benefits: the first was power loss reduction, and the second consisted of multiple goals, including peak shaving, voltage regulation, and load levelling (flattening of the branch currents). To maximise the benefits, the optimal location, power rating, and capacity of the ESS was determined. Firstly, sensitivity analysis of power losses determined the BESS's best location, then the optimisation problem was formulated as MIQCQP and solved using a pattern search method (D-XEMS13) integrated into the optimisation procedure in a MATLAB environment to determine the best sizing of BESS.

In [39], the main application of the BESS was for load levelling and voltage profile improvement. A new BESS-planning MILP optimisation model, including a novel linearised model of BESS considering reactive power, was proposed, which was implemented in GAMS and solved by CPLEX. The purpose of the solution was to determine the optimal location, power rating, and capacity of the BESS by minimising total costs (operational and investment costs) and voltage deviations.

In [48], a primal dual-interior point method was used to solve a formulated mixed-integer second-order cone programming problem (MISOCP) subject to relaxed (linearised) constraints. The two objective functions were minimising the investment and maintenance costs of dispersed DESSs and minimising virtual operation costs represented by voltage deviation, losses, operation costs, power flows in lines, and load curtailment.

In [44], a two-stage stochastic mixed-integer linear programming optimisation model (MILP) was formulated and subjected to relaxed constraints. Determining the optimal location, capacity, and power rating of an ESS could minimise the total cost

(investment and expected operational costs). An ESS was installed to optimally manage the voltage profile, congestion, wind spillage, and load curtailment. In [61], MILP is formulated and solved using MOSEK solver in Matlab to determine the best sizing and sitting of ESS in a transmission network. The formulation considers both short- and long-term planning to improve system's flexibility and reliability.

2.6.2 Metaheuristic optimisation techniques

The most popular method used to solve the optimal configuration problem of ESSs in recent research was metaheuristic optimisation algorithms. These algorithms are highly efficient in managing complex optimisation problems involving multiple non-linear objective functions, many linear and non-linear constraints, a large search space, and a discrete system [65, 66]. Another application of a metaheuristic optimisation algorithm is to determine the optimal sites and sizes of different types of FACTS devices and ESSs simultaneously [19].

In [33], a whale optimisation algorithm was used to find the best site and size of a lithium-ion BESS to minimise power losses in a distribution system. This work proved that obtaining the best site and size of a BESS simultaneously was more efficient than using a two-step optimisation method. In [34], an improved coyote optimisation algorithm (ICOA) was proposed to perform the same work done in [33].

In [43], the optimal location, capacity, and power ratings were optimised using PSO to minimise the cost of energy not supplied and the ESS cost. The main application of the utilised ESS was reliability enhancement in radial distribution systems. A simple operational strategy was developed whereby the ESS charged during low demand, discharged during peak demand, and disconnected from the system in other periods.

In [38], a genetic algorithm (GA) was utilised to find the optimal location, type, and size of an ESS to achieve minimum investment and operational costs and minimise the interruption cost caused by contingency cases. Both islanding and grid-connected operational strategy modes were adopted to enhance the reliability of the studied distribution system, which was considered the main application of an ESS in this work. Monte Carlo simulation was used to generate some scenarios for non-dispatchable DG s and loads. The methodology in this work included two stages to be performed inside the GA. Stage 1 determined the required active and reactive power of DS for different uncertainty scenarios in every island formed by considering all line contingencies. Stage 2 applied the DS operational strategy (an islanding and grid-connected mode) to determine load points to be shed to calculate annual interruption costs.

In [45], the optimal configuration (location, capacity, and power rating) of a sodium-sulphur BESS was determined using an intelligent single-particle optimiser (ISPO) for reliability enhancement. The objective function included maximising annual profits from the BESS, from a new operational strategy-based economic perspective, by fully utilising peak–valley electricity price differences. In [35], a new probabilistic unit commitment problem, based on cost–benefit analysis, was solved by PSO to find the best size of lithium-ion batteries for non- dispatchable DGs. The purpose of installing these batteries in the microgrid (MG) was to maximise MG's total benefit in a grid-connected mode (GCM) and minimise MG's total cost in standalone mode (SAM). Minimising the expected CO emissions from thermal units was an additional objective function in [42]. In [27], maximising wind power utilisation and minimising the cost of the system was accomplished by optimising the location, power rating, and capacity of installed ESSs. The main applications of the ESSs were time shift, energy arbitrage, and the distribution of wind power.

In [47], an improved grey wolf optimisation (IGWO) algorithm was proposed to obtain the optimal placement, capacities, power ratings, and types of installed BESSs in a microgrid. The objective function to be minimised was summarised as the total daily cost represented by the investment cost of the selected BESS type (lithium-ion or sodium-sulphur) and the operational cost of conventional generators, selected BESSs, wind turbines, and photovoltaic. In [37], a bi-level multi-objective optimisation problem was modelled based on cost–benefit analysis for planning and operation issues. The upper layer adopted MOPSO to find the best sites, power rating, and capacities for large-scale BESSs to maximize their direct and indirect benefits (network loss reduction, wind power curtailment mitigation, and increased arbitrage profit from the peak–valley electricity price). The inner layer, which handled optimal scheduling and coordination between the BESSs (charging/discharging), wind farms, and conventional generators, was solved using unit commitment to minimise the total operational cost.

2.6.3 Hybrid techniques

In [7], a new hybrid probabilistic optimisation method was proposed to obtain the optimal site and power ratings of an ESS considering the uncertainties of correlated wind farms. Three objective functions, minimised simultaneously, included the expected cost, voltage deviation, and carbon emissions. Generating a joint power distribution of two correlated wind farms based on the Clayton copula method, the study discretised the model into 25 scenarios for two wind farms using a newly derived probabilistic method based on 5-PEM.

In [41], a hybrid MOPSO-NSGAII was utilised to find the optimal location and size of an ESS to improve the voltage profile. Two objective functions included minimising expected total operational costs and minimising expected voltage deviations. A five-

point estimation method was utilised to generate five scenarios for one wind farm. Investment costs were not included, which meant that this work only dealt with power system operational problems. The optimal location of the ESS could be included because the problem became impractical. In [47], a hybrid multi-objective NSGAII-MOPSO algorithm was utilised to obtain the best site and power rating for an ESS considering the uncertainty of wind power. A five-point estimation method was derived to discretise the Weibull probability density function into five points. The multiple objectives included minimising the expected operational costs, emissions, and voltage deviations, restricted by the investment cost of the installed ESS. In [20], optimal planning of Zn/Br batteries was performed using a two-stage optimisation problem: long-term planning for 25 years and short-term planning for 24 hours. The objective functions aimed to minimise total cost (investment, operational, and reliability costs). The Zn/Br applications were peak shaving, voltage regulation, and reliability enhancement. Islanding mode management was adopted as an operational strategy for optimal charging/discharging scheduling of an ESS to decrease the amount of energy not supplied due to fault occurrence.

In [40], a three-stage hierarchical model was proposed to install lead-acid batteries in radial distribution networks for the purpose of cost effectiveness and voltage support in the presence of renewable DGs (wind and solar resources). In the first stage, the required number of BESSs was determined using voltage sensitivity analysis. The location and capacity of the assigned number of BESSs from the first stage were the decision variables considered in the second stage, and they were initialised randomly. The third stage used the active/reactive power of BESSs as a decision variable to consider optimal scheduling and coordination between different units in the system, including charging/discharging BESSs, conventional units, and renewable resources

(wind and solar). Table 2.4 summarizes the recent research studies related to ESS including optimal allocation, objective functions, optimization methods and case of studies.

Table 2.4: Different solving methods for ESS optimal allocation problems

#	Optimal solution	Objective function	Optimization method	Case of study
[20]	Location, capacity and power ratings of ESS	Minimize total cost (investment, operational and reliability cost)	1. long term planning: PSO 2. Short term planning: TS	21- node Distributio n system
[41]	Location and power ratings of ESS	Minimize total expected operational cost and total expected voltage deviation	Hybrid MOPSO-NSGAII	IEEE 30-bus system
[42]	Location and power ratings of ESS	Minimize total expected operational cost, total expected voltage deviation and total expected emission	1. Hybrid MOPSO-NSGAII 2. MOGSA	IEEE 30-bus system
[7]	Location and power ratings of ESS	Minimize total expected operational cost, total expected voltage deviation and total expected emission	Hybrid MOPSO-NSGAII	IEEE 30-bus system and IEEE 57-bus system
[27]	Location, capacity and power ratings of ESS	1. Maximize wind power utilization 2. Minimize social cost of the system	GA	IEEE 24-bus system (deregulate d power system)
[43]	Location, power ratings and capacity of ESS	1. Minimize cost of energy not supplied (ENS) 2. Minimize ESSs costs	PSO	Radial 30-bus distributio n network
[38]	1. location, type and size of ESS 2. load points to be shed	1. Minimize investment and operational cost of DSs 2. Minimize interruption cost	GA	33-bus radial distributio n system
[33]	Location and power ratings of ESS	Minimize power loss	WOA	50 -node distributio n system
[34]	Location and power ratings of ESS	Minimize power loss	Improved cayote optimization algorithm (ICOA)	50 -node distributio n system
[36]	Location, capacity and power	Minimize power loss	Optimization problem is formulated as MIQCQP and solved using a	1. CIGRE European MV RDN

	ratings of ESS		pattern search method integrated within the optimization procedure named D-XEMS13 in MATLAB environment	2. 17-node RDN
[39]	Location, capacity and power ratings of ESS	Minimize total cost (investment and operational) Minimize voltage deviation	Two stage optimization model solved by CPLEX	33 -node distributio n system
[44]	Location, capacity and power ratings of ESS	Minimize total cost (investment and expected operational cost)	two-stage stochastic mixed-integer linear programming optimization model was implemented using GAMS and solved by XPRESS solver	33 -node distributio n system
[45]	Location, capacity and power ratings of ESS	Maximize annual net profit of BESS	ISPO	33 -node distributio n system
[46]	Location, capacity type and power ratings of BESS	Minimize total daily cost	IGWO	32 -node microgrid
[26]	Location	Minimize total operational cost	MIP in GAMS and solved by CPLEX solver	312 bus ERCOT transmissio n system
[35]	capacity	Minimize total operational cost and Maximize total benefits	PSO	MG
[37]	Location, capacity and power ratings of BESS	Minimize total operational cost and Maximize total benefits	MOPSO	IEEE 39-node system
[40]	Number, location, capacity and power ratings of BESS	Minimize total operational and maintenance cost Minimize Investment cost	1. Voltage sensitivity analysis 2. Natural aggregation evolutionary algorithm (NAA). 3. Relaxation power flow technique	IEEE 15-bus and IEEE 69-bus radial distributio n system
[47]	Location and power ratings of ESS	Minimize total expected operational cost, total expected voltage deviation and total expected emission	Hybrid MOPSO-NSGAII	IEEE 30-bus system
[48]	Location, capacity and power	1. Minimize investment and maintenance cost of DESSs	primal-dual interior point method	IEEE 34 bus radial distributio n system

	ratings of ESS	2. Minimize virtual operation cost (voltage deviation, losses, operation cost, power flow in lines, load curtailment)	

Chapter 3

WIND POWER DISTRIBUTION MODELLING AND DISCRITIZATION

3.1 Wind speed probabilistic model

The non-linear relationship between wind speed and the wind power, directs most of the research works to adopt Weibull distribution function to fit the wind speed data as it can be seen in Figure 3.1. Weibull distribution function can model the wind speed forecasting mathematically as in [67]. Although hourly forecasted wind speed data can be utilized for more accurate probabilistic modelling of wind speed, it should be noted that the wind speed distribution is assumed to be stationary in this thesis.

$$f(x \mid \lambda, k) = \frac{k}{\lambda}\left(\frac{x}{\lambda}\right)^{k-1} e^{-\left(\frac{x}{\lambda}\right)^{k}} \tag{3.1}$$

Where
$$\begin{cases} k = \left(\dfrac{0.9874}{\dfrac{\sigma}{\tilde{x}}}\right)^{1.0983} \\ \tilde{x} = \dfrac{1}{n}\sum_{i=1}^{n} x_i \\ \sigma = \sqrt{\dfrac{1}{n}\sum_{i=1}^{n}\left(x_i - \tilde{x}\right)^2} \\ \lambda = \dfrac{\tilde{x}}{\Gamma\left(1+\dfrac{1}{k}\right)} \end{cases} \tag{3.2}$$

Where x is the actual wind speed; k is called the shape parameter, λ is the scale parameter, σ is the standard deviation, x_i is the wind speed for sample i, $\tilde{x}$ is the mean

value of all wind speed samples, n is the number of wind speed samples and Γ is the gamma function.

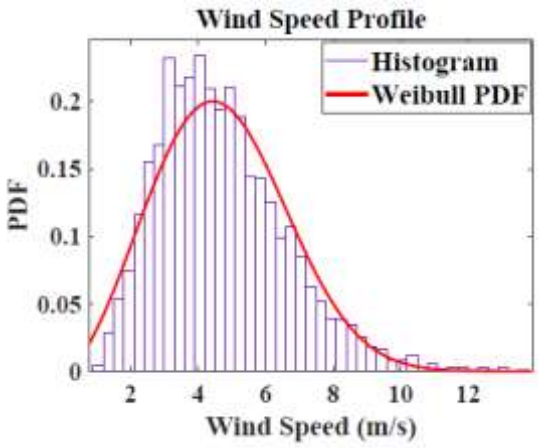

Figure 3.1: wind speed profile fitted with Weibull probability density function

A linear approximation equation is used to obtain the wind power distribution is as follow [68]

$$\begin{cases} Y = \begin{cases} 0 & if\ X \le V_{ci}\ or\ X > V_{co} \\ \alpha + \beta X & if\ V_{ci} \le X \le V_{no} \\ M & if\ V_{no} \le X \le V_{co} \end{cases} \\ where\ \alpha = \dfrac{-M \times V_{ci}}{V_{no} - V_{ci}}\ \ \&\ \ \beta = \dfrac{M}{V_{no} - V_{ci}} \end{cases} \tag{3.3}$$

Where Y is the wind power; X is the actual wind speed; M is the wind farm's maximum power; α and β are the linear coefficients; and V_{ci}, V_{co}, and V_{no} are the cut-in wind speed, cut-out wind speed, and normal wind speed, in m/s respectively.

3.2 Probabilistic load flow

Probabilistic load flow (PLF) was first introduced by Borkowska in 1974 [69] and it is considered as an efficacious tool to assess the effect of the uncertain factors such as loads, non-dispatchable sources, electricity prices, probability of failure and other factors on the functioning of power system over a variety of operating conditions. PLF

is used widely in network planning studies. PLF mathematically is utilized to find the statistical characteristic of the output random variables with the input random variables and it can be classified into three categories: Monte Carlo (MC) simulation, analytic method and point estimate method (PEM).

MC simulation method [70] can handle various complex problems without any simplification and use deterministic routines to solve the problem in each simulation step. However, MC requires long computing time for numerous simulations to reach convergence. Instead, analytic techniques are commonly based on convolution method or cumulant method and it can be combined with copulas to deal with correlations [71, 72]. However, analytic methods use approximate formulas for calculating the statistical moments of output random variables in OPF, including bus voltages, branch power flows and generation cost, based on the moments of the input variables including wind speeds, loads and other random variable inputs. However, large error can result from this approximation. To avoid the disadvantages of MC and analytic approaches, point estimation method PEM [73, 74] requires only the first few moments instead of complete PDF as compared to MC results in less computational burden. Moreover, like MC, PEM uses deterministic routines in solving probabilistic problems which provides accurate results. However, this accuracy depends on the number of uncertain input random variables which makes PEM impractical in large-scale problems. PEM is utilized in PLF and POPF considering the correlation between input random variables mainly wind speed and loads as in [75, 76, 77, 78, 79].

3.3 Proposed probabilistic load flow method

The aim of this thesis in both sections is determining the optimal location and power ratings of ESSs considering the uncertainties of wind power distribution and the

correlation among them. Instead of Monet Carlo simulation, five-point estimation method is utilized in the literature to discretize the continuous probability distribution of wind power into 5-point discrete probability function. In this thesis, a new method based 5-PEM is proposed to replace the power distribution of each wind farm with 5^{nw} discrete points associated with their 5^{nw} joint probabilities where *nw* is the number of wind farms. The procedure of the new proposed 5^{nw} method is divided into 4-steps. The first step can be achieved by applying the 5-point estimation method separately on each wind farm as explained in section 3.3.1. Figure 3.2 is a graphical representation of the proposed method where two Wind farms are utilized to explain the steps of the proposed algorithm. Figure 3.2 can be detailed in table 3.1. The red color represents vertices, the brown color represents edges and the blue color represents the interior points. Each color represents a step in the procedure. Section 3.3.1, Section 3.3.2 and Section 3.3.3 describe the remaining 3-steps. After implementing the required 4-steps, 5^{nw} points for each wind farm are substituted instead of its wind power distribution associated with their 5^{nw} joint probabilities.

Table 3.1: Required discrete boundary and interior points for two wind farms

Boundary Points								Interior Points (j=2,3,4)		
Vertices				Edges (j=2,3,4)						
(1,1)	(1,5)	(5,1)	(5,5)	(1, j)	(j,1)	(5, j)	(j,5)	(j,2)	(j,3)	(j,4)
								(2, j)	(3, j)	(4, j)

3.3.1 Step 1: Applying the 5-point estimation method separately on each wind farm

Step 1 can be summarized by applying the 5-point estimation method separately on each wind farm presented by superscript i. The importance of the discretization method is to replace the continuous random variable which is the wind farm distribution in this

case by five finite elements. The probability of the zero and maximum power can be calculated as follows:

$$\begin{cases} P_1^{(i)} = prob\left\{Y^{(i)} = 0\right\} = prob\left(X^{(i)} \le V_{ci}\right) + prob\left(X^{(i)} > V_{co}\right) \\ \qquad = \int_0^{V_{ci}} f_{X^{(i)}}(x^{(i)} \mid \lambda_i, k_i)dx^{(i)} + \int_{V_{co}}^{\infty} f_{X^{(i)}}(x^{(i)} \mid \lambda_i, k_i)dx^{(i)} \\ P_5^{(i)} = prob\left\{Y^{(i)} = M_i\right\} = prob\left(V_{no} \le X^{(i)} \le V_{co}\right) = \int_{V_{no}}^{V_{co}} f_{X^{(i)}}(x^{(i)} \mid \lambda_i, k_i)dx^{(i)} \end{cases} \tag{3.4}$$

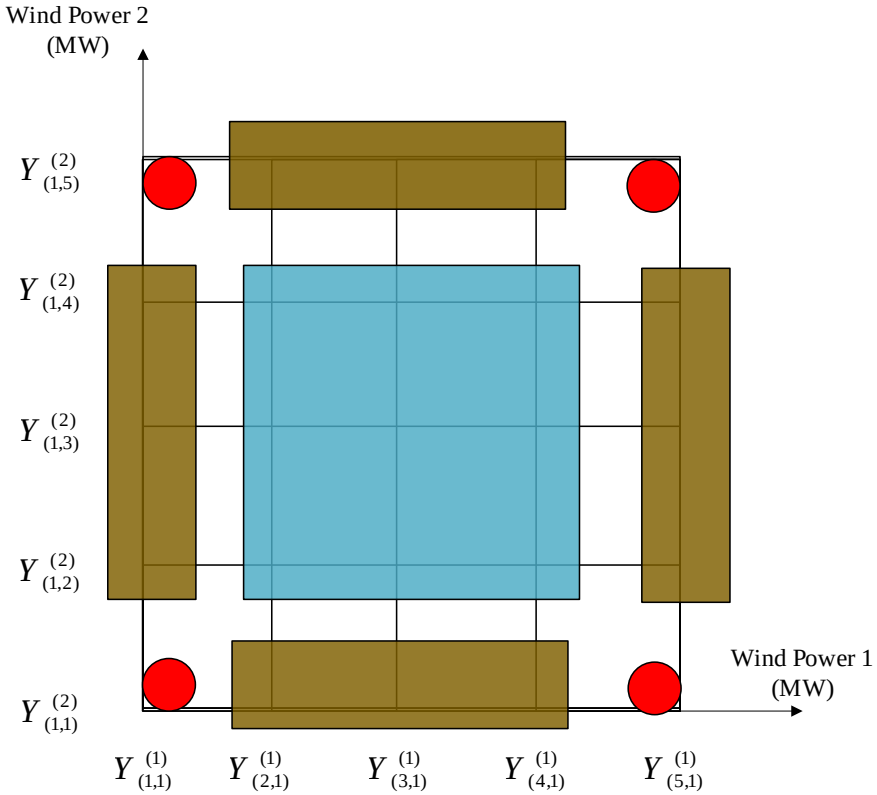

Figure 3.2: Graphical representation of the proposed 5^{nw} method

Where $Y^{(i)}$ consists of one random variable $X^{(i)}$, then

$$f_{Y^{(i)}}(y^{(i)}) = \sum_{k=1}^{n} \frac{f_{X^{(i)}}(x_k^{(i)})}{\left|g'(x_k^{(i)})\right|} \tag{3.5}$$

Where

$$x_1^{(i)} = \left(\frac{y^{(i)} - \alpha_i}{\beta_i} \right) \quad \text{and} \quad g(x^{(i)}) = Y^{(i)} \text{ and } g'(x_1^{(i)}) = \beta_i \tag{3.6}$$

The probability density function (PDF) of $Y^{(i)}$

$$f_{Y^{(i)}}(y^{(i)}) = \frac{f_{X^{(i)}}(x_1^{(i)})}{\left| g'(x_1^{(i)}) \right|} = \frac{f\left(\frac{Y^{(i)} - \alpha_i}{\beta_i} \mid \lambda_i, k_i \right)}{\beta_i} \tag{3.7}$$

The conditional probability density function (PDF) of $Y^{(i)}$

$$f_{Y^{(i)}}(y^{(i)} \mid \lambda_i, k_i) = \frac{\frac{1}{\beta_i} f\left(\frac{y^{(i)} - \alpha_i}{\beta_i} \mid \lambda_i, k_i \right)}{1 - P_1^{(i)} - P_5^{(i)}} \tag{3.8}$$

Notice that for proper PDF

$$\int_0^{M_i} f_{Y^{(i)}}(y^{(i)} \mid \lambda_i, k_i) dx = 1 \tag{3.9}$$

Define

$$\begin{cases} m_{Y^{(i)}} = \int_0^{M_i} y^{(i)} f_{Y^{(i)}}(y^{(i)} \mid \lambda_i, k_i) dy^{(i)} \\ \sigma_{Y^{(i)}}^2 = \int_0^{M_i} (y^{(i)} - m_{Y^{(i)}})^2 f_{Y^{(i)}}(y^{(i)} \mid \lambda_i, k_i) dy^{(i)} \\ L_m^{(i)} = \int_0^{M_i} \left(\frac{y^{(i)} - m_{Y^{(i)}}}{\sigma_{Y^{(i)}}} \right)^m f_{Y^{(i)}}(y^{(i)} \mid \lambda_1, k_1) dy^{(i)} \end{cases} \tag{3.10}$$

Where

$m_{Y^{(i)}}$ is the mean of $Y^{(i)}$

$\sigma_{Y^{(i)}}$ is the standard deviation of $Y^{(i)}$

$L_m^{(i)}$ is the mth central moment of $Y^{(i)}$

Define the standardized value of $Y^{(i)}$ as follows

$$z^{(i)} = \frac{y^{(i)} - m_{Y^{(i)}}}{\sigma_{Y^{(i)}}} \tag{3.11}$$

Then, the moment of equations is given by [73]

$$\sum_{j=2}^{4} p_j^{(i)} \left(z_j^{(i)}\right)^m = L_m^{(i)} \qquad for\ m = 1,2,3,4 \tag{3.12}$$

Where $p_j^{(i)}$ is the probability corresponding to $z_j^{(i)}$. Solve for the nonlinear equation (3.12), we can obtain

$$\begin{cases} z_2^{(i)} = \dfrac{L_3^{(i)}}{2} - \sqrt{L_4^{(i)} - \dfrac{3\left(L_3^{(i)}\right)^2}{4}} \\ z_3^{(i)} = 0 \\ z_4^{(i)} = \dfrac{L_3^{(i)}}{2} + \sqrt{L_4^{(i)} - \dfrac{3\left(L_3^{(i)}\right)^2}{4}} \end{cases} \tag{3.13}$$

$$\begin{cases} p_2^{(i)} = \dfrac{-1}{z_2^{(i)}(z_4^{(i)} - z_2^{(i)})} \\ p_3^{(i)} = 1 - p_2^{(i)} - p_4^{(i)} \\ p_4^{(i)} = \dfrac{1}{z_4^{(i)}(z_4^{(i)} - z_2^{(i)})} \end{cases} \tag{3.14}$$

We can estimate the remaining three discrete points distribution $p_2^{(i)}$, $p_3^{(i)}$, and $p_4^{(i)}$ with corresponding location $z_2^{(i)}$, $z_3^{(i)}$, and $z_4^{(i)}$ for $f_{Y^{(i)}}(y^{(i)} \mid \lambda_i, k_i)$. Then estimated point $Y_j^{(i)}$ and associated probabilities $P_j^{(i)}$ can be obtained as

$$\begin{cases} Y_2^{(i)} = m_{Y^{(i)}} + \sigma_{Y^{(i)}} z_2^{(i)} \\ Y_3^{(i)} = m_{Y^{(i)}} \\ Y_4^{(i)} = m_{Y^{(i)}} + \sigma_{Y^{(i)}} z_4^{(i)} \end{cases} \quad \text{and} \quad \begin{cases} P_2^{(i)} = p_2^{(i)} \times (1 - P_1^{(i)} - P_5^{(i)}) \\ P_3^{(i)} = p_3^{(i)} \times (1 - P_1^{(i)} - P_5^{(i)}) \\ P_4^{(i)} = p_4^{(i)} \times (1 - P_1^{(i)} - P_5^{(i)}) \end{cases} \tag{3.15}$$

At the end of step 1, Table 3.2 presents the 5-discrete points for each wind farm $Y^{(i)}$ with their associated probabilities $P^{(i)}$ where two wind farms are used as an example.

Moreover, Figure 3.3 presents a flowchart summarize all required mathematical steps for implementing five-point estimation method.

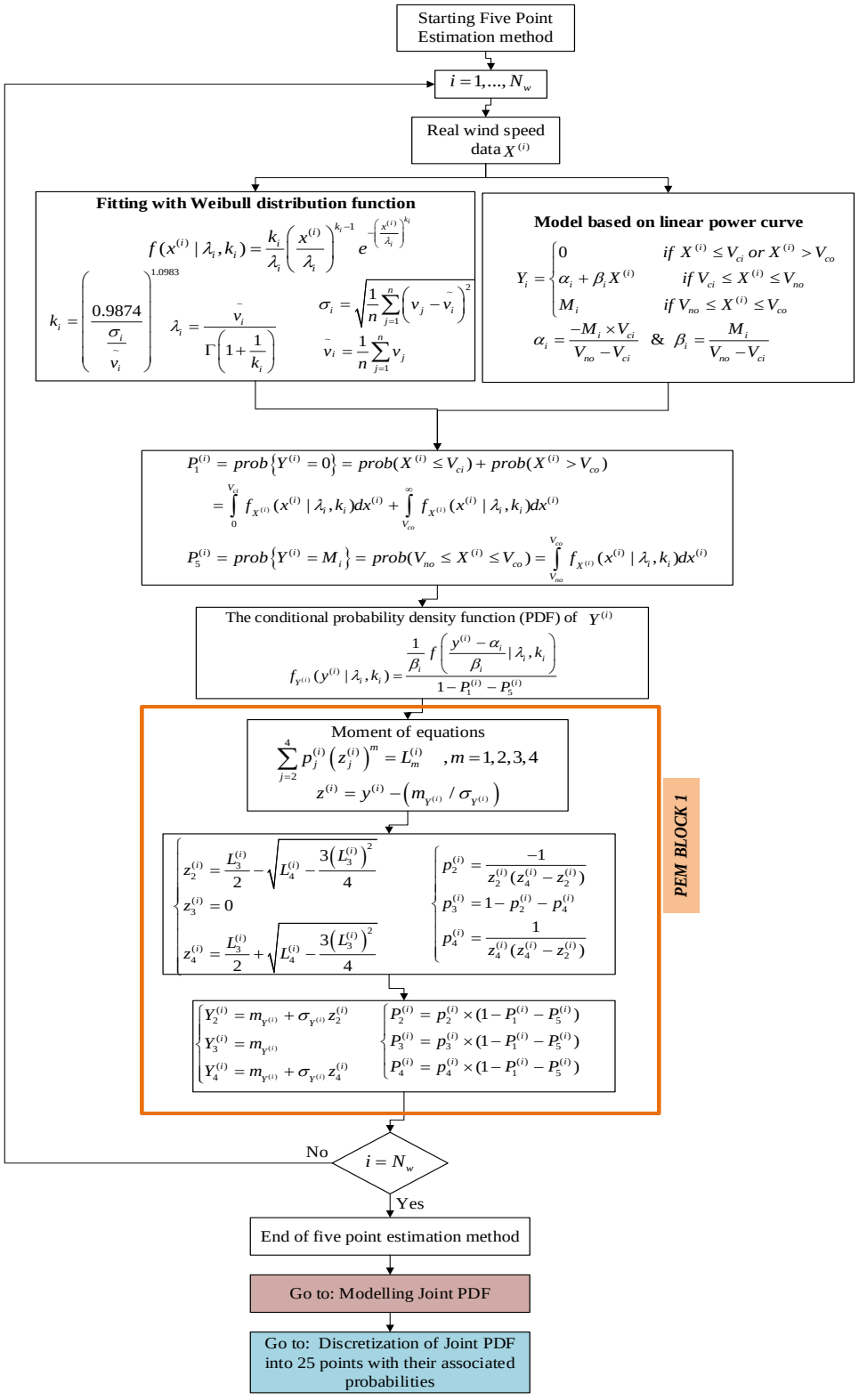

Figure 3.3: Five-point estimation method, modeling and discretizing wind power distribution

Table 3.2: Five-discrete points for each wind farm power $Y^{(i)}$ with their associated probabilities $P^{(i)}$ at the end of step1

	Probabilities					Power (MW)				
Windfarm 1	$P_1^{(1)}$	$P_2^{(1)}$	$P_3^{(1)}$	$P_4^{(1)}$	$P_5^{(1)}$	$Y_1^{(1)}$	$Y_2^{(1)}$	$Y_3^{(1)}$	$Y_4^{(1)}$	$Y_5^{(1)}$
Windfarm 2	$P_1^{(2)}$	$P_2^{(2)}$	$P_3^{(2)}$	$P_4^{(2)}$	$P_5^{(2)}$	$Y_1^{(2)}$	$Y_2^{(2)}$	$Y_3^{(2)}$	$Y_4^{(2)}$	$Y_5^{(2)}$

3.3.2 Step 2: Determining marginal power and joint probabilities at boundaries (vertices)

According Figure 3.2, the red color represents the vertices at points (1,1), (1,5), (5,1) and (5,5) as stated in table 3.1. The number of boundary points at vertices is equal 2^{Nw} where N_w is the number of wind farms. For two wind farms, the joint probabilities at vertices are computed as following:

$$\begin{cases} P_{(1,1)}^{(Y^{(1)},Y^{(2)})} = \int_0^{V_{ci}} \int_0^{V_{ci}} f_{X^{(1)}X^{(2)}}\left(x^{(1)},x^{(2)} \mid \lambda_1,\lambda_2,k_1,k_2\right)dx^{(1)}dx^{(2)} + \ldots \\ \quad \int_0^{V_{ci}} \int_{V_{co}}^{\infty} f_{X^{(1)}X^{(2)}}\left(x^{(1)},x^{(2)} \mid \lambda_1,\lambda_2,k_1,k_2\right)dx^{(1)}dx^{(2)} + \ldots \\ \quad \int_{V_{co}}^{\infty} \int_{V_{co}}^{\infty} f_{X^{(1)}X^{(2)}}\left(x^{(1)},x^{(2)} \mid \lambda_1,\lambda_2,k_1,k_2\right)dx^{(1)}dx^{(2)} + \ldots \\ \quad \int_{V_{co}}^{\infty} \int_0^{V_{ci}} f_{X^{(1)}X^{(2)}}\left(x^{(1)},x^{(2)} \mid \lambda_1,\lambda_2,k_1,k_2\right)dx^{(1)}dx^{(2)} \\ P_{(1,5)}^{(Y^{(1)},Y^{(2)})} = \int_0^{V_{ci}} \int_{V_{no}}^{V_{co}} f_{X^{(1)}X^{(2)}}\left(x^{(1)},x^{(2)} \mid \lambda_1,\lambda_2,k_1,k_2\right)dx^{(1)}dx^{(2)}{}_2 + \ldots \\ \quad \int_{V_{co}}^{\infty} \int_{V_{no}}^{V_{co}} f_{X^{(1)}X^{(2)}}\left(x^{(1)},x^{(2)} \mid \lambda_1,\lambda_2,k_1,k_2\right)dx^{(1)}dx^{(2)} \\ P_{(5,1)}^{(Y^{(1)},Y^{(2)})} = \int_{V_{no}}^{V_{co}} \int_0^{V_{ci}} f_{X^{(1)}X^{(2)}}\left(x^{(1)},x^{(2)} \mid \lambda_1,\lambda_2,k_1,k_2\right)dx^{(1)}dx^{(2)} + \ldots \\ \quad \int_{V_{no}}^{V_{co}} \int_{V_{co}}^{\infty} f_{X^{(1)}X^{(2)}}\left(x^{(1)},x^{(2)} \mid \lambda_1,\lambda_2,k_1,k_2\right)dx^{(1)}dx^{(2)} \\ P_{(5,5)}^{(Y^{(1)},Y^{(2)})} = \int_{V_{no}}^{V_{co}} \int_{V_{no}}^{V_{co}} f_{X^{(1)}X^{(2)}}\left(x^{(1)},x^{(2)} \mid \lambda_1,\lambda_2,k_1,k_2\right)dx^{(1)}dx^{(2)} \end{cases} \quad (3.16)$$

For two independent wind speeds, the joint probability density function (PDF) for two wind speeds can be expressed as following:

$$f_{X^{(1)}X^{(2)}}\left(x^{(1)},x^{(2)}|\lambda_1,\lambda_2,k_1,k_2\right)=f_{X^{(1)}}\left(x^{(1)}|\lambda_1,k_1\right)f_{X^{(2)}}\left(x^{(2)}|\lambda_2,k_2\right) \quad (3.17)$$

However, for correlated wind speeds, the bivariate distribution is modeled by using of the copula method. Correlation is any statistical association which refers to the degree to which bivariate wind speed distributions of wind farms are linearly related. It is useful because they can indicate a predictive relationship between bivariate wind speed distribution that can be exploited in practice. Figure 3.4 presents the relationship between the wind speeds of two wind farms which seems to be very near to exact linear relationship which can be defined by a factor with value very close to 1 called correlation coefficient which equals to 0.94 in this case.

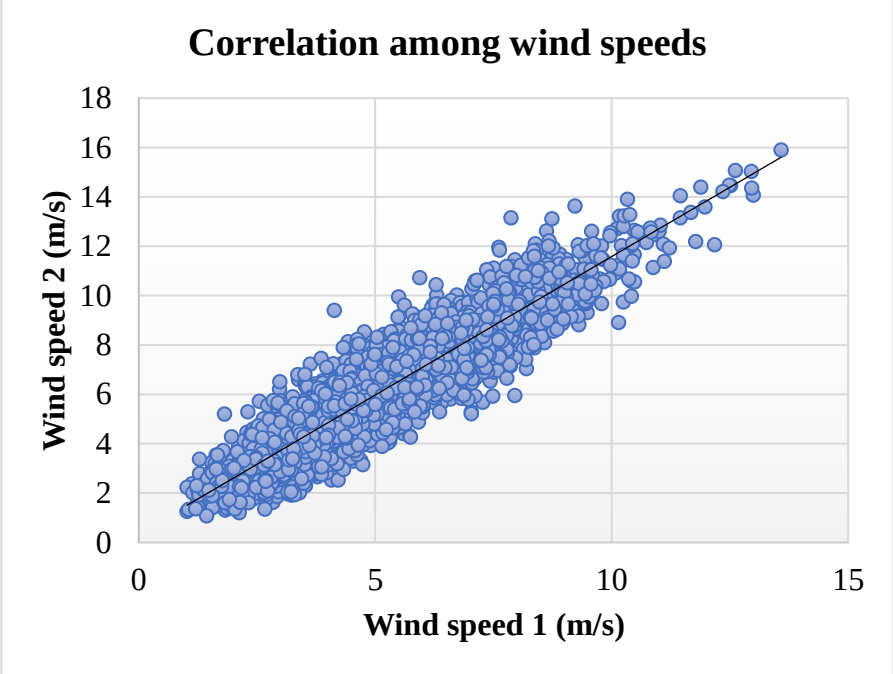

Figure 3.4: Correlation between bivariate wind speed distributions of two wind farms

The copulas are functions that combines multi-variate distribution functions to their one-dimensional marginal [68]. Let $F_{X_1X_2}(x_1,x_2)$ denote the joint cumulative distribution function (CDF) of multi-correlated wind speeds with marginal $F_{X_1}(x_1)$ and $F_{X_2}(x_2)$. Then there exists Clayton-Copula such that for all x_1 and x_2.

$$F_{X_1X_2}(x_1,x_2)=C(F_{X_1}(x_1),F_{X_2}(x_2)) \tag{3.18}$$

Clayton Copula Function is chosen such that;

$$F_{X_1X_2}(x_1,x_2)=(F_{X_1}(x_1)^{-a}+F_{X_2}(x_2)^{-a}-1)^{\frac{-1}{a}} \tag{3.19}$$

Where a is the correlation coefficient. The bivariate distribution PDF is obtained as follows:

$$\begin{aligned} f_{X_1X_2}(x_1,x_2)&=\frac{\partial^2 F_{X_1X_2}(x_1,x_2)}{\partial x_1\partial x_2}=a\left(\frac{1}{a}+1\right)F_{X_1}(x_1)^{-a-1}F_{X_2}(x_2)^{-a-1}\\ &.(F_{X_1}(x_1)^{-a}+F_{X_2}(x_2)^{-a}-1)^{\frac{-1}{a}-2}.f_{X_1}(x_1)f_{X_2}(x_2)\end{aligned} \tag{3.20}$$

Where;

$$\begin{cases} f_{X^{(i)}}(x^{(i)}/\lambda_i,k_i)=\dfrac{k_i}{\lambda_i}\left(\dfrac{x^{(i)}}{\lambda_i}\right)^{k_i-1}\times\exp\left(-\left(\left(\dfrac{x^{(i)}}{\lambda_i}\right)^{k_i}\right)\right) & i=1,...,N_w \\ F_{X^{(i)}}(x^{(i)})=1-\exp\left(-\left(\dfrac{x^{(i)}}{\lambda_i}\right)^{k_i}\right) & i=1...N_w \end{cases} \tag{3.21}$$

After all, the joint pdf of two wind speeds can be expressed as follows:

$$\begin{aligned} f_{X^{(1)}X^{(2)}}(x^{(1)},x^{(2)})&=a\left(\frac{1}{a}+1\right)\times\left(1-\exp\left(-\left(\frac{x^{(1)}}{\lambda_1}\right)^{k_1}\right)\right)^{-a-1}\times\left(1-\exp\left(-\left(\frac{x^{(2)}}{\lambda_2}\right)^{k_2}\right)\right)^{-a-1}\\ &\times\left(\left(1-\exp\left(-\left(\frac{x^{(1)}}{\lambda_1}\right)^{k_1}\right)\right)^{-a}+\left(1-\exp\left(-\left(\frac{x^{(2)}}{\lambda_2}\right)^{k_2}\right)\right)^{-a}+1\right)^{\frac{-1}{a}-2}\\ &\times\frac{k_1}{\lambda_1}\left(\frac{x^{(1)}}{\lambda_1}\right)^{k_1-1}\times\exp\left(-\left(\frac{x^{(1)}}{\lambda_1}\right)^{k_1}\right)\times\frac{k_2}{\lambda_2}\left(\frac{x^{(2)}}{\lambda_2}\right)^{k_2-1}\times\exp\left(-\left(\frac{x^{(2)}}{\lambda_2}\right)^{k_2}\right)\end{aligned} \tag{3.22}$$

$Y^{(1)}$ and $Y^{(2)}$ are the output power for wind farm 1 and wind farm 2; $P_{(1,1)}^{(Y^{(1)},Y^{(2)})}$ is the joint probability at point (1,1) in Figure 3.2 for two wind farms having output power $Y^{(1)}=Y_1^{(1)}=0$ and $Y^{(2)}=Y_1^{(2)}=0$; $P_{(1,5)}^{(Y^{(1)},Y^{(2)})}$ is the joint probability at point (1,5) in Figure 3.2 for two wind farms having output power $Y^{(1)}=Y_1^{(1)}=0$ and

$Y^{(2)} = Y_5^{(2)} = M_2$; $P_{(5,1)}^{(Y^{(1)},Y^{(2)})}$ is the joint probability at point (5,1) in Figure 3.2 for two wind farms having output power $Y^{(1)} = Y_5^{(1)} = M_1$ and $Y^{(2)} = Y_1^{(2)} = 0$; $P_{(5,5)}^{(Y^{(1)},Y^{(2)})}$ is the joint probability at point (5,5) in Figure 3.2 for two wind farms having output power $Y^{(1)} = Y_5^{(1)} = M_1$ and $Y^{(2)} = Y_5^{(2)} = M_2$ At the end of step 2, Four vertices represent the joint probabilities and marginal output power for two wind farms are computed and presented in table 3.3. Figure 3.5 presents modelling of joint PDF for both wind speed and wind power. Figure 3.6 presents a flowchart about steps required for discretizing the joint PDF of wind power into 25 scenarios associated with their probabilities.

Table 3.3: Boundaries (vertices) joint probabilities and marginal output power for two wind farms

	Output Power (MW)			
Joint Vertices Probabilities	$P_{(1,1)}^{(Y^{(1)},Y^{(2)})}$	$P_{(1,5)}^{(Y^{(1)},Y^{(2)})}$	$P_{(5,1)}^{(Y^{(1)},Y^{(2)})}$	$P_{(5,5)}^{(Y^{(1)},Y^{(2)})}$
Wind Farm 1	0	0	M_1	M_1
Wind Farm 2	0	M_2	0	M_2

3.3.3 Step 3: Determining marginal power and joint probabilities at boundaries (edges)

According to Figure 3.2, the rectangular brown color represents the edges as stated in table 3.1. The number of the boundary points at edges is equal to $N_w \times 2^{N_w-1} \times N_{int}$ where N_{int} is the number of interior points presented in five-point estimation method which is equal to 3.

According to Figure 3.2, the procedures of step 3 are as follows:

Step 3 (a) For $Y^{(2)} = Y_{(1,1)}^{(2)} = Y_1^{(2)} = 0$, determine $(Y_{(2,1)}^{(1)}, Y_{(3,1)}^{(1)} \text{ and } Y_{(4,1)}^{(1)})$

Define the followings:

$$\begin{cases} m_{Y^{(1)}/Y^{(2)}}(Y^{(1)}/Y^{(2)}_{(1,1)}) = \int_0^{M_1} Y^{(1)} f_{Y^{(1)}/Y^{(2)}}(Y^{(1)}/Y^{(2)}_{(1,1)} \mid \lambda_1, k_1, \lambda_2, k_2) dy^{(1)} \\ \sigma^2_{Y^{(1)}/Y^{(2)}}(Y^{(1)}/Y^{(2)}_{(1,1)}) = \int_0^{M_1} \left(Y^{(1)} - m^2{}_{Y^{(1)}/Y^{(2)}}(Y^{(1)}/Y^{(2)}_{(1,1)})\right) f_{Y^{(1)}/Y^{(2)}}(Y^{(1)}/Y^{(2)}_{(1,1)} \mid \lambda_1, k_1, \lambda_2, k_2) dy^{(1)} \\ L_m^{(Y^{(1)}/Y^{(2)})} = \int_0^{M_1} \left(\frac{Y^{(1)} - m_{Y^{(1)}/Y^{(2)}}(Y^{(1)}/Y^{(2)}_{(1,1)})}{\sigma_{Y^{(1)}/Y^{(2)}}(Y^{(1)}/Y^{(2)}_{(1,1)})} \right)^m f_{Y^{(1)}/Y^{(2)}}(Y^{(1)}/Y^{(2)}_{(1,1)} \mid \lambda_1, k_1, \lambda_2, k_2) dy^{(1)} \end{cases} \quad (3.23)$$

Where

$m_{Y^{(1)}/Y^{(2)}}(Y^{(1)}/Y^{(2)}_{(1,1)})$ is the conditional mean of $Y^{(1)}$ given that $Y^{(2)} = Y^{(2)}_{(1,1)} = Y^{(2)}_1 = 0$

$\sigma^2_{Y^{(1)}/Y^{(2)}}(Y^{(1)}/Y^{(2)}_{(1,1)})$ is the conditional variance of $Y^{(1)}$ given that $Y^{(2)} = Y^{(2)}_{(1,1)} = Y^{(2)}_1 = 0$

$L_m^{(Y^{(1)}/Y^{(2)})}$ is the conditional mth central moments of $Y^{(1)}$ given that $Y^{(2)} = Y^{(2)}_{(1,1)} = Y^{(2)}_1 = 0$

For two independent wind farms, the conditional PDF of $Y^{(1)}$ given $Y^{(2)}$

$$f_{Y^{(1)}/Y^{(2)}}(Y^{(1)}/Y^{(2)} \mid \lambda_1, k_1, \lambda_2, k_2) = f_{Y^{(1)}}(Y^{(1)} \mid \lambda_1, k_1) \quad (3.24)$$

However, for two correlated wind farms, the conditional PDF of $Y^{(1)}$ given $Y^{(2)}$

$$f_{Y^{(1)}/Y^{(2)}}(y^{(1)}/y^{(2)} \mid \lambda_1, k_1, \lambda_2, k_2) = f_{Y^{(1)}Y^{(2)}}(y^{(1)}, y^{(2)} \mid \lambda_1, k_1, \lambda_2, k_2) / f_{Y^{(2)}}(y^{(2)} \mid \lambda_2, k_2) \quad (3.25)$$

Where the pdf of each wind farm output power is as follows;

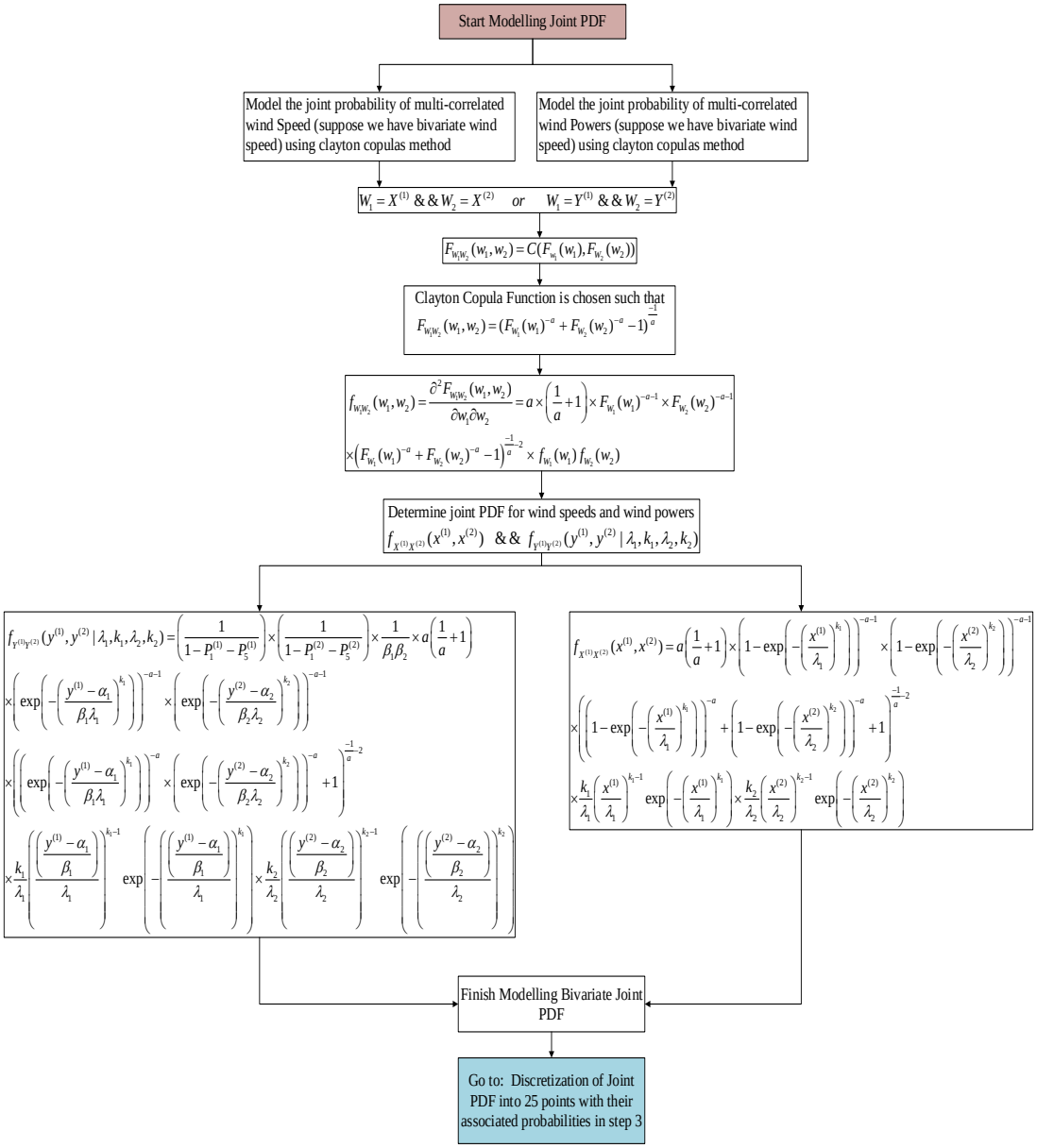

Figure 3.5: Modelling of joint PDF for both wind speed and wind power

$$f_{Y^{(i)}}(y^{(i)} \mid \lambda_i, k_i) = \frac{\frac{1}{\beta_i} f\left(\frac{y^{(i)} - \alpha_i}{\beta_i} \mid \lambda_i, k_i\right)}{1 - P_1^{(i)} - P_5^{(i)}} \tag{3.26}$$

The joint pdf for the output powers of two wind farms can be represented using clayton copula as follows;

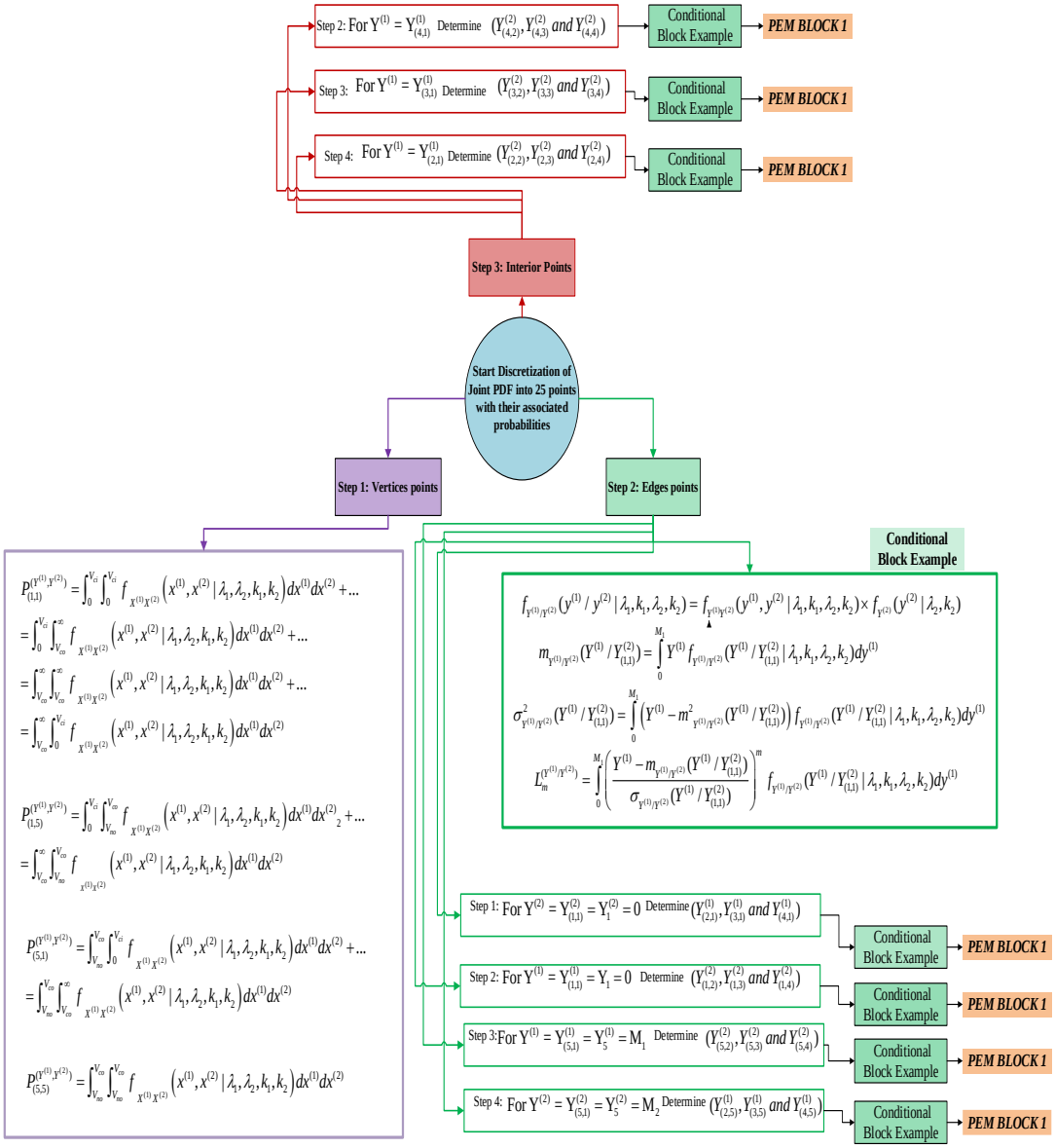

Figure 3.6: The steps required for wind power distribution discretization

$$f_{Y^{(1)}Y^{(2)}}(y^{(1)},y^{(2)} \mid \lambda_1,k_1,\lambda_2,k_2) = \left(\frac{1}{1-P_1^{(1)}-P_5^{(1)}}\right)\times\left(\frac{1}{1-P_1^{(2)}-P_5^{(2)}}\right)\times\frac{1}{\beta_1\beta_2}\times a\left(\frac{1}{a}+1\right)$$
$$\times\left(\exp\left(-\left(\frac{y^{(1)}-\alpha_1}{\beta_1\lambda_1}\right)^{k_1}\right)\right)^{-a-1}\times\left(\exp\left(-\left(\frac{y^{(2)}-\alpha_2}{\beta_2\lambda_2}\right)^{k_2}\right)\right)^{-a-1}$$
$$\times\left(\left(\exp\left(-\left(\frac{y^{(1)}-\alpha_1}{\beta_1\lambda_1}\right)^{k_1}\right)\right)^{-a}\times\left(\exp\left(-\left(\frac{y^{(2)}-\alpha_2}{\beta_2\lambda_2}\right)^{k_2}\right)\right)^{-a}+1\right)^{\frac{-1}{a}-2} \quad (3.27)$$
$$\times\frac{k_1}{\lambda_1}\left(\frac{\left(\frac{y^{(1)}-\alpha_1}{\beta_1}\right)}{\lambda_1}\right)^{k_1-1}\times\exp\left(-\left(\frac{\left(\frac{y^{(1)}-\alpha_1}{\beta_1}\right)}{\lambda_1}\right)^{k_1}\right)\times\frac{k_2}{\lambda_2}\left(\frac{\left(\frac{y^{(2)}-\alpha_2}{\beta_2}\right)}{\lambda_2}\right)^{k_2-1}\times\exp\left(-\left(\frac{\left(\frac{y^{(2)}-\alpha_2}{\beta_2}\right)}{\lambda_2}\right)^{k_2}\right)$$

Then, the moment of equations is given by

$$\sum_{j=2}^{4} p_{(j,1)}^{(Y^{(1)}/Y^{(2)})} \left(z_{(j,1)}^{(Y^{(1)}/Y^{(2)})} \right)^m = L_m^{(Y^{(1)}/Y^{(2)})} \qquad for\ m = 1,2,3,4 \tag{3.28}$$

Where $p_{(j,1)}^{(Y^{(1)}/Y^{(2)})}$ is the conditional probability of $Y^{(1)}$ given $Y^{(2)}$ corresponding to $z_{(j,1)}^{(Y^{(1)}/Y^{(2)})}$

Solve for the above equation, we can obtain

$$\begin{cases} z_{(2,1)}^{(Y^{(1)}/Y^{(2)})} = \dfrac{L_3^{(Y^{(1)}/Y^{(2)})}}{2} - \sqrt{L_4^{(Y^{(1)}/Y^{(2)})} - \dfrac{3\left(L_3^{(Y^{(1)}/Y^{(2)})}\right)^2}{4}} \\ z_{(3,1)}^{(Y^{(1)}/Y^{(2)})} = 0 \\ z_{(4,1)}^{(Y^{(1)}/Y^{(2)})} = \dfrac{L_3^{(Y^{(1)}/Y^{(2)})}}{2} + \sqrt{L_4^{(Y^{(1)}/Y^{(2)})} - \dfrac{3\left(L_3^{(Y^{(1)}/Y^{(2)})}\right)^2}{4}} \end{cases} \tag{3.29}$$

$$\begin{cases} p_{(2,1)}^{(Y^{(1)}/Y^{(2)})} = \dfrac{-1}{z_{(2,1)}^{(Y^{(1)}/Y^{(2)})}\left(z_{(4,1)}^{(Y^{(1)}/Y^{(2)})} - z_{(2,1)}^{(Y^{(1)}/Y^{(2)})}\right)} \\ p_{(3,1)}^{(Y^{(1)}/Y^{(2)})} = 1 - p_{(2,1)}^{(Y^{(1)}/Y^{(2)})} - p_{(2,1)}^{(Y^{(1)}/Y^{(2)})} \\ p_{(4,1)}^{(Y^{(1)}/Y^{(2)})} = \dfrac{1}{z_{(4,1)}^{(Y^{(1)}/Y^{(2)})}\left(z_{(4,1)}^{(Y^{(1)}/Y^{(2)})} - z_{(2,1)}^{(Y^{(1)}/Y^{(2)})}\right)} \end{cases} \tag{3.30}$$

we can estimate three discrete points distribution $p_{(2,1)}^{(Y^{(1)}/Y^{(2)})}$, $p_{(3,1)}^{(Y^{(1)}/Y^{(2)})}$, and $p_{(4,1)}^{(Y^{(1)}/Y^{(2)})}$ with corresponding location $z_{(2,1)}^{(Y^{(1)}/Y^{(2)})}$, $z_{(3,1)}^{(Y^{(1)}/Y^{(2)})}$, and $z_{(4,1)}^{(Y^{(1)}/Y^{(2)})}$. Then the estimated point $Y_{(j,1)}^{(1)}$ and the associated probabilities $P_{(j,1)}^{(Y^{(1)}/Y^{(2)})}$ can be obtained as:

$$\begin{cases} Y_{(2,1)}^{(1)} = \left(m_{Y^{(1)}/Y^{(2)}}(Y^{(1)} / Y_{(1,1)}^{(2)})\right) + \left(\sigma_{Y^{(1)}/Y^{(2)}}(Y^{(1)} / Y_{(1,1)}^{(2)})\right) \times z_{(2,1)}^{(Y^{(1)}/Y^{(2)})} \\ Y_{(3,1)}^{(1)} = \left(m_{Y^{(1)}/Y^{(2)}}(Y^{(1)} / Y_{(1,1)}^{(2)})\right) \\ Y_{(4,1)}^{(1)} = \left(m_{Y^{(1)}/Y^{(2)}}(Y^{(1)} / Y_{(1,1)}^{(2)})\right) + \left(\sigma_{Y^{(1)}/Y^{(2)}}(Y^{(1)} / Y_{(1,1)}^{(2)})\right) \times z_{(4,1)}^{(Y^{(1)}/Y^{(2)})} \end{cases} \tag{3.31}$$

Joint Probabilities for two Independent/correlated wind farms can be computed as follows:

$$p_{(j,1)}^{(Y^{(1)},Y^{(2)})} = p_{(j,1)}^{(Y^{(1)}/Y^{(2)})} \times P_1^{Y^{(2)}} \times (1 - P_1^{Y^{(1)}} - P_5^{Y^{(1)}}) \quad j = 2,3,4 \tag{3.32}$$

At the end of step 3 (a), 3-points represent the joint probabilities and marginal output power for two wind farms are computed and stated in table 3.4.

Table 3.4: Boundary (Edges) joint probabilities and marginal output power for two wind farms at end of step 3 (a)

Joint Probabilities $P_{(j,1)}^{(Y^{(1)},Y^{(2)})}$	$P_{(2,1)}^{(Y^{(1)},Y^{(2)})}$	$P_{(3,1)}^{(Y^{(1)},Y^{(2)})}$	$P_{(4,1)}^{(Y^{(1)},Y^{(2)})}$
Output power of wind farms 1: $Y^{(1)}$ (MW)	$Y_{(2,1)}^{(1)}$	$Y_{(3,1)}^{(1)}$	$Y_{(4,1)}^{(1)}$
Output power of wind farms 2: $Y^{(2)}$ (MW)	$Y_{(1,1)}^{(2)} = Y_1^{(2)}$	$Y_{(1,1)}^{(2)} = Y_1^{(2)}$	$Y_{(1,1)}^{(2)} = Y_1^{(2)}$

Step 3 (b) For $Y^{(1)} = Y_{(1,1)}^{(1)} = Y_1^{(1)} = 0$, determine $(Y_{(1,2)}^{(2)}, Y_{(1,3)}^{(2)} \text{ and } Y_{(1,4)}^{(2)})$

Apply same procedures as in step 3 (a), At the end of step 3 (b). we have the following:

Joint Probabilities for two Independent/correlated wind farms can be computed as follows:

$$p_{(1,j)}^{(Y^{(1)},Y^{(2)})} = p_{(1,j)}^{(Y^{(2)}/Y^{(1)})} \times P_1^{Y^{(1)}} \times (1 - P_1^{Y^{(2)}} - P_5^{Y^{(2)}}) \quad j = 2,3,4 \tag{3.33}$$

At the end of step 3 (b), 3-points represent the joint probabilities and marginal output power for two wind farms are computed and stated in table 3.5.

Table 3.5: Boundary (Edges) joint probabilities and marginal output power for two wind farms at end of step 3 (b)

Joint Probabilities $P_{(1,j)}^{(Y^{(1)},Y^{(2)})}$	$P_{(1,2)}^{(Y^{(1)},Y^{(2)})}$	$P_{(1,3)}^{(Y^{(1)},Y^{(2)})}$	$P_{(1,4)}^{(Y^{(1)},Y^{(2)})}$
Output power of wind farms 1: $Y^{(1)}$ (MW)	$Y_{(1,1)}^{(1)} = Y_1^{(1)}$	$Y_{(1,1)}^{(1)} = Y_1^{(1)}$	$Y_{(1,1)}^{(1)} = Y_1^{(1)}$
Output power of wind farms 2: $Y^{(2)}$ (MW)	$Y_{(1,2)}^{(2)}$	$Y_{(1,3)}^{(2)}$	$Y_{(1,4)}^{(2)}$

Step 3 (c) For $Y^{(1)} = Y_{(5,1)}^{(1)} = Y_5^{(1)} = M_1$, determine $(Y_{(5,2)}^{(2)}, Y_{(5,3)}^{(2)} \text{ and } Y_{(5,4)}^{(2)})$

Apply same procedures as in step 3 (a), At the end of step 3 (c). we have the following:

Joint Probabilities for two Independent/correlated wind farms can be computed as follows:

$$p_{(5,j)}^{(Y^{(1)},Y^{(2)})} = p_{(5,j)}^{(Y^{(2)}/Y^{(1)})} \times P_5^{Y^{(1)}} \times (1 - P_1^{Y^{(2)}} - P_5^{Y^{(2)}}) \quad j = 2,3,4 \tag{3.34}$$

At the end of step 3 (c), 3-points represent the joint probabilities and marginal output power for two wind farms are computed and stated in table 3.6.

Table 3.6: Boundary (Edges) joint probabilities and marginal output power for two wind farms at end of step 3 (c)

Joint Probabilities $P_{(5,j)}^{(Y^{(1)},Y^{(2)})}$	$P_{(5,2)}^{(Y^{(1)},Y^{(2)})}$	$P_{(5,3)}^{(Y^{(1)},Y^{(2)})}$	$P_{(5,4)}^{(Y^{(1)},Y^{(2)})}$
Output power of wind farms 1: $Y^{(1)}$ (MW)	$Y_{(5,1)}^{(1)} = Y_5^{(1)}$	$Y_{(5,1)}^{(1)} = Y_5^{(1)}$	$Y_{(5,1)}^{(1)} = Y_5^{(1)}$
Output power of wind farms 2: $Y^{(2)}$ (MW)	$Y_{(5,2)}^{(2)}$	$Y_{(5,3)}^{(2)}$	$Y_{(5,4)}^{(2)}$

Step 3 (d) For $Y^{(2)} = Y_{(5,1)}^{(2)} = Y_5^{(2)} = M_2$, determine $(Y_{(2,5)}^{(1)}, Y_{(3,5)}^{(1)} \text{ and } Y_{(4,5)}^{(1)})$

Apply same procedures as in step 3 (a), At the end of step 3 (d) we have the following:

Joint Probabilities for two Independent/correlated wind farms can be computed as follows:

$$p_{(j,5)}^{(Y^{(1)},Y^{(2)})} = p_{(j,5)}^{(Y^{(1)}/Y^{(2)})} \times P_5^{Y^{(2)}} \times (1 - P_1^{Y^{(1)}} - P_5^{Y^{(1)}}) \quad j = 2,3,4 \tag{3.35}$$

At the end of step 3 (d), 3-points represent the joint probabilities and marginal output power for two wind farms are computed and stated in table 3.7.

Table 3.7: Boundary (Edges) joint probabilities and marginal output power for two wind farms at end of step 3 (d)

Joint Probabilities $P_{(j,5)}^{(Y^{(1)},Y^{(2)})}$	$P_{(2,5)}^{(Y^{(1)},Y^{(2)})}$	$P_{(3,5)}^{(Y^{(1)},Y^{(2)})}$	$P_{(4,5)}^{(Y^{(1)},Y^{(2)})}$
Output power of wind farms 1: $Y^{(1)}$ (MW)	$Y_{(2,5)}^{(1)}$	$Y_{(3,5)}^{(1)}$	$Y_{(4,5)}^{(1)}$
Output power of wind farms 2: $Y^{(2)}$ (MW)	$Y_{(1,5)}^{(2)} = Y_5^{(2)}$	$Y_{(1,5)}^{(2)} = Y_5^{(2)}$	$Y_{(1,5)}^{(2)} = Y_5^{(2)}$

3.3.4 Step 4: Determining marginal power and joint probabilities for interior points

According to Figure 3.2, the blue square color contains the interior points as stated in table 3.1. The number of interior points with duplicating points is equal to $5^{(N_w-1)-1} \times N_{\text{int}} \times N_w \times (N_w-1)! \times N_{\text{int}}$. The number of interior points without duplicating points is equal to 5^{Nw} - *Number of Boundary points* where the number of boundary points is the sum of the number of points at vertices and edges.

The procedures of step 4 are as follows:

Step 4 (a) For $Y^{(1)} = Y^{(1)}_{(2,1)}$, determine $(Y^{(2)}_{(2,2)}, Y^{(2)}_{(2,3)}\ and\ Y^{(2)}_{(2,4)})$

Define the followings

$$\begin{cases} m_{Y^{(2)}/Y^{(1)}}(Y^{(2)} / Y^{(1)}_{(2,1)}) = \int_0^{M_2} Y^{(2)} f_{Y^{(2)}/Y^{(1)}}(Y^{(2)} / Y^{(1)}_{(2,1)} \mid \lambda_1, k_1, \lambda_2, k_2) dy^{(2)} \\ \sigma^2_{Y^{(2)}/Y^{(1)}}(Y^{(2)} / Y^{(1)}_{(2,1)}) = \int_0^{M_2} \left(Y^{(2)} - m^2_{Y^{(2)}/Y^{(1)}}(Y^{(2)} / Y^{(1)}_{(2,1)})\right) \times \\ \quad f_{Y^{(2)}/Y^{(1)}}(Y^{(2)} / Y^{(1)}_{(2,1)} \mid \lambda_1, k_1, \lambda_2, k_2) dy^{(2)} \\ L_m^{(Y^{(2)}/Y^{(1)})} = \int_0^{M_2} \left(\frac{Y^{(2)} - m_{Y^{(2)}/Y^{(1)}}(Y^{(2)} / Y^{(1)}_{(2,1)})}{\sigma_{Y^{(2)}/Y^{(1)}}(Y^{(2)} / Y^{(1)}_{(2,1)})} \right)^m f_{Y^{(2)}/Y^{(1)}}(Y^{(2)} / Y^{(1)}_{(2,1)} \mid \lambda_1, k_1, \lambda_2, k_2) dy^{(2)} \end{cases} \quad (3.36)$$

Apply same procedures as in step 3 (a), At the end of step 4 (a). we have the following:

Joint Probabilities for two independent wind farms can be computed as follows:

$$p^{(Y^{(1)}, Y^{(2)})}_{(2,j)} = p^{(Y^{(2)}/Y^{(1)})}_{(2,j)} \times P_2^{Y^{(1)}} \times (1 - P_1^{Y^{(2)}} - P_5^{Y^{(2)}}) \qquad j = 2,3,4 \quad (3.37)$$

Joint Probabilities for two correlated wind farms are different from the independent case. Then, we have

$$p^{(Y^{(2)}/(Y^{(1)}_{(2,1)}/Y^{(2)}_1))}_{(2,j)} = \frac{p^{(Y^{(2)}, (Y^{(1)}_{(2,1)}/Y^{(2)}_1))}_{(2,j)}}{\left(p^{(Y^{(1)}/Y^{(2)})}_{(2,1)} \times (1 - P_1^{Y^{(1)}} - P_5^{Y^{(1)}}) \right)} \qquad j = 2,3,4 \quad (3.38)$$

According to Figure 3.1, $p^{(Y^{(2)}/(Y^{(1)}_{(2,1)}/Y^{(2)}_1))}_{(2,j)}$ is being calculated in this step by applying the same procedures as in step 3.1. It represents the probability of $Y^{(2)}_{(2,2)}$ at point (2,2) given

$Y_{(2,1)}^{(1)}$ which is calculated given that $Y_1^{(2)}$ in step of boundary vertices (step 3 (a)). The conditional probability $p_{(2,1)}^{(Y^{(1)}/Y^{(2)})}$ is calculated in step 3 (a). Then $p_{(2,j)}^{(Y^{(2)},(Y_{(2,1)}^{(1)}/Y_1^{(2)}))}$ can be calculated and represents the conditional joint probability of both wind powers at points (2,1), (2,2) and (2,3) according to Figure 3.2 given the wind speed at wind farm 2. Finally, the joint probability of both wind powers can be calculated as follows:

$$p_{(2,j)}^{(Y^{(1)},Y_1^{(2)})} = p_{(2,j)}^{(Y^{(2)},(Y_{(2,1)}^{(1)}/Y_1^{(2)}))} \times (1 - P_1^{Y^{(2)}} - P_5^{Y^{(2)}}) \qquad j = 2,3,4 \tag{3.39}$$

At the end of step 4 (a), 3-points represent the joint interior probabilities and marginal output power for two wind farms are computed as stated in table 3.8.

Table 3.8: Interior joint probabilities and marginal output power for two wind farms at end of step 4 (a)

Joint Probabilities $P_{(2,j)}^{(Y^{(1)},Y^{(2)})}$	$P_{(2,2)}^{(Y^{(1)},Y^{(2)})}$	$P_{(2,3)}^{(Y^{(1)},Y^{(2)})}$	$P_{(2,4)}^{(Y^{(1)},Y^{(2)})}$
Output power of wind farm 1: $Y^{(1)}$ (MW)	$Y_{(2,1)}^{(1)}$	$Y_{(2,1)}^{(1)}$	$Y_{(2,1)}^{(1)}$
Output power of wind farm 2: $Y^{(2)}$ (MW)	$Y_{(2,2)}^{(2)}$	$Y_{(2,3)}^{(2)}$	$Y_{(2,4)}^{(2)}$

Step 4 (b) For $Y^{(1)} = Y_{(3,1)}^{(1)}$, determine $(Y_{(3,2)}^{(2)}, Y_{(3,3)}^{(2)}$ *and* $Y_{(3,4)}^{(2)})$

Apply same procedures as in step 3 (a), At the end of step 4 (b). we have the following:

Joint Probabilities for two independent wind farms can be computed as follows:

$$p_{(3,j)}^{(Y^{(1)},Y^{(2)})} = p_{(3,j)}^{(Y^{(2)}/Y^{(1)})} \times P_3^{Y^{(1)}} \times (1 - P_1^{Y^{(2)}} - P_5^{Y^{(2)}}) \qquad j = 2,3,4 \tag{3.40}$$

Conditional Joint Probabilities $p_{(3,j)}^{(Y^{(2)},(Y_{(3,1)}^{(1)}/Y_1^{(2)}))}$ for two correlated wind farms can be computed as follows:

$$p_{(3,j)}^{(Y^{(2)}/(Y_{(3,1)}^{(1)}/Y_1^{(2)}))} = \frac{p_{(3,j)}^{(Y^{(2)},(Y_{(3,1)}^{(1)}/Y_1^{(2)}))}}{\left(p_{(3,1)}^{(Y^{(1)}/Y^{(2)})} \times (1 - P_1^{Y^{(1)}} - P_5^{Y^{(1)}})\right)} \qquad j = 2,3,4 \tag{3.41}$$

Joint Probabilities $p_{(3,j)}^{(Y^{(1)},Y_1^{(2)})}$ for two correlated wind farms can be computed as follows:

$$p_{(3,j)}^{(Y^{(1)},Y_1^{(2)})} = p_{(3,j)}^{(Y^{(2)},(Y_{(3,1)}^{(1)}/Y_1^{(2)}))} \times (1 - P_1^{Y^{(2)}} - P_5^{Y^{(2)}}) \qquad j = 2,3,4 \tag{3.42}$$

At the end of step 4 (b), 3-points represent the joint interior probabilities and marginal output power for two wind farms are computed and stated in table 3.9.

Table 3.9: Interior joint probabilities and marginal output power for two wind farms at end of step 4 (b)

Joint Probabilities $P_{(3,j)}^{(Y^{(1)},Y^{(2)})}$	$P_{(3,2)}^{(Y^{(1)},Y^{(2)})}$	$P_{(3,3)}^{(Y^{(1)},Y^{(2)})}$	$P_{(3,4)}^{(Y^{(1)},Y^{(2)})}$
Output power of wind farm 1: $Y^{(1)}$ (MW)	$Y_{(3,1)}^{(1)}$	$Y_{(3,1)}^{(1)}$	$Y_{(3,1)}^{(1)}$
Output power of wind farm 2: $Y^{(2)}$ (MW)	$Y_{(3,2)}^{(2)}$	$Y_{(3,3)}^{(2)}$	$Y_{(3,4)}^{(2)}$

<u>Step 4 (c)</u> For $Y^{(1)} = Y_{(4,1)}^{(1)}$, determine $(Y_{(4,2)}^{(2)}, Y_{(4,3)}^{(2)}$ *and* $Y_{(4,4)}^{(2)})$

Apply same procedures as in step 3 (a), At the end of step 4 (c). we have the following:

Joint Probabilities for two independent wind farms can be computed as follows

$$p_{(4,j)}^{(Y^{(1)},Y^{(2)})} = p_{(4,j)}^{(Y^{(2)}/Y^{(1)})} \times P_4^{Y^{(1)}} \times (1 - P_1^{Y^{(2)}} - P_5^{Y^{(2)}}) \qquad j = 2,3,4 \tag{3.43}$$

Conditional Joint Probabilities $p_{(4,j)}^{(Y^{(2)},(Y_{(4,1)}^{(1)}/Y_1^{(2)}))}$ for two correlated wind farms can be computed as follows:

$$p_{(4,j)}^{(Y^{(2)}/(Y_{(4,1)}^{(1)}/Y_1^{(2)}))} = \frac{p_{(4,j)}^{(Y^{(2)},(Y_{(4,1)}^{(1)}/Y_1^{(2)}))}}{\left(p_{(4,1)}^{(Y^{(1)}/Y^{(2)})} \times (1 - P_1^{Y^{(1)}} - P_5^{Y^{(1)}})\right)} \qquad j = 2,3,4 \tag{3.44}$$

Joint Probabilities $p_{(4,j)}^{(Y^{(1)},Y_1^{(2)})}$ for two correlated wind farms can be computed as follows

$$p_{(4,j)}^{(Y^{(1)},Y_1^{(2)})} = p_{(4,j)}^{(Y^{(2)},(Y_{(4,1)}^{(1)}/Y_1^{(2)}))} \times (1 - P_1^{Y^{(2)}} - P_5^{Y^{(2)}}) \qquad j = 2,3,4 \tag{3.45}$$

At the end of step 4 (c), 3-points represent the joint interior probabilities and marginal output power for two wind farms are computed and stated in table 3.10.

Table 3.10: Interior joint probabilities and marginal output power for two wind farms at end of step 4 (c)

Joint Probabilities $P_{(4,j)}^{(Y^{(1)},Y^{(2)})}$	$P_{(4,2)}^{(Y^{(1)},Y^{(2)})}$	$P_{(4,3)}^{(Y^{(1)},Y^{(2)})}$	$P_{(4,4)}^{(Y^{(1)},Y^{(2)})}$
Output power of wind farm 1: $Y^{(1)}$ (MW)	$Y_{(4,1)}^{(1)}$	$Y_{(4,1)}^{(1)}$	$Y_{(4,1)}^{(1)}$
Output power of wind farm 2: $Y^{(2)}$ (MW)	$Y_{(4,2)}^{(2)}$	$Y_{(4,3)}^{(2)}$	$Y_{(4,4)}^{(2)}$

3.4 Conclusion

A probabilistic method based 5-PEM is proposed to replace the power distribution of each wind farm with 5^{nw} discrete points associated with their 5^{nw} joint probabilities. The purpose of this method is to consider the uncertainties of wind power distribution and the correlation among them in the optimal allocation problem of energy storage system.

Chapter 4

OPTIMAL ALLOCATION OF ENERGY STORAGE SYSTEM CONSIDERING WIND FARMS

4.1 Problem formulation

The optimal location and sizing problem of ESS is formulated as a constrained mixed integer non-linear optimization problem. Three objective functions are including minimization of the system's total expected cost keeping the total cost of the optimal sizes of ESSs within constraints of the proposed budget on the total investment cost of ESSs, voltage profile improvement, and carbon emission reduction. The objective function is subjected to some technical and economic equality and inequality constraints. The three objective functions are incompatible, nonlinear and non-convex functions to be minimized simultaneously without converting them into single weighted objective function. Minimization of multiple objective functions simultaneously rather than minimizing them as single weighted objective function would result in better values and avoiding the required algorithms for determining the weights or relative importance of each objective function. The steps for minimizing multiple objective functions without using single weighted objective function is stated in section 4.2.4.

4.1.1 Objective function

The aim of this thesis in the first section is to determine the optimal location of ESSs, optimal generator's output power and optimal values of voltages at each bus to minimise the system's total expected cost, considering an economic constraint on the

obtained total investment cost of ESSs, and the total emissions of generating units considering the uncertainties of wind power generation and correlation among them.

The economic factor is very important during any optimal planning problem in power system. So, minimizing the total expected cost should be considered as one of the objective functions refers to acquiring the best performance for the system with minimum cost. On the other hand, due to the global climate change associated with serious environmental pollution problems and global warming, decreasing the amount of carbon emission is very important from environmental point of view and considered to be the second objective function in this thesis. The voltage at some buses will experience some fluctuations due to the intermittent nature of wind power. Although reactive power compensators like SVC, TCSC and other FACTs devices can be utilized for improving the voltage profile for the given power network, many research works in the liteature proves the ability of ESS in maintaining the voltage at each bus within constraints with minimum deviation. So the third objective function is to improve voltage profile by minimising voltage deviation at each bus. The multi-objective functions are as followings:

$$\begin{cases} \min f_1 = \sum_{i=1}^{Nscen} prob_i.\mathrm{Cos}t_i = \sum_{i=1}^{Nscen} prob_i.\left(\begin{array}{l} \sum_{j=1}^{NG} C_i\left(P_{i,G_j}\right) + \sum_{j=1}^{Nw}\left(C_{i,w_j}\right) + \\ \sum_{j=1}^{NESS}\left(C_{i,ESS_j}\right) \end{array} \right) \times t = \\ \quad = \sum_{i=1}^{Nscen} prob_i.\left(\begin{array}{l} \sum_{j=1}^{NG}\left(c_j + b_j.P_{i,G_j} + a_j.P_{i,G_j}{}^2\right) + \sum_{j=1}^{Nw}\left(C^{opw,i}.P_{i,w_j}\right) + \\ \sum_{j=1}^{NESS}\left(C^{ops,i}.P_{i,ESS_j}\right) \end{array} \right) \times t \\ \min f_2 = \sum_{i=1}^{Nscen} prob_i.\left(\sum_{k=1}^{nb}\left(\frac{v_{k,i} - v_{k,i}^{spec}}{\Delta v_{k,i}^{\max}} \right)^2 \right) \\ \min f_3 = \sum_{i=1}^{Nscen} prob_i.Emission_i = \sum_{i=1}^{Nscen} prob_i.\sum_{j=1}^{NG} 10^{-2}\left(\gamma_j + \phi_j.P_{i,G_j} + \theta_j.P_{i,G_j}{}^2\right) \times t \end{cases} \quad (4.1)$$

Where $prob_i$ is the probability of operation cost at the i^{th} scenario which is the joint probability of multiple wind farms; nb is the total number of buses; $v_{k,i}$ is the voltage at bus k in scenario i; $v_{k,i}^{spec}$ is the specified voltage in scenario i which is assumed to be 1pu; N_{scen} is the total number of scenarios which is the summation of boundary (vertices and edges) and interior joint probability points which is equal to 25 scenarios for two wind farms; $\Delta v_{k,i}^{\max}$ is the maximum of voltage deviation in scenario i which is equal to 0.12pu; Cost_i is the total operation cost at the i scenario ($/h); NG is the number of generators; $Emission_i$ is the total emission (kg/h) at the scenario i; $C_i\left(P_{i,G_j}\right)$ is the fuel cost of generator j in scenario i ($/h); C_{i,w_j} is the cost of wind power generator in scenario i ($/h); C_{i,ESS_j} is the cost of ESS in scenario i ($/h); $C^{opw,i}$ is the operation cost of wind power generator including (maintenance and operation cost) which is 30 ($/MWh) according to [80] and [81]; $C^{ops,i}$ is the operation cost of energy storage system in scenario i which is considered to be 35 ($/MWh) [82]; a_j ($/MW^2h), b_j ($/MWh) and c_j ($/h) are the fuel cost coefficients of generator j; γ_j (kg/h), ϕ_j (kg/MWh) and θ_j (kg/MW^{2}h) are the carbon emission coefficients of generator j; N_w is the number of wind farms; $NESS$ is the total number of energy storage systems; P_{i,G_j} is the power of generator j in scenario i; P_{i,w_j} is the power of wind farm j in scenario i; P_{i,ESS_j} is the power rating of the ESS j in scenario i; t_i is the duration time which is assumed to be equal to one hour in this case (peak-load condition).

4.1.2 Problem Constraints

The objective function is subjected to some equality and inequality constraints:

1. *Equality Constraints:* These constrainst are related to power balance and power

flow as stated in the below equations.

1.1. Power balance constraint: The total generated power by the power plants should equal to the summation of total load demand and total transmission line losses.

$$\sum_{j=1}^{NG}\left(P_{i,G_j}\right)+\sum_{j=1}^{Nw}\left(P_{i,w_j}\right)+\sum_{j=1}^{NESS}\left(P_{i,ESS_j}\right)-\sum_{j=1}^{nb}P_{d\,j}-\sum_{j=1}^{NTL}P_{Loss_j}=0 \tag{4.2}$$

Where $P_{d\,j}$ is the load demand at bus j; P_{Loss_j} is the power loss in transmission line j; N_{TL} is the total number of transmission lines in the studied bus system.

1.2. Power flow equations: they are applied using the Newton-Raphson method.

$$\left.\begin{aligned} P_m - V_m\sum_{n=1}^{nb}V_n\left(G_{mn}\cos\delta_{mn}+B_{mn}\sin\delta_{mn}\right)=0 \\ Q_m - V_m\sum_{n=1}^{nb}V_n\left(G_{mn}\sin\delta_{mn}-B_{mn}\cos\delta_{mn}\right)=0 \end{aligned}\right\} \tag{4.3}$$

P_m and Q_m are the injected active and reactive power at bus m ; V_m is the voltage at bus m; G_{mn} and B_{mn} are the conductance and susceptance between buses m and n. δ_{mn} is the phase difference between voltages in buses m and n.

2. *Inequality Constraints:* These constrainst are related to bus voltages, generation active and reactive power, and ESS power rating

2.1. Voltage constaint: The voltage at each bus should remains within its upper and lower boundaries which they are mainly considered between 0.96pu and 1.05pu.

$$V_i^{\min}\le V_i\le V_i^{\max}\qquad i=1,...,nb \tag{4.4}$$

2.2. Power plants generation capacity constraint: The active and reactive power generation for each generator should remains within its upper and lower boundaries.

$$\begin{cases} P_{g,i}^{\min}\le P_{g,i}\le P_{g,i}^{\max} & i=1,...,NG \\ Q_{g,i}^{\min}\le Q_{g,i}\le Q_{g,i}^{\max} & i=1,...,NG \end{cases} \tag{4.5}$$

2.3. Storage power rating: The ESS output power should not exceed the maximum power rating

$$0 \le P_{ESS,i} \le P_{ESS,i}^{\max} \qquad i = 1, ..., NESS \tag{4.6}$$

2.4. Storage total investment cost: The total investment cost IC for ESSs should not exceed its proposed budget PB. The investment cost for each ESS $C_{ESS_j}^{INS}$ is 125000$/MW [9] and [25].

$$IC = \sum_{j=1}^{NESS} \left(C_{ESS_j}^{INS} \times P_{ESS_j} \right) \le PB \tag{4.7}$$

4.2 Proposed hybrid probabilistic optimisation method

4.2.1 TOPSIS method

It is difficult to determine the optimal solution from a set of non-dominated solutions represeneted by pareto front. Technique for Order Preference by Similarity to Ideal Solution (TOPSIS) [83] is used in this work due to its simple procedures for determining the best solution from as set of solutions. The steps of TOPSIS method are detailed as follows.

Step 1: The decision matrix D in (4.8) represents the non-dominated solutions in the archive of size n of the hybrid algorithm and it is updated before the end of each iteration. Each non-dominated solution has three objective values or so called criterions according to (4.1).

$$D = \begin{bmatrix} x_{11} & x_{12} & x_{13} \\ x_{21} & x_{22} & x_{23} \\ \vdots & \vdots & \vdots \\ x_{n1} & x_{n2} & x_{n3} \end{bmatrix} \tag{4.8}$$

Where n is the number of non-dominated solutions in the archive, x_{n1} is the first objective function value for the n[th] non-dominated solution, x_{n2} is the second objective function value for the n[th] non-dominated solution and x_{n3} is the third objective function value for the n[th] non-dominated solution.

Step 2: Normalize the decision matrix by transforming it into a non-dimensional attribute matrix as follows:

$$v_{ij} = \frac{x_{ij}}{\sqrt{\sum_{i=1}^{n} x_{ij}^{2}}} \qquad j = 1,2,3 \tag{4.9}$$

Where x_{ij} is the j[th] objective function value for the i[th] non-dominated solution and v_{ij} is the normalized j[th] objective function value for the i[th] non-dominated solution.

Step 3: Assign a set of weight vector W (equal weight coefficients are assigned in this work according to [83] and [84]) expressed as the relative importance for each objective function value (criterion).

$$\begin{cases} W = [w_1 \;\; w_2 \;\; w_3]^T \\ \sum_{i=1}^{i=3} w_i = 1 \end{cases} \tag{4.10}$$

Step 4: Determine the weighted normalized decision matrix by multiplying the decision matrix with the weight vector.

Step 5: Determine the positive ideal v_j^+ and negative ideal solution v_j^- based on the weighted normalized decision matrix as follows:

$$\begin{cases} v_j^+ = \max(v_{ij} \mid j \in J^+) \,\&\, \min(v_{ij} \mid j \in J^-) \mid i = 1,2,3...,n \\ v_j^- = \min(v_{ij} \mid j \in J^+) \,\&\, \max(v_{ij} \mid j \in J^-) \mid i = 1,2,3...,n \end{cases} \tag{4.11}$$

Where

$J^+ = \{ j = 1, 2, ..., n \}$ associated with the objective function having a positive impact and $J^- = \{ j = 1, 2, ..., n \}$ associated with the objective function having a negative impact.

Step 6: Determine the Euclidean distance S_i^+ between each solution v_i and positive ideal v_j^+ and the Euclidean distance S_i^- between each solution v_i and negative ideal v_j^- solution as follows

$$\begin{cases} S_i^+ = \sqrt{\sum_{j=1}^{3} \left(v_{ij} - v_j^+ \right)^2} & i = 1, 2, 3, ..., n \\ S_i^- = \sqrt{\sum_{j=1}^{3} \left(v_{ij} - v_j^- \right)^2} & i = 1, 2, 3, ..., n \end{cases} \tag{4.12}$$

Where n is the number of non-dominated solutions.

Step 7: Determine the relative closeness $C_i^+ [0,1]$ in descending order for each solution v_i and the ideal solutions as in (4.13). The best solution among the non-dominated solutions in the archive is the one has greatest C_i^+.

$$C_i^+ = \frac{S_i^-}{S_i^+ + S_i^-} \tag{4.13}$$

4.2.2 Non-dominated sorting genetic algorithm (NSGAII)

The three special characteristics of this algorithm include fast non-dominated sorting approach, fast crowded distance estimation procedure and simple crowded comparison operator [85]. The crowded-comparison operator guides the selection process of the algorithm toward a uniformly spread-out Pareto optimal front (better

diversity). On the other hand, Eltisim can preserves the good solutions [86]. NSGAII algorithm is described in details.

Combining the population P of size N and the population Q of same size N, a new population M of size 2N would be generated. The members of the new population M are then sorted based on the nondomination [87, 88] Each member of the new population is assigned with a front number where F_1 is the set contains the best solutions and F_2 is the next best set and so on until reaching the last Front F_L. Then, N best solutions are selected starting from F_1 untill front F_i to renew the population of size N for the next iteration. If the combined size of F_1, F_2 and F_i is less than N, then some members of F_{i+1} should be selected using crowed- comparsion operator to ensure the new population P of size N. Then new population Q (offsprings) is generated by applying genetic operators (crossover and mutation) on the memebers of population P.

4.2.3 Particle swarm optimization algorithm (PSO)

PSO is a meta-heuristic optimization technique developed by Eberhart and Kennedy in 1995. The main idea of this algorithm is generating randomly a population called swarm consists of N particles mimic the social behavior of flock birds [89]. The algorithm updates continoulsy the position and velocity of each particle until finding the best position according to (4.14).

$$\begin{cases} v_i^{t+1} = wv_i^t + c_1 r_1 \left(pbest_i^t - x_i^t \right) + c_2 r_2 \left(gbest^t - x_i^t \right) \\ x_i^{t+1} = x_i^t + v_i^{t+1} \end{cases} \tag{4.14}$$

Where x is the particle position; v is the particle velocity; t is the current iteration number; w is the inertia weight; c_1 and c_2 are the acceleration constants; r_1 and r_2 are two random numbers in the range of [0,1]; *pbest* is the best position of particle i acquired based on its own experience; *gbest* is the best particle of position i based on

overall swarm's experience. The function of w is to control the previous history of particle velocity and hence to control the balance between the local and global exploration abilities [90]. *w* is often decreasing linearly from maximum $w_{\max}$ value to minimum $w_{\min}$ according to the following equation

$$w^{it} = w_{\max} - \frac{w_{\max} - w_{\min}}{it_{\max}}.it \tag{4.15}$$

Where it is the current iteration and $it_{\max}$ is the maximum iteration number. In addition to w, time variant acceleration coefficients are introduced in [91] in order to make better compromise between exploration and exploitation of the search space. Higher values of c_1 ensure the exploration while higher values of c_2 ensure the exploitation. Both time variant acceleration coefficients are decreasing linearly with the iteration as described in (4.16). The best particle with the best fitness value is the position has the minimum cost, emission, and voltage deviation

$$\begin{cases} c_{1,t} = c_{1,i} + \left(c_{1,f} - c_{1,i}\right) \times \dfrac{it}{it_{\max}} \\ c_{2,t} = c_{2,i} + \left(c_{2,f} - c_{2,i}\right) \times \dfrac{it}{it_{\max}} \end{cases} \tag{4.16}$$

Where $c_{1,i}$ is the initial value of the acceleration constant c_1, $c_{1,f}$ is the final value of the acceleration constant c_1, $c_{2,i}$ is the initial value of the acceleration constant c_2, $c_{2,f}$ is the final value of the acceleration constant c_2

4.2.4 Hybrid probabilistic optimization algorithm (PLF-NSGAII-MOPSO)

The proposed solution method is a hybrid algorithm obtained by combining multi-objective NSGAII-MOPSO algorithm and new proposed probabilistic load flow PLF (probabilistic discretising method 5^{Nw} and Newton Raphson power flow) for determining the best location and power rating of ESSs.

The advantages of PSO algorithm inlcude simple implementation, robustness and short computational time. However, PSO can converge prematurely and be trapped into a local minimum especially with complex problems [89]. To overcome such drawback, incorporating the advantages of NSGAII (better diversity of solutions using crowed-comparison operator, the ability to save the good solutions once they have been found using elitism) within PSO can improve the performance of this hybrid algorithm (NSGAII-PSO) due to widely diversification of the search space. The flowchart in Figure 4.1 describes the required steps for a full operation of the hybrid algorithm (PLF-NSGAII-MOPSO) and they are stated as follows:

Start: Initialize NSGAII and MOPSO parameters as follows: The primary population size and maximum number of iterations are selected to be 100; $w_{\max}$, $w_{\min}$, $c_{1,i}$, $c_{1,f}$, $c_{2,i}$ and $c_{2,f}$ are selected to be equal to 0.7, 0.4, 2.5, 0.5, 0.5 and 2.5 for MOPSO, crossover and mutation probabilities are selected to be equal to 0.75 and 0.2 for NSGAII. Also initialize the personnel best, global best and best solution.

Step 1: the hybrid algorithm initializes randomly a main initial population within constraints and it is divided into sub-populations according to the representation in (4.17). It is clear the decision variables consist of voltage of all buses, thermal generators output power, location and size of ESSs on all buses except generator buses.

$$\begin{cases} pop_1 = [V_1, ..., V_{nb}] \\ pop_2 = [Pg_1, ..., Pg_{NG}] \\ pop_3 = [Loc_1, ..., Loc_{nb-nPV}] \\ pop_4 = [Size_1, ..., Size_{nb-nPV}] \\ pop = [pop_1, pop_2, pop_3, pop_4] \end{cases} \tag{4.17}$$

Step 2: In Figure 4.1, the uncertainty method (blue colored) represents the new probabilistic discretising method responsible for generating 25 scenarios for the two correlated wind farm's output power.

Step 3: The three expected objective functions (fitness values) are evaluated through the newly proposed PLF (probabilistic discretising method and Newton Raphson power flow) represented by BLOCK 1 in Figure 4.1. The calculated total investment cost related to the sizes of ESSs should not exceed the proposed budget according to (4.7). Until this step, the three expected objective values are evaluated for every candidate solution (called chromosome or particle) in the generated population.

Step 4: Start the main iteration of the proposed hybrid method and initialize the personnel best directly after the beginning of each new iteration.

Step 5: Start the operation of NSGAII algorithm as decribed in section 4.1 and represented by a dashed rectangular shape titled NSGAII in Figure 4.1. By the end of this step, a new population of size N with new three expected objective values for each candidate solution and new archive contains all non-dominated candidate solutions are generated.

Step 6: Select the leader (global best) randomly from the new archive and move the particles of the new population within constraints using (4.14). Apply BLOCK 1 on the newly generated population to determine the three expected objective values and the investment cost for each particle. After that, update the current archive by adding the non- dominated solutions in the new population to the current archive and delete

all the dominated solutions in the current archive. Figure 4.1 representes MOPSO by a dashed red colored rectangle.

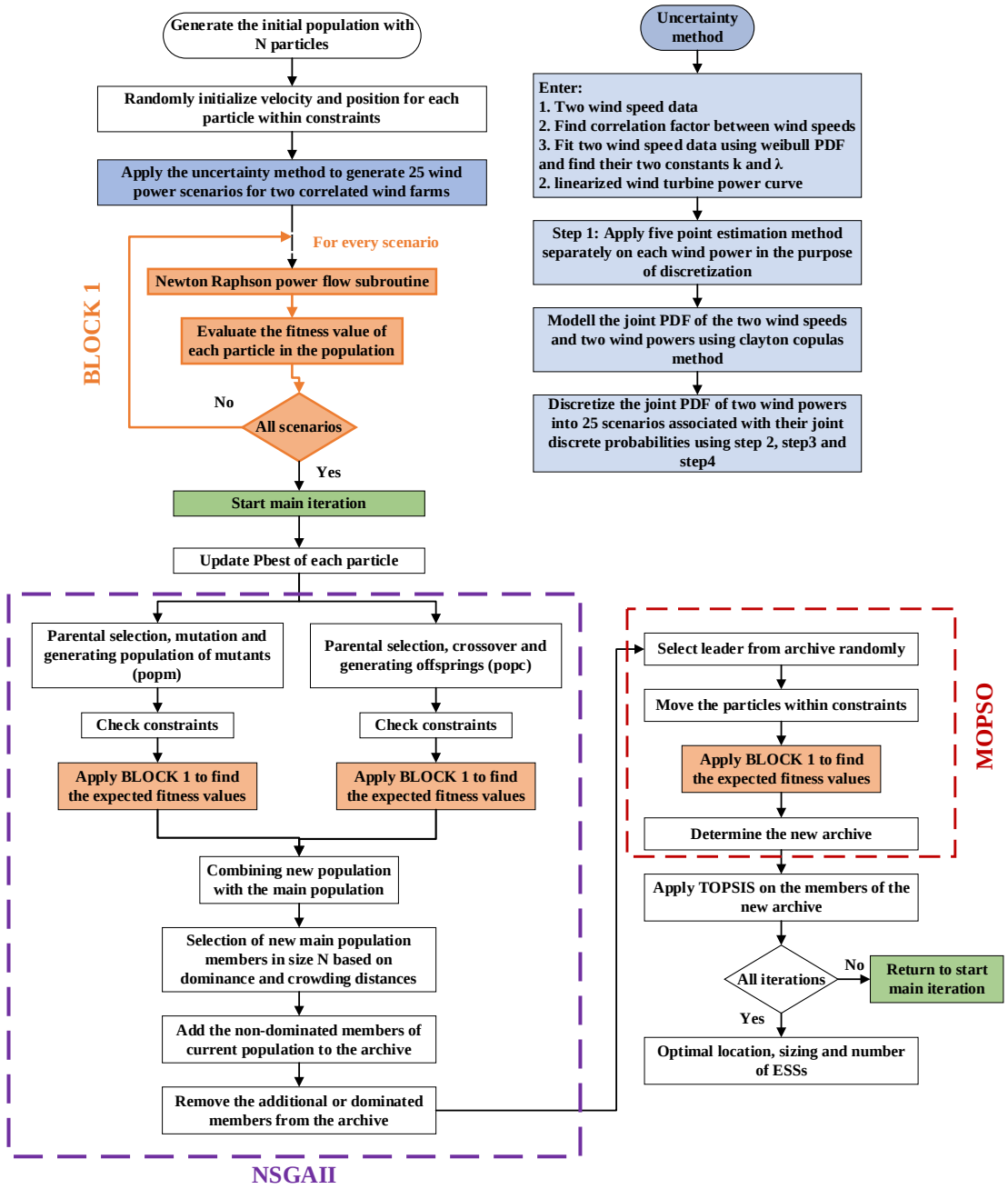

Figure 4.1: The proposed flowchart using hybrid algorithm of PLF-NSGAII MOPSO

Step 7: Before the end of each iteration, apply TOPSIS method as described in section 4.3 on the last updated archive to select only one solution (best solution) from a set of non-dominated solutions.

Step 8: If all the iterations are performed, then the optimal solution represents the optimal location and sizing of ESS is obtained.Otherwise, returns to step 4.

End: After performing all the iterations,the selected solution from TOPSIS method before the end of each iteration has three objective values where every objective function value can be plotted as a function of number of iterations.

4.3 Conclusion

Mixed integer non-linear programming constrained MINLP optimization problem is formulated to determine the optimal locations and sizes of ESSs. Three objective functions are including minimization of the system's total expected cost keeping the total cost of the optimal sizes of ESSs within constraints of the proposed budget on the total investment cost of ESSs, voltage profile improvement, and carbon emission reduction. The objective function is subjected to some technical and economic equality and inequality constraints. Hybrid NSGAII-MOPSO algorithm is proposed and combined with decision making technique ''TOPSIS'' to solve the MINLP optimisation problem to find the best locations and power ratings of ESSs.

Chapter 5

OPTIMAL PLANNING AND OPERATION OF ENERGY STORAGE SYSTEMS

5.1 Wind power distribution discretization

The bi-variate wind power distribution will be discretized into 25 points. Each point corresponds to a scenario composed of two wind power values (two wind farms) associated with its probability. The previous chapters of this thesis derived and detailed all the required steps for discretizing the joint PDF of wind power into 25 scenarios for the case of independent and correlated wind farms. The discretized points are available in table 5.1 for both cases of independent and correlated wind farms. The scenarios related to independent case are the same but the scenarios related to correlated case are different because a new correlation factor $a = 0.84$ in this work is calculated based on statistical wind speed data for Madison and Milwaukee cities in USA [92].

5.2 Energy storage system modelling

Time shift of electric energy from renewable sources is one of the main applications of ESS. Compressed air energy storage (CAES) and pumped hydroelectric storage (PHES) have large sizes and an economic characteristic that render them to be the best solutions in storing the excess energy from wind farms and the other generating units at a certain period and discharge the stored energy whenever required. However, PHS requires a special geographical position for installation purposes which renders CAES

as a viable technology in this work. According to [93], USA natural geographical locations are suitable for CAES installation.

Table 5.1: Table Parameters of wind farms distribution

Wind Power uncertainties								
Number of scenarios	Joint Probabilities		Wind Power (MW)					
			Independent wind farms			Correlated wind farms		
	Independent	Correlated	PW1	PW2	penetration level (%)	PW1	PW2	penetration level (%)
1	0.004	0.029	0.000	0.000	0.000	0.000	0.000	0.000
2	0.016	0.002	0.000	330.000	26.383	0.000	330.000	26.383
3	0.007	0.001	45.000	0.000	3.598	45.000	0.000	3.598
4	0.028	0.045	45.000	330.000	29.981	45.000	330.000	29.981
5	0.012	0.012	5.790	0.000	0.463	3.451	0.000	0.276
6	0.023	0.024	22.234	0.000	1.778	19.211	0.000	1.536
7	0.011	0.011	39.085	0.000	3.125	35.453	0.000	2.834
8	0.012	0.013	0.000	46.566	3.723	0.000	31.170	2.492
9	0.013	0.022	0.000	173.964	13.908	0.000	175.270	14.013
10	0.024	0.014	0.000	293.177	23.439	0.000	262.725	21.005
11	0.022	0.065	45.000	46.566	7.321	45.000	102.898	11.824
12	0.023	0.021	45.000	173.964	17.506	45.000	153.005	15.830
13	0.043	0.001	45.000	293.177	27.037	45.000	307.485	28.181
14	0.047	0.040	5.790	330.000	26.846	7.446	330.000	26.978
15	0.046	0.051	22.234	330.000	28.161	26.007	330.000	28.462
16	0.093	0.093	39.085	330.000	29.508	40.491	330.000	29.620
17	0.036	0.039	5.790	46.566	4.186	3.451	32.105	2.843
18	0.038	0.065	5.790	173.964	14.371	3.451	177.178	14.441
19	0.071	0.039	5.790	293.177	23.902	3.451	263.729	21.361
20	0.071	0.075	22.234	46.566	5.501	19.211	39.771	4.716
21	0.076	0.133	22.234	173.964	15.686	19.211	189.896	16.718
22	0.141	0.086	22.234	293.177	25.217	19.211	274.541	23.485
23	0.035	0.033	39.085	46.566	6.848	35.453	61.533	7.754
24	0.038	0.034	39.085	173.964	17.033	35.453	186.133	17.716
25	0.070	0.073	39.085	293.177	26.564	35.453	306.542	27.342

5.2.1 Two stage model description

To ensure the maximum benefits from utilizing CAES, the configuration (location, capacity, power ratings, hourly charging/discharging schedule and hourly generating units schedule in every scenario) should be determined optimally. In this case, an optimization model should be formulated with an objective function (single or multiple) to be minimized or maximized subjected to some technical and economic constraints. The formulated model can be single stage or multiple stages. In the second

section of this thesis, two stage optimization model is proposed and formulated as an upper and lower optimization problem. The decision variables of the upper layer include the locations and capacities of ESSs. However, the decision variables in the inner layer consists of active power of thermal generators and the active power of the allocated storage devices (CAESs). The upper layer minimizes three objective functions simultaneously including the total daily expected planning and operation cost, total daily expected emission and the maximum expected voltage deviation. However, the inner optimization layer minimizes the difference between the total daily expected operational cost of conventional units and the arbitrage benefits of ESSs. Hybrid NSGAII-MOPSO is adopted to solve the outer problem and tabu search algorithm (TS) is adopted to solve the inner optimization problem considering peak shaving operational strategy of ESSs and PLF algorithm for independent and correlated wind farms. The two main stages are briefly presented in Figure 5.1. From the economic point of view, the operation strategy composed of three states for the allocated ESSs including the charging, discharging and floating modes. CAESs will charge (stores the energy) during valley and low demand or low energy price, discharge during the high and peak demand (dispatch the stored energy) or high energy price and float during the moderate demand. This strategy can support some benefits like peak shaving, valley filling, arbitrage benefits, active power loss mitigation, reduction of overall energy purchase from the thermal generating units and emission reduction.

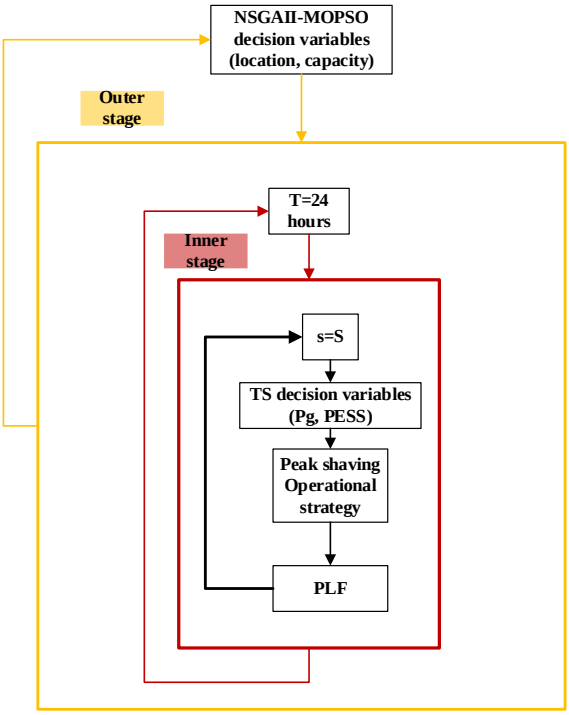

Figure 5.1: Two main stages for the optimal planning and operation of CAES

5.2.2 Inner stage

The inner layer (lower level) is responsible for the optimal operation of the allocated CAESs from the outer layer (upper level). The objective function to be minimized in (5.1) include the difference between the total daily expected operation cost of thermal generating units (5.2) and total daily expected arbitrage benefits of ESSs (5.3).

$$\min F_{inner} = TEOCG(P^{Gens}) - TEArb(P^{ESSs}) \tag{5.1}$$

$$TEOCG(P^{Gen}) = \sum_{t=1}^{T}\sum_{s=1}^{S}\left(prob_s \times \left(\sum_{g=1}^{G} a_g \left(P_{(g,s,t)}^{Gen}\right)^2 + b_g P_{(g,s,t)}^{Gen} + c_g \right)\right) \tag{5.2}$$

$$\forall t \in \psi_T,\ s \in \psi_S,\ g \in \psi_G$$

$$TEArb = \sum_{t=1}^{T} C_e \times \left(\sum_{s=1}^{S}\sum_{n=1}^{N} prob_s \times PESS_{(n,s,t)}^{ESS} \right) \quad \forall t \in \psi_T,\ s \in \psi_S,\ n \in \psi_N \tag{5.3}$$

Where TEOCG is the total daily expected operation cost of thermal generating units due to its active power generation, TEArb is the total daily expected arbitrage benefits of CAESs due to the process of buying (charging) and selling (discharging) the

electrical energy, $prob_s$ is the associated probability for each wind power scenario in the case of independent or correlated wind farms, $P_{(g,s,t)}^{Gen}$ is the active power of gth thermal generating unit in sth scenario in each hour t, a_g , b_g and c_g are the cost coefficients of gth thermal unit, $PESS_{(n,s,t)}^{ESS}$ is the active power of the nth CAES in the sth scenario in each hour t, *Ce* is the active power price ($/MWh) and F_{inner} is the objective function of the inner optimization layer. The inner optimization problem is subjected to some network technical constraints as follows:

1. Bus voltage

$$V_{i,\min} \le V_{i,s,t} \le V_{i,\max} \quad \forall t \in \psi_T,\ s \in \psi_S,\ i \in \psi_I \tag{5.4}$$

2. Thermal generator active and reactive power

$$P_{g,\min}^{Gen} \le P_{g,s,t}^{Gen} \le P_{g,\max}^{Gen} \quad \forall t \in \psi_T,\ s \in \psi_S,\ g \in \psi_G \tag{5.5}$$

$$Q_{g,\min}^{Gen} \le Q_{g,s,t}^{Gen} \le Q_{g,\max}^{Gen} \quad \forall t \in \psi_T,\ s \in \psi_S,\ g \in \psi_G \tag{5.6}$$

3. Transmission line capacity limits

$$S_{tl,\min}^{TL} \le S_{tl,s,t}^{TL} \le S_{tl,\max}^{TL} \quad \forall t \in \psi_T,\ s \in \psi_S,\ tl \in \psi_{TL} \tag{5.7}$$

4. Active power injection balance at every bus

$$PESS_{(i,t,s)}^{char} + P_{(i,t)}^{load} + P_{(i,t,s)}^{injec} = P_{(i,t,s)}^{Gens} + P_{(i,t,s)}^{WF} + PESS_{(i,t,s)}^{dischar}$$
$$\forall t \in \psi_T,\ s \in \psi_S,\ i \in \psi_I \tag{5.8}$$

5. Reactive power injection balance at every bus

$$Q_{(i,t)}^{load} + Q_{(i,t,s)}^{injec} = Q_{(i,t,s)}^{Gens} + Q_{(i,t,s)}^{WF} \qquad \forall t \in \psi_T,\ s \in \psi_S,\ i \in \psi_I \tag{5.9}$$

6. State of charge for the allocated ESSs

$$SOC_{(n,s,t+1)}^{ESS} = \begin{Bmatrix} (1-d_n^{ESS}) \times SOC_{(n,s,t)}^{ESS} - \eta_{ch} \times \Delta t \times PESS_{n,s,t} & if\ PESS_{n,s,t} \le 0 \\ (1-d_n^{ESS}) \times SOC_{(n,s,t)}^{ESS} - \dfrac{\Delta t \times PESS_{n,s,t}}{\eta_{disch}} & if\ PESS_{n,s,t} > 0 \end{Bmatrix} \tag{5.10}$$
$$\forall t \in \psi_T,\ s \in \psi_S,\ n \in \psi_N$$

7. State of charge limits for the allocated ESSs

$$SOC_{n,\min}^{ESS} \le SOC_{n,s,t}^{ESS} \le SOC_{n,\max}^{ESS} \quad \forall t \in \psi_T,\ s \in \psi_S,\ n \in \psi_N \tag{5.11}$$

Where $V_{i,s,t}$ is the voltage of ith bus in sth scenario in each hour t, $V_{i,\min}$ and $V_{i,\max}$ are the minimum and maximum voltages of ith bus, $P_{g,\min}^{Gen}$, $P_{g,\max}^{Gen}$, $Q_{g,\min}^{Gen}$ and $Q_{g,\max}^{Gen}$ are the limits of active and reactive power of gth unit, $S_{tl,s,t}^{TL}$ is the capacity of each transmission line tl in sth scenario in every hour t, $S_{tl,\min}^{TL}$ and $S_{tl,\max}^{TL}$ are the limits of every transmission line capacity, $P_{tl,s,t}^{Loss}$ is the power loss in each transmission line in the sth scenario in each hour t, ψ_T is the set of time interval, ψ_S is the set of wind power scenarios, ψ_G is the set of thermal generating units, ψ_W is the set of wind farms, ψ_N is the set of allocated CAESs, $SOC_{(n,s,t)}^{ESS}$ and $SOC_{(n,s,t+1)}^{ESS}$ are the old and new state of charge of nth CAES in the sth scenario in each time t, η_{ch} and η_{disch} are the overall efficiency of CAES, $PESS_{n,s,t}$ is the active power of nth CAES in the sth scenario in each hour t, d_n^{ESS} is the hourly self-discharge of nth CAES, $SOC_{n,\min}^{ESS}$ and $SOC_{n,\max}^{ESS}$ are the limits of state of charge of nth CAES, $PESS_{(i,t,s)}^{char}$ and $PESS_{(i,t,s)}^{dischar}$ are the negative (charging) and positive (discharging) active power of nth CAES in the sth scenario in each time t allocated at ith bus, $P_{(i,t)}^{load}$ and $Q_{(i,t)}^{load}$ are the active and reactive power of load at ith bus, $P_{(i,t,s)}^{injec}$ and $Q_{(i,t,s)}^{injec}$ are the injected active and reactive power at ith bus in the sth scenario in each hour t and $P_{(i,t,s)}^{WF}$ and $Q_{(i,t,s)}^{WF}$ are the active and reactive power of each wind farm at ith bus in the sth scenario in each hour t. The fuel cost, emission and other technical data related to the thermal generating units are shown in table 5.2 [21] and [31]. Note that the reactive power of the allocated CAES is not considered in this work.

Table 5.2: Fuel cost, emission and generator active power limits data

Gen	**Cost Coefficients**			**Emission Coefficients**			**Gen. limit**	
	a	*b*	*c*	θ	Φ	ɣ	P_{min}	P_{max}

	($/MW^{2}h)	($/MWh)	($/h)	(kg/MW^{2}h)	(kg/MWh)	(kg/h)	(MW)	(MW)
1	0.0775795	20	0	7.632	-5.876	3.965	0	575.88
3	0.25	20	0	5.638	-6.047	2.543	0	140
6	0.01	40	0	4.586	-5.094	4.258	0	100
9	0.01	40	0	4.586	-5.094	4.258	0	100
12	0.0323	20	0	5.449	-4.663	4.872	0	410

5.2.3 Outer stage/Upper layer

The outer stage optimization problem is responsible for sending the locations and capacities of multiple storage devices to the inner layer. The multi-objective function in (5.12) is to be minimized and composed of three objective functions. The first objective function (5.13) minimizes the total daily expected planning and operation cost including the summation of the total daily expected variable operation cost of thermal generating units (TEOCG), the total daily expected variable operational cost of storage devices (TEVOCS), the total daily fixed operation and maintenance cost of allocated storage devices (TFOMCS), total daily investment cost (IC) of all allocated ESSs and the negative value of the total daily expected arbitrage benefits from all allocated ESSs. The second objective function (5.14) minimizes the total daily expected carbon emission. The third objective function (5.15) minimize the maximum expected hourly voltage deviation.

$$\min F_{outer} = \min(F_1, F_2, F_3) \tag{5.12}$$

$$F_1 = \begin{pmatrix} TEOCG(P^{Gens}) + TEVOCS(S^{ESSs}) + TFOMCS(S^{ESS}) + \dfrac{\sigma \times IC^{total}}{365} \\ -TEArb(P^{ESSs}) \end{pmatrix} \tag{5.13}$$

$$F_2 = \sum_{t=1}^{T}\sum_{s=1}^{S}\left(prob_s \times \left(\sum_{g=1}^{G} \theta_g \left(P_{(g,s,t)}^{Gen}\right)^2 + \phi_g P_{(g,s,t)}^{Gen} + \gamma_g \right)\right) \tag{5.14}$$

$\forall t \in \psi_T,\ s \in \psi_S,\ g \in \psi_G$

$$F_3 = \max\left[\sum_{s=1}^{S} prob_s \times \left(\sum_{i=1}^{I}\left(\frac{v_{i,s,t} - v_i^{spec}}{\Delta v_i^{\max}}\right)^2\right)\right]_{t=1,\ldots T} \quad \forall t \in \psi_T,\ s \in \psi_S,\ i \in \psi_I \qquad (5.15)$$

Where γ_g (kg/h), ϕ_g (kg/MWh) and θ_g (kg/MW^2h) are the carbon emission coefficients of generator, $v_{i,s,t}$ is the per unit voltage at ith bus in the sth scenario at tth hour, v_i^{spec} is the specified per unit voltage at each ith bus equals to one, $\Delta v_i^{\max}$ is the maximum allowed voltage deviation in at each ith bus which is equal to 0.12pu, σ is a constant used to convert investment cost into daily cost.

The three objective functions (F_1, F_2 and F_3) in (5.13) - (5.15) depend on the expected values that can be determined in the inner layer. The total daily expected operational cost of the allocated CAESs is divided into two parts. The first part is the total daily expected variable operational cost (fuel cost) as in (5.16) and the second part is the total daily fixed operation and maintenance cost (5.17).

$$TEVOCS = \sum_{t=1}^{T}\sum_{s=1}^{S}\left(prob_s \times \left(\sum_{n=1}^{N} HR \times C_{n,s,t}^{ESS} \times C_{NG}\right)\right) \quad \forall t \in \psi_T,\ s \in \psi_S,\ n \in \psi_N \qquad (5.16)$$

$$TFOMCS = \frac{\sum_{n=1}^{N} C_n^{OM}\left(P_n^{ESS}\right)}{365} \quad \forall n \in \psi_N \qquad (5.17)$$

Where HR is the heat rate of turbine of CAES, $C_{n,s,t}^{ESS}$ is the capacity of nth CAES in the sth scenario at tth hour, C_{NG} is the natural gas cost for CAES, C_n^{OM} is the operation and maintenance cost of nth allocated CAES and P_n^{ESS} is the rated power of nth allocated CAES.

Since the fixed operational and maintenance cost of CAES TFOMCS depends on the rated power of each allocated CAES, power rating of every CAES should be

determined according to (5.18). This can limit power (charging or discharging) of CAES in every scenario in each hour within maximum apparent power rating. In this study, it is assumed that all CAESs are having reactive power controller and their reactive power is not considerable [49]. Note that QESS is not considered in this work which make P^{ESS} equals to S^{ESS}.

$$S_n^{ESS} = \arg\max_{\substack{s=1,\ldots,S \\ t=1,\ldots,T}} \left[\sqrt{\left(PESS_{(n,s,t)}^{ESS}\right)^2 + \left(QESS_{(n,s,t)}^{ESS}\right)^2} \right] \tag{5.18}$$

Moreover, the investment cost is included in the first objective function f_1 of the outer layer problem. It can be determined according to (5.19). The constant which is responsible for converting the investment cost into daily cost is defined in (5.20). The life time L_f of CAES is determined in this work according to the obtained number of cycles.

$$IC^{total} = \sum_{n=1}^{N} C_P \times S_n^{ESS} + C_C \times S_n^{ESS} + C_E \times C_n^{ESS} \tag{5.19}$$

$$\sigma = \frac{Intr\left(1+Intr\right)^{Lf}}{\left(1+Intr\right)^{Lf} - 1} \tag{5.20}$$

Where C_P is unit cost of power rating of CAES ($/MW) and C_C is the unit cost of the compressor power rating ($/MW) and C_E is the energy cost of CAES ($/MWh) and *Intr* is the interest rate. Table 5.3 summarizes all the economic and technical features of CAES [9] and [25].

Table 5.3: CAES characteristics

Features	Value	Unit
Heat rate of turbine (*HR*)	4300	Btu/kWh
Natural gas cost (C_{NG})	5	MBtu
Fixed O&M cost ($C^{OM)}$	2.5	$/kW-yr

Power rating cost (*CP*)	425	$/kW
Compressor power rating cost (*CP*)	425	$/kW
Capacity cost (*CE*)	3	$/kWh
Minimum depth of discharge (SOC_{min})	10	%
Maximum allowed state of charge (SOC_{max})	90	%
Initial stored energy	90	%
Overall efficiency (μ)	80	%
hourly self-discharge (*d*)	3/24	%
Interest rate (*Intr*)	10	%
Life time L_f	15000	cycles

5.3 Proposed model solving approach

5.3.1 Inner/outer decision variables

A nesting layers of non-linear mixed integer optimization problem is formulated to minimize the objective functions stated in (5.1) and (5.12) subjected to (5.4) - (5.11). In the inner stage, peak shaving operational strategy and PLF are to be implemented inside an optimization algorithm to minimize the objective function stated in (5.1) considering all constraints in (5.4) – (5.12). In this case, a fast-optimal power flow algorithm (OPF) is required. Tabu search algorithm (TS) is adopted to solve the inner optimization problem to determine the optimal scheduling of the thermal generating units and active power profiles (charging/discharging) of the allocated CAESs. On the other hand, hybrid NSGAII-MOPSO is utilized to solve the outer stage problem to

determine the optimal locations and capacities of storage devices by minimizing the multiple objective function F_{outer} stated in (5.12).

So, the decision variables of the outer stage problem (location and capacity) shown in (5.21) will be initialized randomly using the hybrid NSGAII-MOPSO. Then, TS initializes randomly the active power of thermal generating units from one side and the active power of storage devices based on the decision variables of outer stage from another side. Decision variables of inner stage are presented in (5.22). d^{Inner} and d^{Outer} are the decision variables of the upper and lower optimization problem. q is the number of candidate locations specified for storages devices

$$d^{Outer} = \left[Loc_1\, Loc_2\, Loc_3 .....Loc_q, C_1\, C_2\, C_3 .....C_q \right] \tag{5.21}$$

$$d_{t,s}^{Inner} = \left[P_{G1}^{t,s}\ P_{G2}^{t,s}\ P_{G3}^{t,s}\ P_{G4}^{t,s}\ P_{G5}^{t,s}\ P_{ESS1}^{t,s}\ P_{ESS2}^{t,s} \cdots P_{ESSq}^{t,s} \right]_{\substack{t=1,2,...,T \\ s=1,2,...,S}} \tag{5.22}$$

5.3.2 Tabu Search algorithm (TS)

TS algorithm is an efficient combinatorial method capable of converging to the optimal solution with a reasonable short time whenever the dimension of decision variable is not large. TS algorithm initializes randomly a feasible solution as a current solution. Then using some operators, a set of neighbour solutions is generated. The fitness value of each generated neighbour solution is evaluated. The neighbour solution with the best fitness value is selected as the new solution. Then by comparing the objective function values of the current and new solutions, TS continues the local search with the solutions which have the best fitness value until termination criteria is satisfied [20]. The steps of implementing the solver of the inner optimization method (TS) can be summarized as follows:

1. TS will receive the location and capacity from the outer loop at each NSGAII-MOPSO iteration it^{th} as shown in (5.21)

2. Set the counter k=0 for TS
3. Considering the received information, TS will initialize randomly a solution as in (5.22) within constraints and its fitness value in (5.1) is to determined.
4. Set the initialized solution as the current solution
5. A set of neighbourhood solutions is generated stochastically as follows

$$\left.\begin{aligned} P_{g,h}^{t,s} &= P_{g,k}^{t,s} + r\left(P_{g,\max}^{Gen} - P_{g,\min}^{Gen}\right) \;\; \forall t \in \psi_T,\, s \in \psi_S,\, g \in \psi_G,\, h \in \psi_H \\ P_{ESSn,h}^{t,s} &= P_{ESSn,k}^{t,s} + r\left(P_{n,it,\max}^{ESS} - P_{n,it,\min}^{ESS}\right) \;\; \forall t \in \psi_T,\, s \in \psi_S,\, n \in \psi_N,\, h \in \psi_H \end{aligned}\right\} \quad (5.23)$$

Where ψ_H is the set of neighborhoods, $P_{g,h}^{t,s}$ is the hth generated neighbor solution represents the active power of gth generator at tth hour in sth scenario, $P_{ESSn,h}^{t,s}$ is the hth generated neighbor solution represents the active power of nth CAES at tth hour in sth scenario, $P_{n,it,\max}^{ESS}$ is the maximum active power of nth CAES in the itth iteration of NSGAII-MOPSO. The maximum active power in the itth of NSGAII-MOPSO can be determined by dividing nth capacity of CAES (which is fixed value in each itth) by a certain number which represents the ratio between capacity and rated power during itth. $P_{n,it,\min}^{ESS}$ is the minimum value of the nth CAES during itth of NSGAII-MOPSO and it equals to zero and r is a random number in the range of [-1,1].

6. Check the constrains of the newly generated neighbor solutions
7. For each generated neighbor solution, apply the peak shaving operational strategy
8. After that, apply the newton Raphson power flow
9. Check for constraints
10. Determine the objective function value in (5.1) for each neighbor solution
11. Select the best neighbor solution has the most minimum fitness value and set it as the new solution

12. Compare the current and new fitness values and select the best one and set it as the current solution. TS will continue its local search with the best solution
13. Termination criteria is satisfied, then go to step 14. Otherwise, update k=k+1and go to step 5.
14. Stop:
    a. We have established the optimal scheduling of thermal generating units and allocated CAESs by determining the optimal active power of generating units and active power profiles for each allocated CAES in each scenario in every hour.
    b. The optimal objective function in (5.1) is determined.

5.3.3 NSGAII-MOPSO

Hybrid NSGAII-MOPSO is utilized to minimize the multiple objective function in (5.12) simultanously by determining the optimal locations and capacities of CAESs. Combining this hybrid optimization method with the local search method TS, the optimal location, capacity, power ratings and optimal scheduling for thermal generating units and allocated CAESs can be finally determined.

Although MOPSO has a reasonable short computational time and simple procedures, it may trap into a local minimum due to the premature convergence feature [89]. Incorporating NSGAII can overcome the disadvantages in MOPSO. NSGAII has the ability to diversify the search space using crowed-comparsion operation. Moreover, elitism which can save the good solutions is a main feature of NSGAII [86]. Hybridization of NSGAII within MOPSO can improve the performance of MOPSO due to widely diversification of the search space. The work in [7] proves the superiority of hybrid NSGAII-MOPSO in solving optimization problem for minimizing system's total expected cost comparing to MOPSO alone or NSGAII alone. Regarding the

quality of the optimal solutions that can be determined by hybrid NSGAII-MOPSO, it should be noted that the obtained solution after implementing TOPSIS can be considered near to the exact global solution. For small optimisation problems with easy constructed objective funtions and constraints, a lot of comparsion made between conventional and evolutionary optimisation algorithms in the literature which proves the ability of meta-heuristic techniques to obtain a solution very close to the exact solution with much less computational efforts. However, for complex optimisation problem composed of multiple non-linear, nonconvex and incompatible objective functions subjected to thousands of non-linear constraints with huge search space and unknown pareto front, which is the case in this thesis, makes proving theoretically the quality of the obtained solution extremely difficult and seems to be not possible. So, in the literature, running the algorithm multiple times and take the best solution among the obtained solutions was considered a solution for optimality due to lacking of theoretical prove for convergence and the difficulty of using the conventional optimization techniques to determine the exact solution. Also, it should be noted that if the true pareto front is given, then several metrics like generational distance (the distance between the obtained solutions on pareto front and solutions on the given true pareto front) can be utilised to compare between the obatined and the true given pareto front which is not the case in this thesis. The steps for implementing the hybrid optimization method NSGAII-MOPSO are summarized as follows:

Start: Initialize NSGAII and MOPSO parameters as detailed deeply in [7].

Step 1: the hybrid algorithm initializes randomly an initial population with size equals N_p within constraints. It consists of multiple particles according Figure 5.2. Each particle is referred as a candidate solution. The first sub-population composed of

binary variables represented by Loc_q and the second sub-population composed of real valued variables represented by C_q. Initialize also the personnel best Pbest, global best Gbest and the archive.

Step 2: Apply tabu local search algorithm as explained above for every particle initialized in step1.

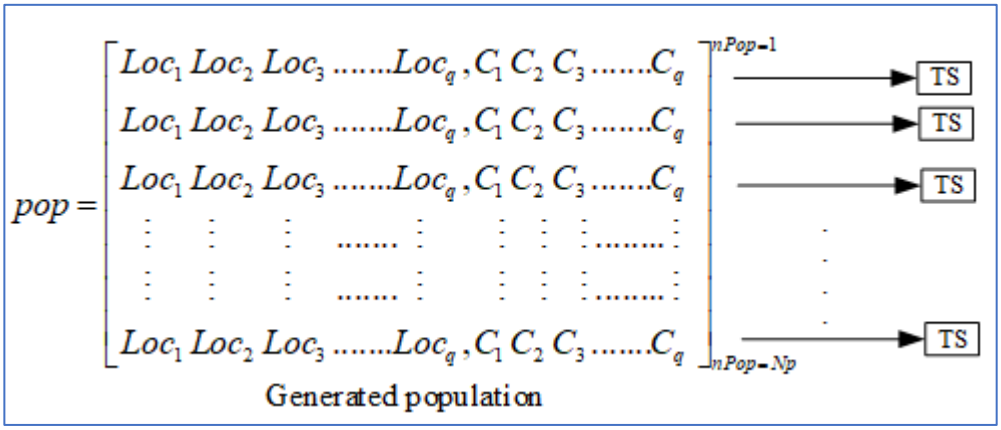

Figure 5.2: TS algorithm is applied for every particle in the generated population

Step 3: Using the objective function F_{inner} determined in step 2, the objective function F_{outer} for every particle stated in (5.12) can be determined. Update the personnel best Pbest. Till this step we initialize the main population and the initial objective function for every particle.

Step 4: Start the main iteration (it) of the hyrbid NSGAII-MOPSO.

Step 5: Apply crossover operator on pop to get popc. Check constraints of every candidate solution in popc.

Step 6: apply mutation operator on pop to get popm. Check constraints of every candidate solution in popm.

Step 7: combine pop, popc and popm to generate a new population (popnew1) of size equal $2N_P$.

Step 8: Apply tabu local search algorithm for every new solution generated in popnew1.

Step 9: Using the objective function F_{inner} determined in Step 8, the objective function F_{outer} for every solution in popnew1 stated in (5.12) can be determined. This means that every solution (particle) inside popnew1 has its own fitness value.

Step 10: Apply fast non-dominated sorting approach, fast crowded distance estimation procedure, simple crowded comparison operator on the population (popnew1). Then, apply the truncate operator to have a new population popnew2 of size N_P.

Step 11: Update the archive by adding the non-dominated particles of the popnew2 into the archive. After that, update the archive again by removing the dominated particles inside the archive.

Step 12: Select the global best Gbest or leader randomly from the archive.

Step 13: Generate a new population (pop) by moving the particles in popnew2 using the well known velocity-position update equation. More details about this equation

and its parameters can be found in chapter 5. Check the constraints of the newly generated population pop.

Step 14: Apply tabu local search algorithm for every newly generated solution in pop.

Step 15: Using the objective function F_{inner} determined in step 14, the objective function F_{outer} for every solution in pop stated in (5.12) can be determined. This means that every solution (particle) inside pop has its own fitness value.

Step 16: Apply step 11 on the generated pop.

Step 17: Before the end of each iteration, apply TOPSIS method as described in chapter 5 on the last updated archive to select only one solution (best solution) from a set of non-dominated solutions.

Step 18: termination criteria is satisfied, then go to the next step. Otherwise go to step 5.

Stop: Stop NSGAII-MOPSO-TS iteration process. The optimal configuration of CAESs (location, capacity, power ratings, optimal charging/discharging schedule) and the optimal objective functions are determined. The steps for implementing hybrid optimization method NSGAII-MOPSO-TS are presented in Figure 5.3.

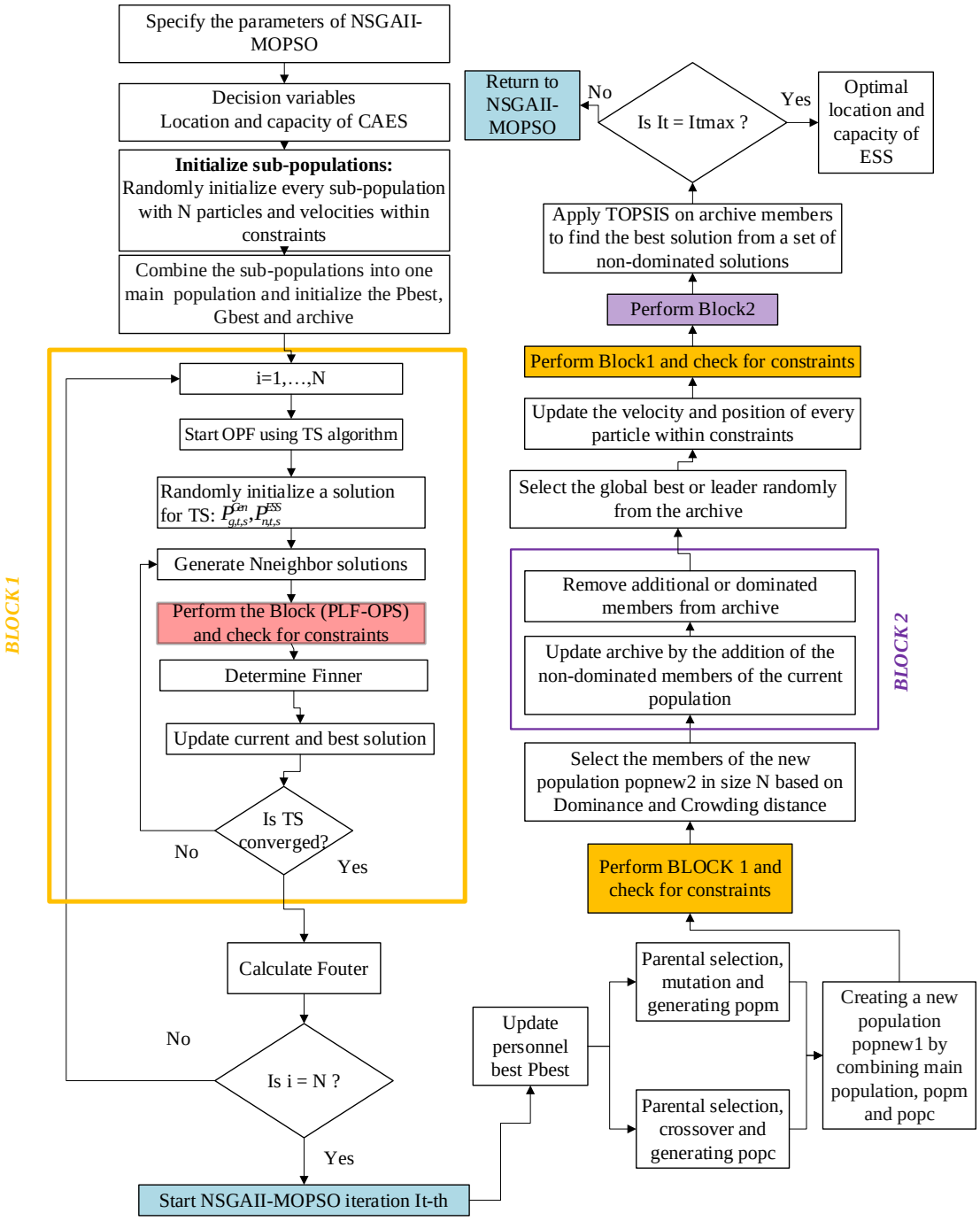

Figure 5.3: The proposed hybrid NSGAII-MOPSO-TS flowchart for solving two-stage non-linear mixed integer optimization problem to determine the optimal configuration of CAES

5.4 Conclusion

Bi-level mixed integer non-linear optimisation planning and operation model is formulated for the optimal configuration (location, capacity and power ratings) of compressed air energy storage system (CAES). The model was formulated with

consideration for independent and correlated wind farms. The single objective function in the inner layer of the bi-level model includes the difference between the total daily expected operational cost of conventional generators and the energy arbitrage benefits derived when considering the operational strategies of ESSs. The outer layer is a multi-objective function composed of three objective functions to be minimised. The objective functions encompass the total daily expected planning and operational cost, total daily expected emission and the maximum expected voltage deviation. Wind power uncertainties in independent and correlated wind farms were also examined. A hybrid non-dominating sorted genetic algorithm NSGAII and multi-objective particle swarm optimisation MOPSO were used to minimise the outer layer objective function, whilst fast Tabu search TS algorithm that considers the probabilistic load flow represented by wind power uncertainties and the operational strategies of ESSs was adopted to minimise the inner layer objective function.

Chapter 6

RESULTS OF OPTIMAL ALLOCATION OF ENERGY STORAGE SYSTEMS IN TRANSMISSION NETWORK

The proposed hybrid algorithm NSGAII-MOPSO-PLF has been applied to IEEE 30 bus and IEEE 57 bus systems and compared to NSGAII and MOPSO to test its quality and robustness. The standarad IEEE 30 bus system consists of five generations and 20 loads, bus 1 is slack bus, buses 13, 22, 23, 27 are PV buses, and other buses are PQ nodes. Wind generation is added to bus 2 rated as 113MW [42] (derived from 40% penetration of total load). The fuel cost coefficients, emission coefficients and active power limits are taken from [42] and shown in table 6.1. The maximum load (283.04MW) is selected as peak load condition to conduct the combined method in this case of study. IEEE 57 bus system consists of five generations and 42 loads, bus 1 is slack bus, buses 3, 6, 9, 12 are PV buses, and other buses are PQ nodes. The fuel cost coefficients, emission coefficients and active power limits are taken from [21] and shown in table 6.1. The wind generations are added to bus 2 and bus 8 with rated power of 45 MW and 330 MW as stated in [21] , derived from 30% penetration. The peak-load condition, which is 1250.80 MW, is used conduct the combined proposed method in this case of study. The distribution data for wind farms in both case of studies is summarized in table 6.2. The proposed budget PB for the total investment cost of ESSs for IEEE 30 bus and IEEE 57 bus system is 10 million dollars and 80 million dollars respectively.

Table 6.1: Fuel cost and emission data

Case of studies	Gen	Cost Coefficients			Emission Coefficients			Gen. limit	
		a ($/MW^{2}h)	*b* ($/MWh)	*c* ($/h)	θ (kg/MW^{2}h)	Φ (kg/MWh)	ɣ (kg/h)	P_{min} (MW)	P_{max} (MW)
IEEE 30 BUS SYSTEM	1	100	200	10	4.091	-5.554	6.49	5	50
	22	40	180	20	4.258	-5.094	4.586	5	100
	27	60	100	10	5.326	-3.55	3.38	5	120
	23	40	180	20	4.258	-5.094	4.586	5	100
	13	100	150	10	6.131	-5.555	5.151	5	60
IEEE 57 BUS SYSTEM	1	0.0775795	20	0	7.632	-5.876	3.965	0	575.88
	3	0.25	20	0	5.638	-6.047	2.543	0	140
	6	0.01	40	0	4.586	-5.094	4.258	0	100
	9	0.01	40	0	4.586	-5.094	4.258	0	100

Table 6.2: Parameters of wind farms distribution

Case of studies	Wind Farms	k	λ	α	β	V_{ci} (m/s)	V_{co} (m/s)	V_{no} (m/s)	Max Power (MW)
IEEE 30 bus system	Bus 2	2.5034	10.0434	-39.55	11.3	3.5	40	13.5	113
IEEE 57 bus system	Bus 2	2.5034	10.0434	-15.75	4.5	3.5	40	13.5	45
	Bus 8	2.4	11.5	-115.5	33	3.5	40	13.5	330

6.1 Case Studies

To demostrate the effectivness of the proposed combined algorithm in solving the optimal allocation of ESS's considering the uncertainty of wind powers and their correlation, two test systems are conducted and compared.

6.1.1 Results of the proposed algorithm for IEEE 30 bus system

Table 6.3 details the optimal values in five wind power scenarios associated with their probabilities resulted from decretization of wind power pdf using the five point estimation method as shown in Figure 6.1. The optimal values including operation

cost, carbon emission, voltage deviation, power losses and ESS allocation (location and size) are discussed and tabulted in four different cases.

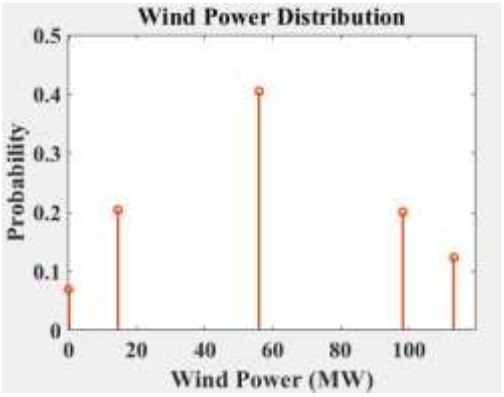

Figure 6.1: Wind Power distribution for one wind farm in IEEE 30 bus system

6.1.1.1 Case 1 (Only wind power)

According to table 6.3, as the wind power increases from 0MW to 113MW, the optimal values of operation cost, carbon emission and power losses decreases from 1019909.96 $/h to 246552.5 $/h, 484.4665 kg/h to 169.1721 kg/h and 3.4167MW to 2.4231MW respectively. Moreover, voltage deviation decreases from 1.5148 pu to 0.9528 pu as wind power penetration level increase from 0% to 19.725% corresponding to 55.83MW. However, as wind power pentration level increases, the voltage at some buses experienced more deviation from the expected voltage which is assumed to be 1 pu. Accordinly, the optimal value of voltage deviation increases slightly to reach 0.9583 pu for 40% wind power penetration due to the intermittent nature of wind power. So, we can conclude that wind power uncertainities causes voltage fluctuation when the penetration level is as high as 20% and above. Using the probabilistic objective function above, the total objective function values can be calculated and tabulted for comparsion purposes with other cases.

6.1.1.2 Case 2 (Optimal allocation of ESS using PLF-NSGAII)

A combined algorithm include PLF-NSGAII is proposed to determine the optimal location and sizing of ESSs considering wind power uncertainties. According to table 6.3, as the wind power increases from 0MW to 55.83MW (penetration level is 19.725%), the optimal values of operation cost, carbon emission and power losses decrease from 633335.3610 $/h to 149232.9030 $/h, 303.8610 kg/h to 106.6075 kg/h and 2.1328MW to 1.7249MW respectively.

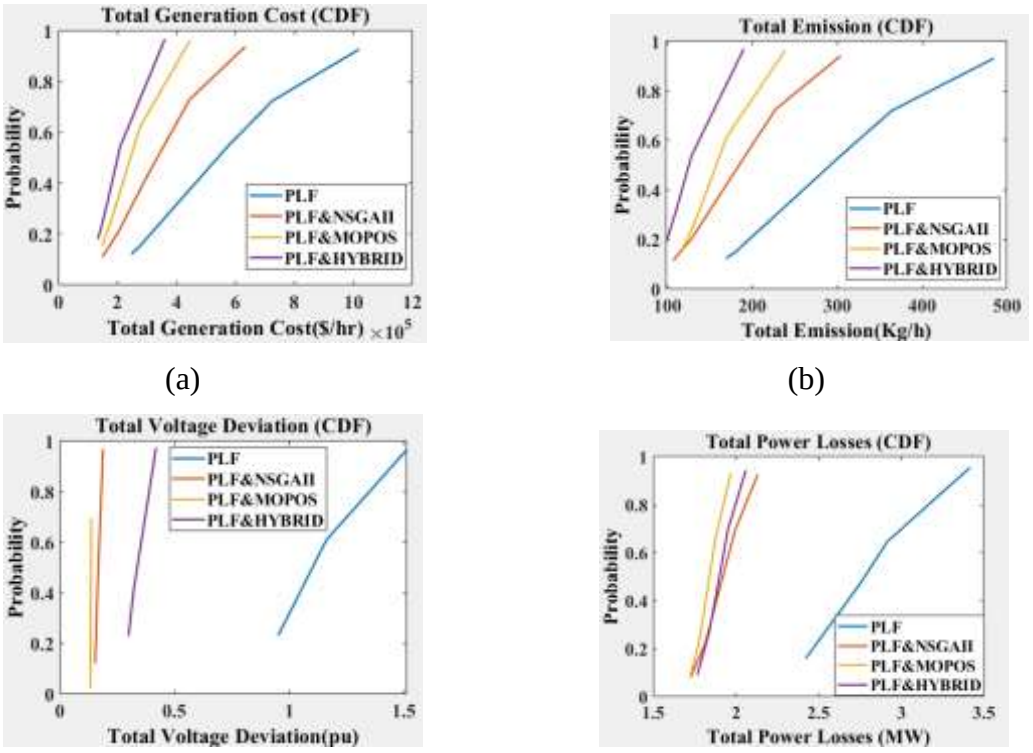

Figure 6.2: The CDF comparsion for different objective functions including generation cost, emission, losses and voltage deviation using different combination algorithms (multi-objective probabilistic-optimization methods) considering one wind farm in IEEE 30 bus system

However, for higher wind power penetration level, these values increased to reach 303209.2 $/h, 170.3928 kg/h and 1.9962 MW respectively for 113MW wind power. Voltage deviation optimal value decreases from 0.1885 pu to 0.1539 pu as wind power

increases to cover only 5.137% from the total peak load which is 283.08 MW. Then, the value of voltage deviation increases to reach 0.1645 pu for peak wind power. In this case, ESS is optimally located at buses 3, 8 and 20 with size of 11.2125MW, 14.8693MW and 8.7638MW. Comparing the case without ESS to the case with ESS using PLF-NSGAII algorithm, the total operation cost, total carbon emission and total power losses are reduced by 54.60%, 49.85% and 33.74% respectively. The optimal allocation of ESS in this case results in annual profits or savings of 2870405722.2360$/year. Moreover, total voltage deviation without ESS is 1.1141 pu. This value decreases by 85.30% to reach 0.1637 after optimally allocating ESS.

6.1.1.3 Case 3 (Optimal allocation of ESS using PLF-MOPSO)

A hybrid probabilistic optimization method PLF-MOPSO is also proposed to determine the optimal location and sizing of ESSs considering wind power uncertainties to prove the validity of PLF-NSGAII. According to table 6.3, as the wind power increases from 0MW to 98.15MW (penetration level is 34.678%), the optimal values of operation cost and carbon emission decreases from 445330.0940 $/h to 147798.0090 $/h and 238.4955 kg/h to 117.7237 kg/h respectively. Also the power losses decreases from 1.8643 to 1.7227MW as wind power penetration reaches 19.725%. However, for higher wind power penetration level, these values increased to reach 172621.6 $/h, 127.9877 kg/h and 1.9709 MW respectively for 113MW wind power (40% penetration). Voltage deviation optimal value experienced slight fluctuation around 0.13 pu for the whole wind power scenarios. In this case, ESS is optimally located at buses 6, 18 and 20 with size of 20MW, 3.0875MW and 19.9908MW. Comparing the case without ESS to the case with ESS using PLF-MOPSO algorithm, the total operation cost, total carbon emission and total power losses are reduced by 58.59%, 49.41% and 34.8265% respectively. However, the total

investment cost increased by 23.63% to reach 5.384787 million dollars which is less than the proposed budget 10 million dollars. Moreover, total voltage deviation without ESS is 1.1141 pu. This value decreases by 87.66% to reach 0.1374 after optimally allocating ESS.

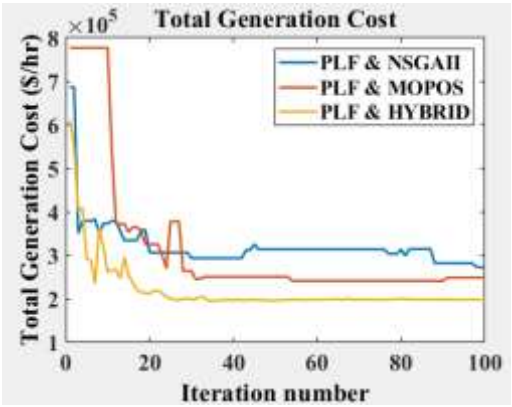

(a)

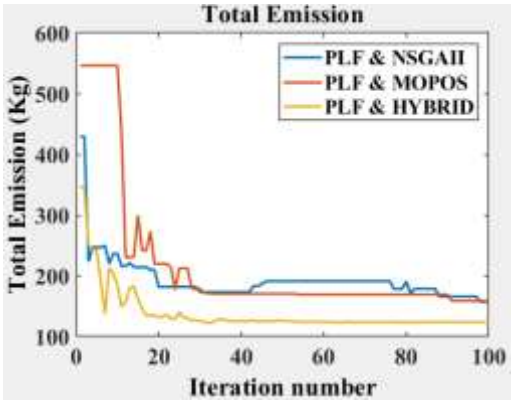

(b)

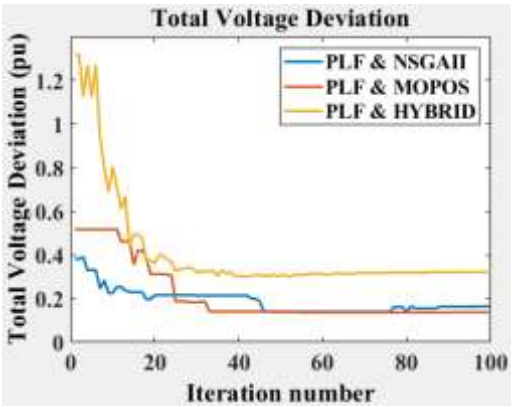

(c)

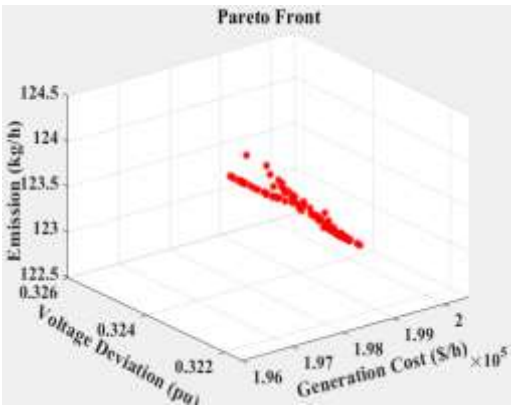

(d)

Figure 6.3: (a), (b) and (c) the objective functions comparison for one wind Farm in IEEE 30 bus system using three combined probabilistic multi-objective optimization methods and d) the objective space for the hybrid method (PLF-NSGAII-MOPSO)

6.1.1.4 Case 4 (Optimal allocation of ESS using PLF-NSGAII-MOPSO)

A hybrid probabilistic optimisation method PLF-NSGAII-MOPSO is proposed to determine the optimal location and sizing of ESSs considering wind power uncertainties. According to table 6.3, as the wind power increases from 0MW to

98.15MW, the optimal values of operation cost, carbon emission and voltage deviation decreases from 360997.9020 $/h to 134107.8380$/h, 189.7611 kg/h to 97.8939kg/h and 0.4202 pu to 0.3000 pu respectively. Also the power losse decreases from 2.0618 to 1.7674 MW as wind power penetration reaches 19.725%. However, for higher wind power penetration level, these values increased to reach 167475.4 $/h, 111.654 kg/h, 0.3002 pu and 1.9531 MW respectively for 113MW wind power (40% penetration). In this case, ESS is optimally located at buses 9, 17 and 30 with size of 19.9972MW, 19.9982MW and 19.9951MW. Comparing the case without ESS to the case with ESS using hybrid algorithm, the total operation cost, total carbon emission and total power loss are reduced by 66.99%, 60.55% and 33.04% respectively. However, the total investment cost increased by 39.26% to reach 7.498812million dollars which is within the range of the proposed budget. Moreover, total voltage deviation without ESS is 1.11 pu. This value decreases by 71.13% to reach 0.3216 after optimally allocating ESS.

Table 6.3: Optimal objective function values and ESS allocation obtained in five wind power scenarios in different cases

Cases	**Wind Power**	**0 (MW)**	**14.54 (MW)**	**55.83 (MW)**	**98.15 (MW)**	**113 (MW)**	**Total**	**% Relative reduction w.r.t. case 1**
	Penetration level (%)	0.0000	5.1370	19.7250	34.6780	40.0000		
	Probability	0.0689	0.2041	0.4050	0.1991	0.1228		
Without ESS (PLF)	Cost ($/h)	1019909.9600	725944.5510	576314.7330	272064.4110	246552.5000	600088.9753	------
	Emission (Kg/h)	484.4665	364.4703	303.4212	179.4978	169.1721	313.1973	
	Volt.Dev (pu)	1.5148	1.1644	0.9528	0.9572	0.9583	1.1141	
	Loss (MW)	3.4167	2.9158	2.7501	2.4235	2.4231	2.7950	
NSGAII	Cost ($/h)	633335.3610	445575.2290	149232.9030	201550.5430	303209.2000	272417.0892	54.60
	Emission (Kg/h)	303.8610	227.2566	106.6075	128.6010	170.3928	157.0432	49.85
	Volt.Dev (pu)	0.1885	0.1539	0.1641	0.1644	0.1645	0.1637	85.30
	Loss (MW)	2.1328	1.9580	1.7249	1.8150	1.9962	1.8519	33.74
	Total Invest. Cost (million $)	-					4.355700	-
	ESS optimal location and size	bus (3) 11.2125MW, bus (8) 14.8693MW and bus (20) 8.7638MW					34.8456 MW	
MOPSO	Cost ($/h)	445330.0940	276249.5940	202651.1160	147798.0090	172621.6000	248471.7118	58.59

	Emission (Kg/h)	238.4955	169.5787	139.6312	117.7237	127.9877	158.4250	49.41
	Volt .Dev (pu)	0.1329	0.1378	0.1378	0.1378	0.1378	0.1374	87.66
	Loss (MW)	1.8643	1.7798	1.7227	1.8742	1.9709	1.8216	34.82
	Total Invest. Cost (million $)	-					5.384787	-
	ESS optimal location and size	bus (6) 20MW, bus (18) 3.0875MW and bus (20) 19.9908MW					43.0783 MW	
Hybrid (PLF-NSGAII-PSO)	Cost ($/h)	360997.9020	209685.7440	148223.7180	134107.8380	167475.4000	198047.7679	66.99
	Emission (Kg/h)	189.7611	128.1170	103.1350	97.8939	111.6540	123.5664	60.54
	Volt.Dev (pu)	0.4202	0.3209	0.3213	0.3000	0.3002	0.3216	71.13
	Loss (MW)	2.0618	1.8390	1.7674	1.8852	1.9531	1.8716	33.03
	Total Invest. Cost (million $)	-					7.498812	-
	ESS optimal location and size	bus (9) 19.9972MW, bus (17) 19.9982MW and bus (30) 19.9951MW					59.9905 MW	

6.1.1.5 Comparsion

The distribution of the different objective functions including system operation cost, carbon emission, voltage deviation and power losses considering wind power uncertainty in four different cases is presented in Figure 6.2. Figure 6.3 (d) presents the objective space for PLF-NSGAII-MOPSO. So, according to Figure 6.3 (d) and as clarified before, it is very difficult to choose one global solution for the hybrid probabilisitic multi-objective optimization algorithm. Accordingly, TOPSIS is applied for each method by the end of each iteration ending with 100 global solutions for 100 iterations considering each of the three objective functions individually as shown in Figure 6.3 (a), (b) and (c).

When NSGAII is utilized a lone or included in the hybrid algorithnm (NSGAII-MOPSO), the objective space is represented by many solutions that can be either a scattered points on the surface or a pareto solution set and this depends on the problem being minimized and the settings of NSGAII. Although NSAGII is included in the hybrid algorithm, Figure 6.3 (d) presents a pareto solution set instead of many points

scattering on the surface of objective space. NSGAII algorithm resulted in a parteo solution set in [94, 95, 96, 97] in two and three dimensional objecive space which proves the ability of NSGAII to give a pareto solution set. So, according to Figure 6.2, Figure 6.3 and table 6.3, it is very clear that case 1 (without ESS) is the worest one considering all objective function values, case 3 (PLF- MOPSO) is the best one considering voltage deviation and power losses and case 4 (PLF- NSGAII-MOPSO) is the so far best method considering system cost and carbon emission. Moreover, the carbon emission reduction using the hybrid method is 10.68% more than PLF-NSGAII and 11.12% more than PLF-MOPSO. On the other hand, the power loss mitigation using PLF-MOPSO (case 3) is slightly more than PLF-NSGII by 1.084% and slightly more than PLF-Hybrid method by 1.78%.

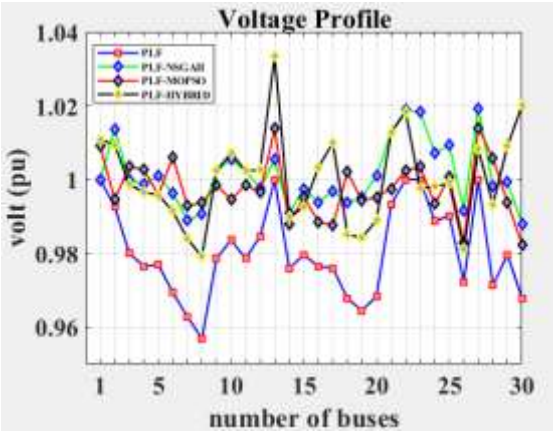

Figure 6.4: Voltage profile comparsion in four different cases including PLF, PLF-NSGAII, PLF-MOPSO and PLF-HYBRID methods for IEEE 30 bus system

Also, voltage deviation reduction using PLF-MOPSO is 2.36% more than PLF-NSGAII and 16.53% more than hyrbid method. According to Figure 6.4, voltage deviation reduction after ESS optimal allocation using three different probabilistic optimization algorithms resulted in voltage profile improvement where the best voltage profile obtained by PLF-MOPSO and the worest one is in the case of wind

power alone without ESS. After all, we conclude that hybrid method is superior compared to the other methods considering cost and emission and PLF-MOPSO is far better than hybrid considering voltage deviation.

6.1.2 Results of the proposed algorithm for IEEE 57 bus system

The discrete wind power joint distribution for two independent and two correlated wind farms are presented in Figure 6.5 (a) and Figure 6.5 (b). Table 6.4 and table 6.5 details the optimal values and their statisitical analysis in 25 wind power scenarios for two independent and two correlated wind farms including thermal generators's output power, system's operation cost, carbon emission, voltage deviation and power loss. Table 6.6 and table 6.7 summarize the optimal values of the objective functions including total expected operation cost, total investment cost, total expected carbon emission, total expected voltage deviation and total expected power losses in four different cases including two independent wind farms without ESS, two correlated wind farms without ESS, two independent wind farms with ESS using hybrid PLF-NSGAII-MOPSO and two correlated wind farms with ESS using hybrid PLF-NSGAII-MOPSO.

6.1.2.1 Case 1 (two independent wind farms without ESS)

According to table 6.6, the optimal values of operation cost, carbon emission, voltage deviation and power losses are 67175.552 $/h, 43266.982 kg/h, 4.043 pu and 63.494MW respectively. Using the probabilistic objective function defined (4.1), the total objective function values can be calculated and tabulted for comparsion purposes with other cases.

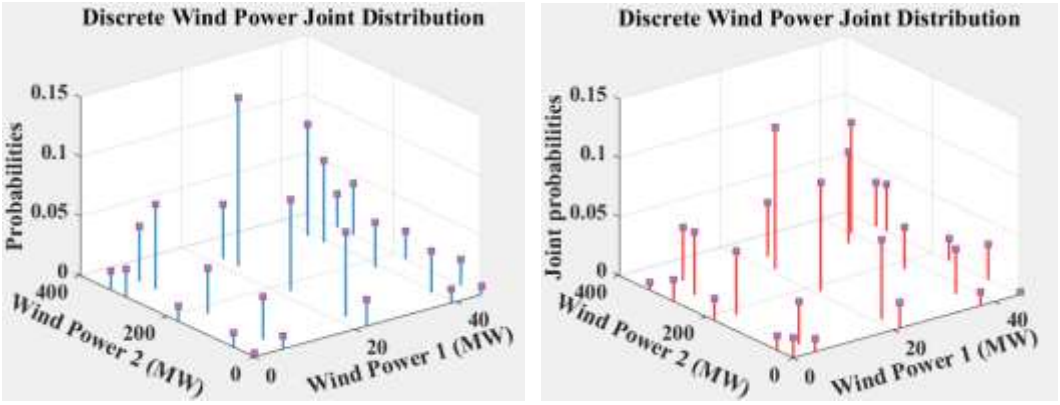

(a) **(b)**

Figure 6.5: Discrete wind power joint distribution for a) two independent wind farms and b) two correlated wind farms

6.1.2.2 Case 2 (two independent wind farms with ESS using PLF-NSGAII-MOPSO

According to table 6.6, the optimal values of total operation cost, carbon emission, power losses and investment cost are 42797.410 $/h, 4994.506 kg/h, 23.339 MW and 64.244000 million dollars respectively. The optimal number of ESSs required to cover the intermittent nature of two independent wind farms is 16 and the optimal location and sizing of these ESSs are given in table 6.6.

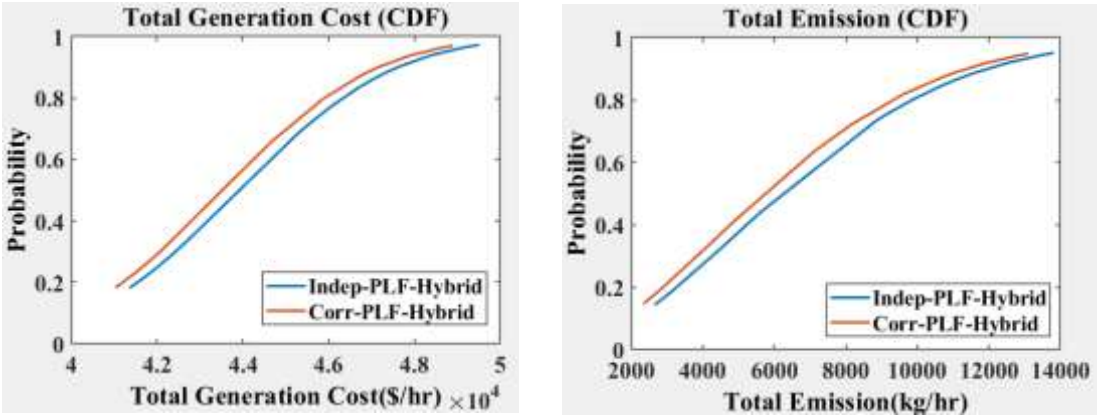

(a) (b)

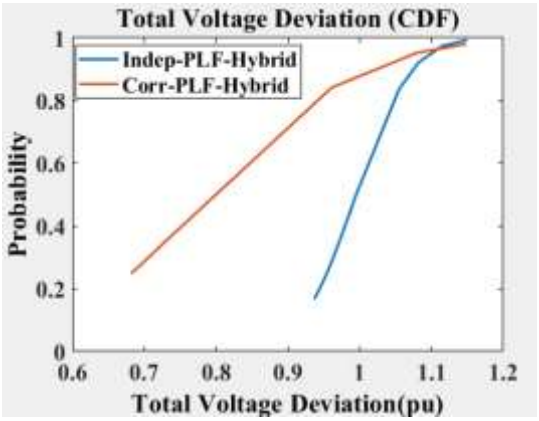

(c)

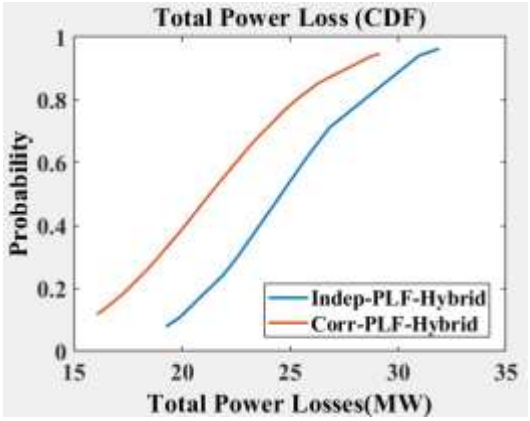

(d)

Figure 6.6: CDF comparsion for different objective functions in IEEE 57 bus system considering two independent/correlated wind farms

Comparing case2 (with ESS) with case 1 (without ESS) for independent wind farms, the total operation cost, total carbon emission and total power losses are reduced by 36.29%, 88.45% and 63.24% respectively after allocation of ESS optimally. Moreover, total voltage deviation during without ESS is 4.043 pu. This value decreases by 76.03% to reach 0.969 after optimally allocating ESS

6.1.2.3 Case 3 (two correlatd wind farms without ESS using PLF)

According to table 6.7, the optimal values of total operation cost, carbon emission, voltage deviation and power losses are 68757.906 $/h, 44517.206 kg/h, 4.209 pu and 65.838MW respectively. Using the probabilistic objective function defined in (4.1), the total objective function values can be calculated and tabulted for comparsion purposes with other cases.

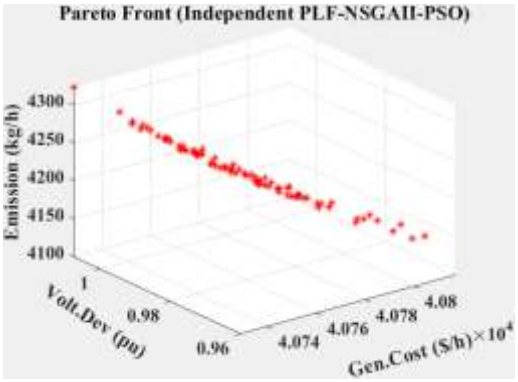

(a)

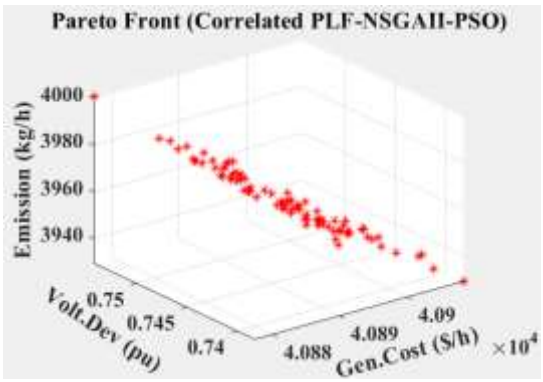

(b)

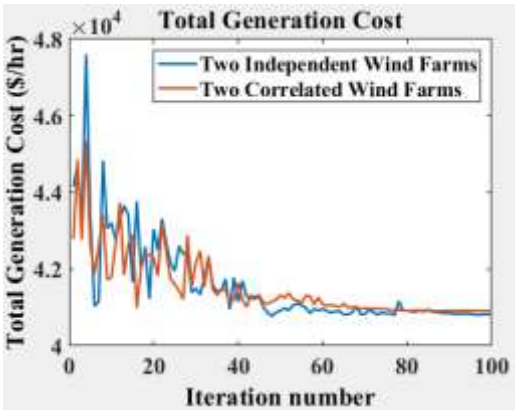

(c)

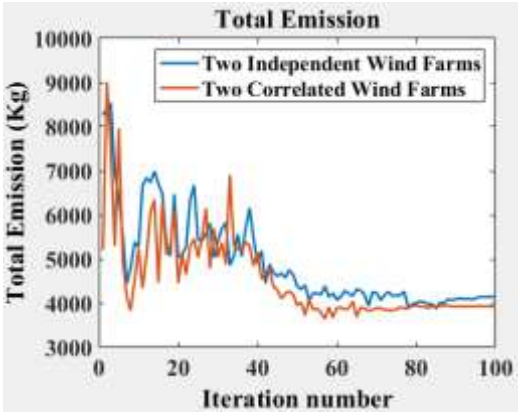

(d)

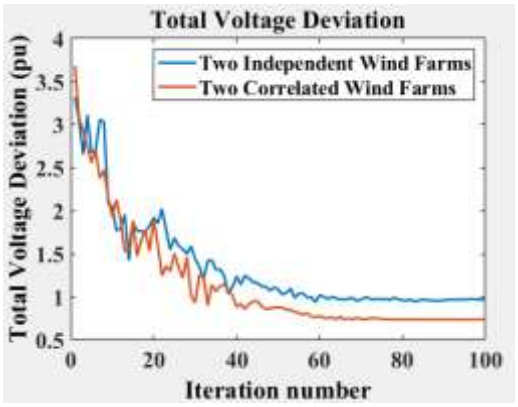

(e)

Figure 6.7: Objective functions and objective spaces : (a) and (b) Non-dominated solutions (pareto front) for this method in both independent and correlated wind farms , (c), (d) and (e) Objective functions comparison for two independent/correlated wind Farms in IEEE 57 bus system using PLF-NSGAII-PSO method

6.1.2.4 Case 4 (two correlated wind farms with ESS using PLF-NSGAII-MOPSO)

According to table 6.7, the optimal values of total operation cost, investment cost, carbon emission, voltage deviation and power losses are 42907.524 $/h, 69. 650350 million dollars, 4802.407 kg/h, 0.738 pu and 20.005 MW respectively. The optimal number of ESSs required to cover the intermittent nature of two correlated wind farms is 20 and the optimal location and sizing of these ESSs are given in table 6.7. Comparing case 4 (with ESS) with case 3 (without ESS) for correlated wind farms, the total operation cost, total carbon emission and total power losses are reduced by 37.59%, 89.21% and 69.61% respectively after allocation of ESS optimally. Moreover, total voltage deviation without ESS in case 3 is 4.209 pu. This value decreases by 82.46% to reach 0.738 after optimally allocating ESS.

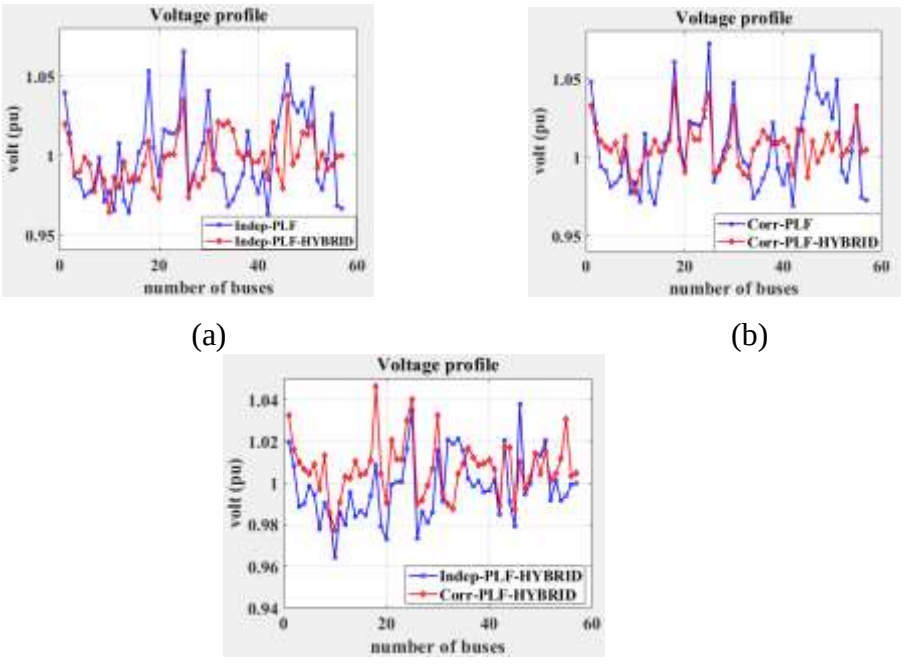

(a) (b)

(c)

Figure 6.8: Voltage profile comparsion in IEEE 57 bus system: a) Independent wind farms with and without ESS; b) Correlated wind farms with and without ESS; c) Independent and correlated wind farms with ESS

6.1.2.5 Comparsion

The distribution of the different objective functions including system's operation cost, carbon emission, voltage deviation and power losses considering the discrete wind power distribution for two independent and two correlated wind farms using hybrid PLF-NSGAII-MOPSO is presented in Figure 6.6 and detailed with their statistical values in table 6.5 and table 6.6 as stated before. Figure 6.7 (a) and (b) present the objective space for hybrid PLF-NSGAII-MOPSO in the case of two independent and two correlated wind farms. Figure 6.7 (c), (d) and (e) present 100 global solutions for 100 iterations for each objective function. So, according to Figure 6.6, Figure 6.7, table 6.6 and table 6.7, it is very clear that case 3 (correlated wind farms without ESS) is the worest case considering all objective function values, case 1 (independent wind farms without ESS) is the second worest case considering all objective function values, case 4 (correlated wind farms using PLF-NSGAII-MOPSO) is the best case considering all the objective function values except that case 2 (independent wind farms using PLF-NSGAII-MOPSO) is slightly betther than case 4 considering total generation cost.

Table 6.4: Optimal values in all power scenarios of two independent wind farms obtained using the proposed combined PLF-NSGAII-MOPSO

IEEE 57 BUS SYSTEM (PLF-NSGAII-MOPSO) - TWO INDEPENDENT WIND FARMS - OPTIMAL VALUES IN EACH SCENARIO													
Points	Joint Probability	PW1 (MW)	PW2 (MW)	% penetration	Pg1 (MW)	Pg3 (MW)	Pg6 (MW)	Pg9 (MW)	Pg12 (MW)	Gen. Cost ($/h)	Emission (kg/h)	Volt. Dev (pu)	Losses (MW)
1	0.004	0.000	0.000	0.000	382.853	37.527	80.507	74.463	193.412	49513.302	13814.506	1.150	31.913
2	0.016	0.000	330.000	26.383	45.927	37.527	80.507	74.463	193.412	41467.106	2808.589	0.995	24.987
3	0.007	45.000	0.000	3.598	336.927	37.527	80.507	74.463	193.412	47380.259	11294.320	1.115	30.987
4	0.028	45.000	330.000	29.981	0.693	37.527	80.507	74.463	193.412	41748.833	2650.306	0.959	24.754
5	0.011	5.790	0.000	0.463	376.209	37.527	80.507	74.463	193.412	49162.935	13430.044	1.055	31.060
6	0.023	22.234	0.000	1.778	359.728	37.527	80.507	74.463	193.412	48385.647	12505.306	1.114	31.023
7	0.011	39.085	0.000	3.125	342.804	37.527	80.507	74.463	193.412	47630.335	11598.904	1.056	30.950
8	0.012	0.000	46.566	3.723	331.214	37.527	80.507	74.463	193.412	47016.917	11003.379	1.082	26.841
9	0.013	0.000	173.964	13.908	196.882	37.527	80.507	74.463	193.412	42648.666	5597.091	0.972	19.907
10	0.024	0.000	293.177	23.439	80.298	37.527	80.507	74.463	193.412	41386.433	3137.687	0.989	22.536
11	0.022	45.000	46.566	7.321	285.258	37.527	80.507	74.463	193.412	45249.872	8843.853	0.994	25.885

12	0.023	45.000	173.964	17.506	151.410	37.527	80.507	74.463	193.412	41860.551	4391.039	0.938	19.434
13	0.043	45.000	293.177	27.037	35.010	37.527	80.507	74.463	193.412	41425.533	2741.796	0.953	22.248
14	0.047	5.790	330.000	26.846	39.499	37.527	80.507	74.463	193.412	41469.668	2767.063	0.957	24.350
15	0.046	22.234	330.000	28.161	23.196	37.527	80.507	74.463	193.412	41557.627	2690.011	0.958	24.491
16	0.093	39.085	330.000	29.508	6.532	37.527	80.507	74.463	193.412	41691.442	2653.182	0.958	24.678
17	0.036	5.790	46.566	4.186	324.500	37.527	80.507	74.463	193.412	46714.751	10667.744	0.993	25.917
18	0.038	5.790	173.964	14.371	190.446	37.527	80.507	74.463	193.412	42500.247	5407.212	0.937	19.260
19	0.071	5.790	293.177	23.902	73.868	37.527	80.507	74.463	193.412	41354.637	3062.412	0.952	21.896
20	0.071	22.234	46.566	5.501	308.013	37.527	80.507	74.463	193.412	46069.359	9872.860	0.993	25.874
21	0.076	22.234	173.964	15.686	174.046	37.527	80.507	74.463	193.412	42201.838	4951.967	0.937	19.305
22	0.141	22.234	293.177	25.217	57.543	37.527	80.507	74.463	193.412	41355.022	2899.640	0.952	22.015
23	0.035	39.085	46.566	6.848	291.162	37.527	80.507	74.463	193.412	45454.561	9103.262	0.994	25.874
24	0.038	39.085	173.964	17.033	157.283	37.527	80.507	74.463	193.412	41941.239	4529.072	0.938	19.393
25	0.070	39.085	293.177	26.564	40.857	37.527	80.507	74.463	193.412	41399.439	2775.307	0.953	22.180
minimum		0.000	0.000	0.000	0.693	37.527	80.507	74.463	193.412	41354.637	2650.306	0.937	19.260
maximum		45.000	330.000	29.981	382.853	37.527	80.507	74.463	193.412	49513.302	13814.506	1.150	31.913
average		22.422	168.741	15.283	184.486	37.527	80.507	74.463	193.412	43943.449	6607.862	0.996	24.710
Standard deviation		18.067	133.007	10.731	136.784	0.000	0.000	0.000	0.000	2920.931	4062.521	0.063	4.037
Total/h										42797.410	4994.506	0.969	23.339

Table 6.5: Optimal values in all power scenarios of two correlated wind farms obtained using the proposed combined PLF-NSGAII-MOPSO

IEEE 57 BUS SYSTEM (PLF-NSGAII-MOPSO) - TWO CORRELATED WIND FARMS - OPTIMAL VALUES IN EACH SCENARIO													
Points	Joint Probability	PW1 (MW)	PW2 (MW)	% penetration	Pg1 (MW)	Pg3 (MW)	Pg6 (MW)	Pg9 (MW)	Pg12 (MW)	Gen. Cost ($/h)	Emission (kg/h)	Volt. Dev (pu)	Losses (MW)
1	0.017	0.000	0.000	0.000	375.927	37.322	57.758	62.756	188.980	48903.894	13104.694	1.143	29.146
2	0.006	0.000	330.000	26.383	36.787	37.322	57.758	62.756	188.980	41162.443	2442.271	0.712	20.006
3	0.002	45.000	0.000	3.598	330.587	37.322	57.758	62.756	188.980	46861.967	10662.576	1.148	28.806
4	0.037	45.000	330.000	29.981	-7.962	37.322	57.758	62.756	188.980	41517.400	2346.457	0.717	20.257
5	0.011	4.386	0.000	0.351	371.229	37.322	57.758	62.756	188.980	48669.220	12837.085	1.079	28.834
6	0.022	21.167	0.000	1.692	354.441	37.322	57.758	62.756	188.980	47891.779	11908.304	1.148	28.827
7	0.012	37.104	0.000	2.966	338.421	37.322	57.758	62.756	188.980	47188.309	11062.078	1.080	28.743
8	0.013	0.000	36.476	2.916	336.656	37.322	57.758	62.756	188.980	47041.765	10971.270	0.961	26.351
9	0.019	0.000	179.701	14.367	183.323	37.322	57.758	62.756	188.980	42086.459	4895.288	0.688	16.243
10	0.018	0.000	275.509	22.027	88.415	37.322	57.758	62.756	188.980	41061.745	2932.561	0.703	17.143
11	0.030	45.000	72.701	9.410	250.866	37.322	57.758	62.756	188.980	43852.439	7129.510	0.686	21.786
12	0.019	45.000	163.685	16.684	154.697	37.322	57.758	62.756	188.980	41632.771	4158.482	0.698	16.601
13	0.039	45.000	307.438	28.177	13.183	37.322	57.758	62.756	188.980	41271.989	2353.640	0.713	18.839
14	0.045	6.634	330.000	26.913	29.975	37.322	57.758	62.756	188.980	41189.942	2407.963	0.716	19.828
15	0.046	23.474	330.000	28.260	13.296	37.322	57.758	62.756	188.980	41305.575	2353.861	0.717	19.989
16	0.094	39.947	330.000	29.577	-2.979	37.322	57.758	62.756	188.980	41461.260	2342.003	0.717	20.188

17	0.037	4.386	37.028	3.311	330.737	37.322	57.758	62.756	188.980	46765.117	10670.155	0.681	25.371
18	0.054	4.386	180.121	14.751	178.335	37.322	57.758	62.756	188.980	41990.920	4757.900	0.692	16.061
19	0.054	4.386	276.537	22.459	82.845	37.322	57.758	62.756	188.980	41038.785	2860.094	0.707	16.988
20	0.068	21.167	41.704	5.026	308.718	37.322	57.758	62.756	188.980	45876.039	9596.805	0.682	24.807
21	0.092	21.167	181.404	16.195	160.307	37.322	57.758	62.756	188.980	41698.658	4293.024	0.693	16.097
22	0.121	21.167	285.154	24.490	57.922	37.322	57.758	62.756	188.980	41030.063	2593.795	0.709	17.462
23	0.039	37.104	56.044	7.447	276.950	37.322	57.758	62.756	188.980	44705.572	8178.705	0.684	23.316
24	0.036	37.104	174.645	16.929	151.357	37.322	57.758	62.756	188.980	41578.617	4080.675	0.692	16.325
25	0.077	37.104	301.613	27.080	26.485	37.322	57.758	62.756	188.980	41167.340	2393.130	0.712	18.421
minimum		0.000	0.000	0.000	-7.962	37.322	57.758	62.756	188.980	41030.063	2342.003	0.681	16.061
maximum		45.000	330.000	29.981	375.927	37.322	57.758	62.756	188.980	48903.894	13104.694	1.148	29.146
average		21.827	168.790	15.240	177.621	37.322	57.758	62.756	188.980	43558.003	6133.293	0.795	21.457
Standard deviation		18.006	132.166	10.739	137.973	0.000	0.000	0.000	0.000	2867.719	3979.351	0.175	4.763
Total/h										42907.524	4802.407	0.738	20.005

Table 6.6: Comparing the objective function values for the cases of independent wind farms with and without allocation of ESS using the proposed hybrid PLF-NSGAII-MOPSO

Cases	**Objective functions**	**Total**	**%Relative reduction relative to case 1**
Case 1	Cost ($/h)	67175.552	
	Emission (Kg/h)	43266.982	
	Volt.Dev (pu)	4.043	
	Loss (MW)	63.494	
Case 2	Cost ($/h)	42797.410	36.290
	Emission (Kg/h)	4994.506	88.457
	Volt.Dev (pu)	0.969	76.036
	Loss (MW)	23.339	63.243
	Total Invest. Cost (million $)	64.244000	-
	ESS optimal location and size	bus 5 (36.5701MW), bus 13 (38.8077MW), bus 14 (33.2857MW), bus 18 (18.1039MW), bus 27 (37.6372MW), bus 28 (35.8762MW), bus 32 (37.7220MW), bus 35 (30.0902MW), bus 38 (39.7668MW), bus 45 (37.0620MW), bus 47 (35.9856MW), bus 48 (35.7204MW), bus 49 (38.0229), bus 50 (29.6551MW), bus 53 (27.9977MW), bus 55 (1.6481MW)	

Table 6.7: Comparing the objective function values for the cases of Correlated wind farms with and without allocation of ESS using the proposed hybrid PLF-NSGAII-MOPSO

Cases	**Objective functions**	**Total**	**%Relative reduction relative to case 3**	**%Relative reduction relative to case 2**	**%Relative reduction relative to case 1**
Case 3	Cost ($/h)	68757.906			
	Emission (Kg/h)	44517.206			
	Volt.Dev (pu)	4.209			
	Loss (MW)	65.838			
Case 4	Cost ($/h)	42907.524	37.59	-0.25	36.12
	Emission (Kg/h)	4802.407	89.21	3.84	88.90
	Volt.Dev (pu)	0.738	82.46	23.80	81.74
	Loss (MW)	20.005	69.61	14.28	68.49
	Total Invest. Cost (million $)	69. 650350			

	ESS optimal location and size	bus 4 (38.1832MW), bus 10 (37.1211MW), bus 11 (12.3182MW), bus 13 (38.6620MW), bus 14 (15.3882MW), bus 19 (12.2766MW), bus 20 (19.1246MW), bus 29 (38.3420MW), bus 30 (27.1945MW), bus 36 (17.9866MW), bus 37 (34.6429MW), bus 38 (31.5892MW), bus 43 (26.1884MW), bus 44 (25.9028 MW), bus 45 (38.5394MW), bus 46 (32.7448MW), bus 48 (39.0714MW), bus 50 (38.4766MW), bus 51 (0.0247MW), bus 53 (33.4256MW)

Reduction in total operation cost in case 4 is 37.59% more than case 3, 36.12% more than case 1 and slightly less than case 2 by 0.257%. In addition, considering the correlation among wind farm would result in 8.42% increase in the required investment cost of ESS.The carbon emission reduction in case 4 is 89.212% more than case 3, 3.84% more than case 2 and 88.90% more than case 1. Also, then power loss mitigation in case 4 is 69.61% more than case 3, 14.282% more than case 2 and 68.49% more than case 1. Moreover, The voltage deviation improvement in case 4 is 82.46% more than case 3, 23.80% more than case 2 and 81.74% more than case 1. Voltage deviation reduction results in voltage profile improvement. Voltage profile is improved when we compare cases without ESS to the cases with ESS as shown in Figure 6.8 (a) and (b). Optimal allocation of ESS in power system considering correlated wind farms results in better voltage profile than considering independent wind farms as it is seen in Figure 6.8 (c). So, correlation between wind farms during optimal planning of ESS should be considered for achieving better voltage stability, loss reduction, and environmental support.

Chapter 7

RESULTS OF OPTIMAL PLANNING AND OPERATIONAL STRATEGY OF ENERGY STORAGE SYSTEMS

7.1 System configuration

The proposed two stage model is applied on IEEE 57-bus system to verify its feasiblity and effectiveness. IEEE 57 consists of five generations and 42 loads, bus 1 is slack bus, buses 2, 6, 9 and 12 are PV buses, and other buses are PQ nodes. The wind farms are located at bus 3 and bus 8 with rated power of 45 MW and 330 MW derived from 30% penetration from peak load (1250.08MW). The active power profile for 24 hours in summer season extracted from [98] is shown in Figure 7.1. The active power prices Ce are presented in Figure 7.2 [37]

7.2 Simulation results

To demonstrate the effectiveness of the proposed model and its hybrid solving method, three cases are studied and compared. Hybrid NSGAII-MOPSO-TS solved the proposed two stage model considering the following cases:

Case 1: Independent wind farms without considering the operational strategy of ESSs.

Case 2: Independent wind farms considering the operational strategy of ESSs.

Case 3: Correlated wind farms considering the operational strategy of ESSs.

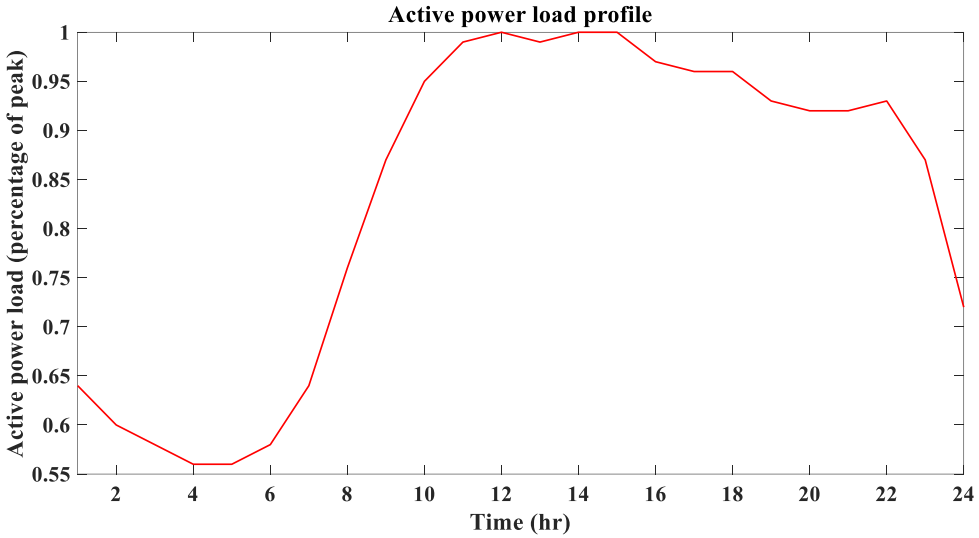

Figure 7.1: Hourly mean value of active power profile in percentage of peak

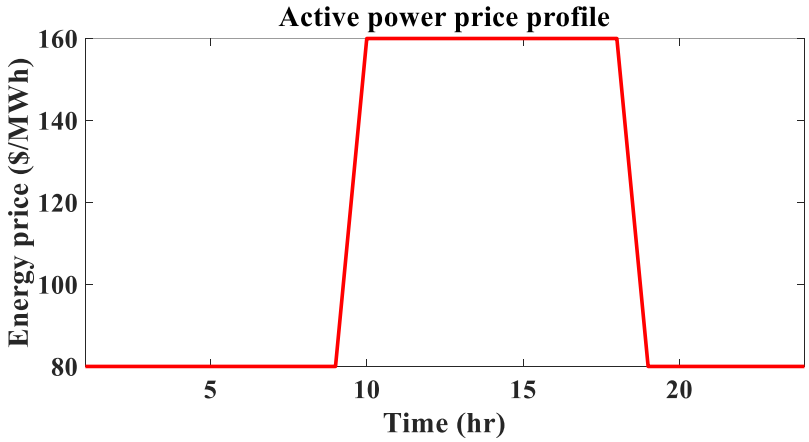

Figure 7.2: Hourly active power price profile

According to table 7.1, three and thirteen CAESs are optimally allocated to achieve the optimal minimum values of the three objective functions F1, F2 and F3 in case 1 and case 2. CAESs of capacities and power ratings between 270MWh/60MW and 276.283MWh/61.396MW are optimally obtained in case 1 and ranges between 270MWh/60MW and 352.141MWh/78.254MW in case 2. The sum of capacities and power ratings of allocated CAESs are 816.283MWh/181.396MW and 3828.165MWh/850.274MW in both cases.

Table 7.1: The obtained optimal values in case 1 and case 2

Optimal Values	**Studied Cases**	
	Case 1	Case 2
	Independent WFs Without OPS	Independent WFs With OPS
CAESs (bus, capacity, and power rating)	bus 4 (270MWh,60MW), bus 18 (270MWh, 60MW) and bus 27 (276.283MWh, 61.396MW)	bus 2 (270MWh,60MW), bus 4 (270MWh,60MW), bus 10 (270.756MWh,60.168MW), bus 11 (352.141MWh,78.254MW), bus 13 (344.202MWh,76.489MW), bus 14 (328.969MWh,73.104MW), bus 15 (270MWh,60MW), bus 17 (340.887MWh,75.753MW), bus 18 (270MWh,60MW), bus 29 (270MWh, 59.571MW), bus 38 (270MWh, 60MW), bus 50 (301.209MWh,66.935MW) and bus 53 (270MWh, 60MW)
Life time (years)	bus 4 (6.322), bus 18 (5.479), bus 27 (5.479)	All ESSs (41.096)
CAES Investment Cost ($)	156635584.049	734217478.377
CAES Variable Operational Cost ($/day)	29076.084	49556.775
CAES Fixed Operational Cost ($/day)	1242.439	5823.795
CAES arbitrage ($/day)	-32200.241	46918.228
Wind Gen Operational Cost ($/day)	191945.209	191945.209
Thermal Gen Operational Cost ($/day)	824274.955	763445.149
Total variable operational cost ($/day)	1077496.490	958028.904
F_{inner} ($/day)	856475.196	716526.921
F_1 (Total daily cost) ($/day)	987788.994	977147.980
F_2 (Total Emission) (Kg/day)	479330.816	408603.077
F_3 (Max Volt.dev) (pu)	4.417	3.487

It is clear that in case 2, the total capacities and power ratings of the allocated CAESs are more than that of case 1 resulted in higher investment cost of 734,217,478.377$ in case 2 and 156,635,584.049$ in case 1. However, the replacement cost occurs every 5 or 6 years in case 1 and after 41 years in case 2. The smaller life time of the allocated CAESs in the case of without considering the operational strategy of ESSs would affect negatively on the obtained total daily expected cost. The system achieved more

economic, technical and environmental benefits in the case of independent wind farms considering the operational strategy of ESSs compared to the case without operational strategy. One of the economic benefits from considering the operational strategy of ESSs include the reduction in the total daily expected operational cost of thermal generators compared to the case without operational strategy to reach 824274.955 $/day and 763445.149 $/day in case 1 and case 2. This can be clearly seen in Figure 7.3 where the system is more dependent on thermal generators during the first eight hours in case 2 (charging mode) compared to case 1. However, after t=9hr, the system in case 2 is far less dependent on thermal generators (discharging mode) and highly depedent on thermal generators in case 1 due to the lack of the operational strategy of CAESs.

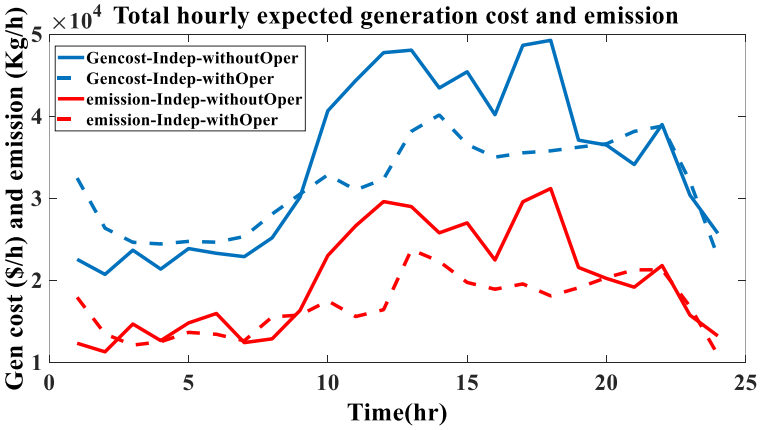

Figure 7.3: Total hourly expected operational cost and emission of thermal generators considering independent wind farms in the case of with and without including the operational strategy of ESSs

Moreover, the reduction in the difference between the total daily expected variable operation cost of CAESs and their daily expected arbitrage is more in case 2 by 95.694% than case 1 to reach 61276.325$/day and 2638.547$/day in case 1 and case 2. The reason behind this huge percentage of reduction is the arbitrage benefits. The obtained optimal daily schedule of charging/discharging process of all allocated

CAESs resulted in paying 32200.241$/day and earning 46918.228 $/day of electric energy in case 1 and case 2.

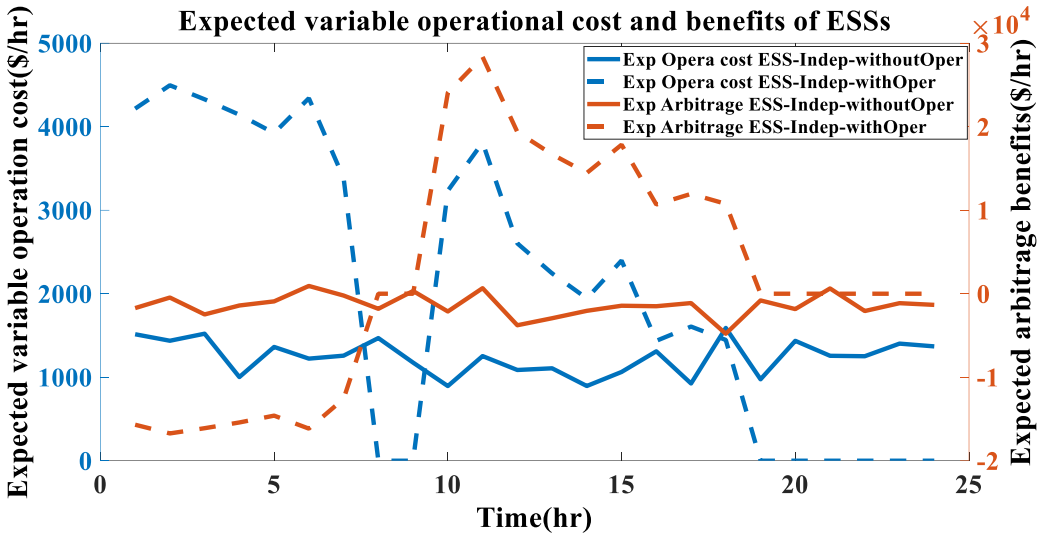

Figure 7.4: Total hourly expected operational cost and arbitrage benefits of ESSs considering independent wind farms in the case of with and without including the operational strategy of ESSs

Also, the arbitrage benefits in case 2 is negative during [1-8]hrs and hits its maximum positive value during peak load at t=11hr to reach 2836$ approximately and remained positive until t=19hr before it goes to zero during floating mode. However, in case 1, the arbitrage benefits are always in negative values which will be added as a positive value to the expected variable operational cost of ESSs results in higher cost as specified numerically in the previous sentences.

The environmental benefit obtained from considering the operational strategy of the allocated ESSs is represented by more reduction in the total daily expected emission of thermal generators compared to the case of without operational strategy to reach 479330.816 kg/day and 408603.077 kg/day in case 1 and case 2. If the operational strategy is considered during the optimal planning of ESSs, then CO emission would be reduced by 17.756% compared to the case of optimal planning without any

consideration of the operational strtagey of ESSs. According to Figure 7.4 and as it stated before, all the allocated CAESs in case 1 started their discharging mode in the time interval of [10-19]hr approximately. During this interval, the system decreased its dependency on thermal generators leads to more reduction of CO emission compared to case 1.

Minimizing the maximum expected voltage deviation is also considered in this research work and represented by the objective function F3. According to table 7.1, F3 equals 4.417pu and 3.487pu in case 1 and case 2. According to Figure 8, the expected voltage deviations hits its maximum value during valley load at t=5hr approximately in both cases and during peak load at t=13hr in case 2.

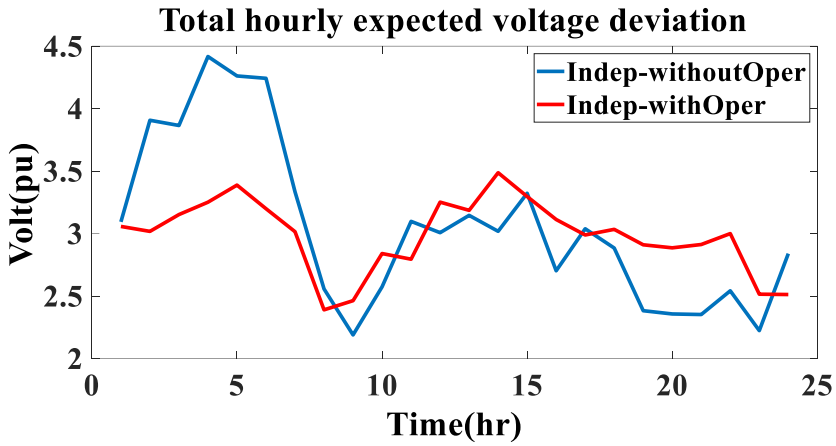

Figure 7.5: Total hourly expected voltage deviation considering independent wind farms in the case of with and without including the operational strategy of ESSs

Although, considering the operational strategy of allocated CAESs reduced the maximum expected voltage deviation by 21% compared to case 1, 3.487pu still considered a high value. One of the reasons is that the first and the worest wind power scenarios can be considered as a double wind power generator outage and the scenarios in the interval [2-3, 5-10] can be considered as single wind generator outage. Every

one of these mentioned scenarios has its own probability that can effect on the operation of the optimization and hence leaves a negative effect on the value of the expected voltage deviation and its maximum value. Moreover, the peak shaving operational strategy adopted in case 2 has more positive weight or impact on the total daily expected cost rather than expected voltage deviation. Also, according to table 7.1, all the obatined optimal locations in both cases did not include bus 25 and bus 30 which are considered the buses of the highest expected voltage deviation in the base case (without ESS). Hence, the optimization method with the operational strategy minimized the total daily expected cost on the expense of expected voltage deviation.

The proposed optimization method combined with the peak shaving operational strategy reduced the expected active power loss in the system during the intervals of the high and peak loads compared to case 1 according to Figure 7.6. The expected active power loss hits its maximum values at t=17hr and t=14hr to reach 71.68MW and 55.48MW in case 1 and case 2. So, considering the operational strategy in case 2 would reduce the maximum expected active power loss by 22.6%.

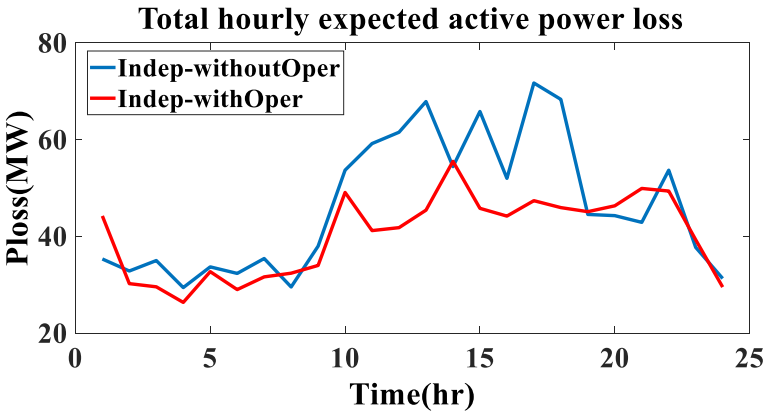

Figure 7.6: Total hourly expected active power loss considering independent wind farms in the case of with and without including the operational strategy of ESSs

Figure 7.7. According to Figure 7.7 and considering the 4th wind power scenario as an example, the state of charge SOC of the three allocated CAESs in case 1 is increasing (charging) sometimes during the hours of high load level which results in a total load even higher than the predefined peak load which results in higher active power losses. For example, at t=17hr, the load is 95% from the peak load and all the three CAESs are in the charging mode resulting in a maximum expected active power loss of 71.68MW.

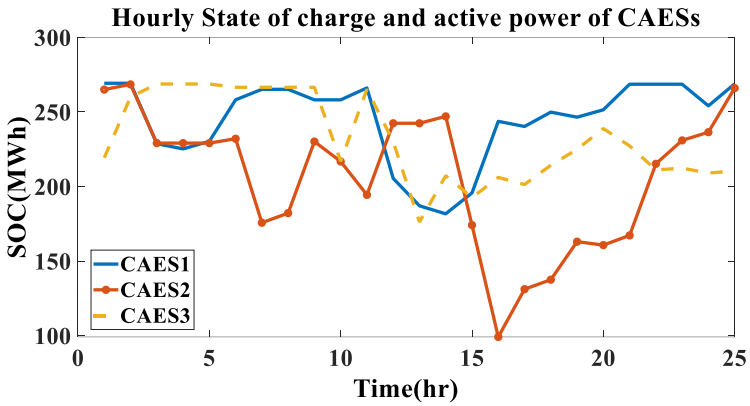

Figure 7.7: Hourly state of charge of CAESs considering independent wind farms in the 4th scenario without including the operational strategy of ESSs

Hybrid NSGAII-MOPSO is utilized to minimize the outer multi-objective function (F1, F2 and F3) with and without considering the peak shaving operational strategy of the allocated CAESs. The total expected daily cost F1 which consists of the daily expected operation cost of thermal generators, daily expected variable and fixed operation cost and arbitrage of all allocated CAESs and the daily investment cost is presented in Figure 7.8 (a) as function of the iteration number of the solving optimization method NSGAII-MOPSO for both case 1 and case 2. Furthermore, Figure 7.8 (b) and Figure 7.8 (c) present the total daily expected emission F2 and the maximum expected voltage deviation F3 as function of the iteration number of the proposed solving method. Although the number of the allocated CAESs in case 2 is

approximately four times of that in case 1, the total expected daily cost is the same in both case 1 and case 2 according to Figure 7.8 (a). The reason is the obtained life time of all allocated CAESs as stated before. According to Figure 7.7, the three allocated CAESs have at least three cycles during charging/discharging process results in smaller life time. As the life time decrease, the constant σ which is used to convert the investment cost into daily cost would rise which in turns increase the total expected daily cost. However, according to Figure 7.9 (a), (b), (c) and (d), all 13 allocated CAESs in case 2 have only one cycle results in higher life time compared to case 1 equals to 41 years. This high value of life time would decrease σ results in total expected daily cost equals to that in case 1 at the end of the iteration. Although both cases have the same total expected daily cost, case 2 is much better compared to case 1 regarding the environmental (total daily expected emission) and technical (maximum expected voltage deviation) benefits according to Figure 7.8 (b) and (c).

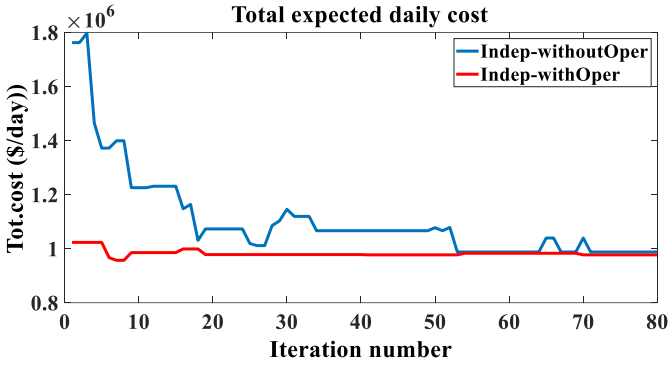

(a)

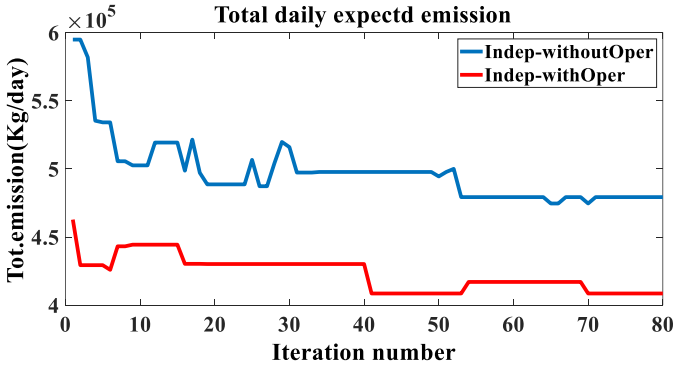

(b)

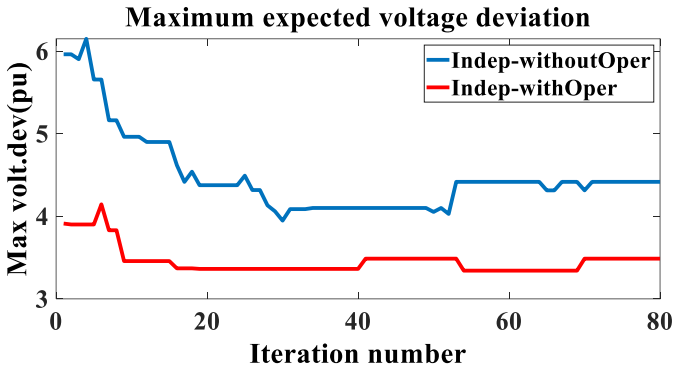

(c)

Figure 7.8: Multi-objective functions as function of the iteration number: (a) total daily expected cost, (b) total daily expected emission and (c) maximum expected voltage deviation

In order to study the hourly SOC and the effect of allocating CAESs on the hourly load level, hourly total thermal generation power, hourly variable operation cost and arbitrage of CAESs and voltage profile, four wind power scenarios are chosen considering independent wind farms with and without including the operational strategy. Scenarios of percentage of penetration level equals to 0% (s=1), 13.908% (s=9), 23.902% (s=19) and 29.981% (s=4) are selected as examples for deep analysis. According to Figure 7.9 (a), (b), (c) and (d), all 13 allocated CAESs in case 2 through all the selected scenarios are in charging mode during low load level (1-8hrs) and discharging mode during high load level (10-19hrs) and floating mode during moderate load level (other hours). Every allocated CAES has only one cycle during charging and discharging process for duration of 24hours. This strategy increased the life time of allocated CAESs and effect positively on total cost as stated before.

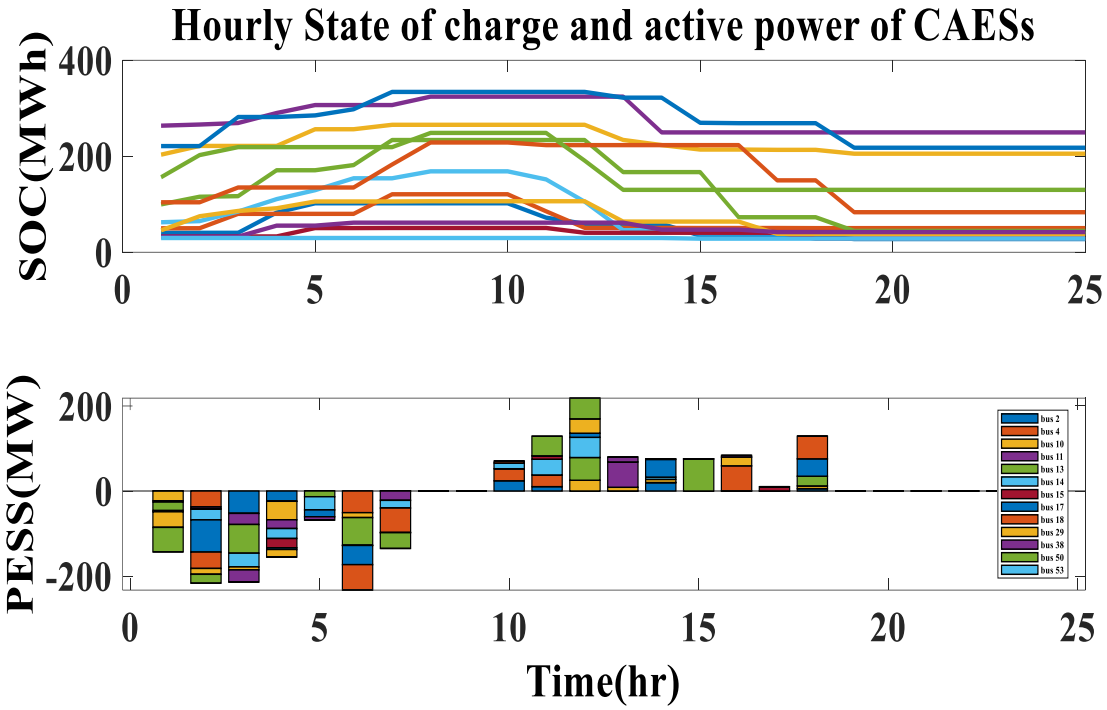
Hourly State of charge and active power of CAESs
SOC(MWh)
400
200
0
0
5
10
15
20
25
PESS(MW)
200
0
-200
0
5
10
15
20
25
Time(hr)
bus 2
bus 4
bus 10
bus 11
bus 13
bus 14
bus 15
bus 17
bus 18
bus 29
bus 38
bus 50
bus 53

(a)

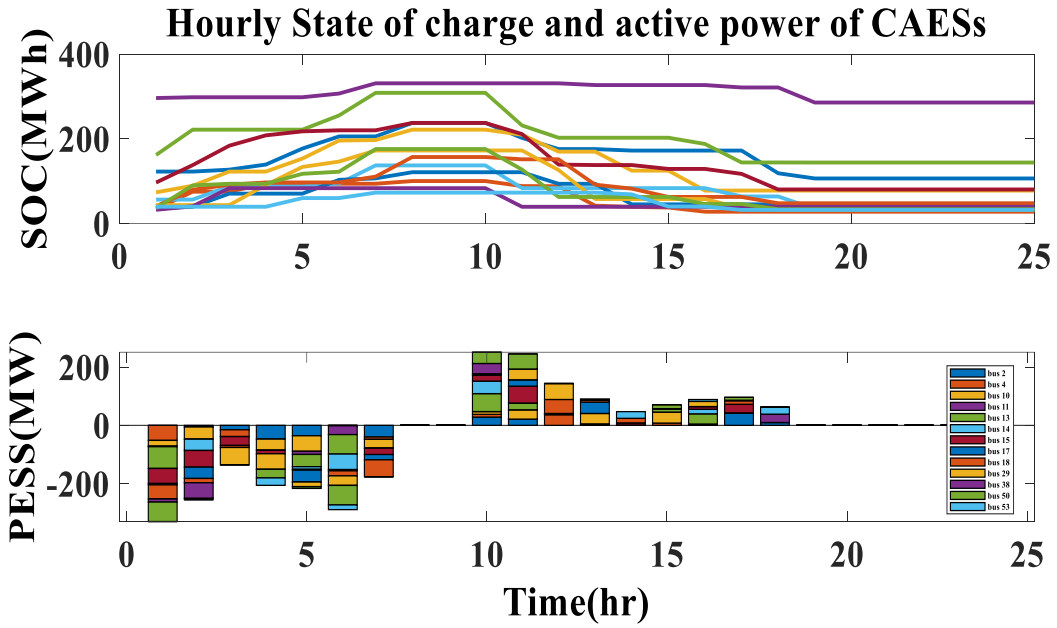
Hourly State of charge and active power of CAESs
SOC(MWh)
400
200
0
0
5
10
15
20
25
PESS(MW)
200
0
-200
0
5
10
15
20
25
Time(hr)
bus 2
bus 4
bus 10
bus 11
bus 13
bus 14
bus 15
bus 17
bus 18
bus 29
bus 38
bus 50
bus 53

(b)

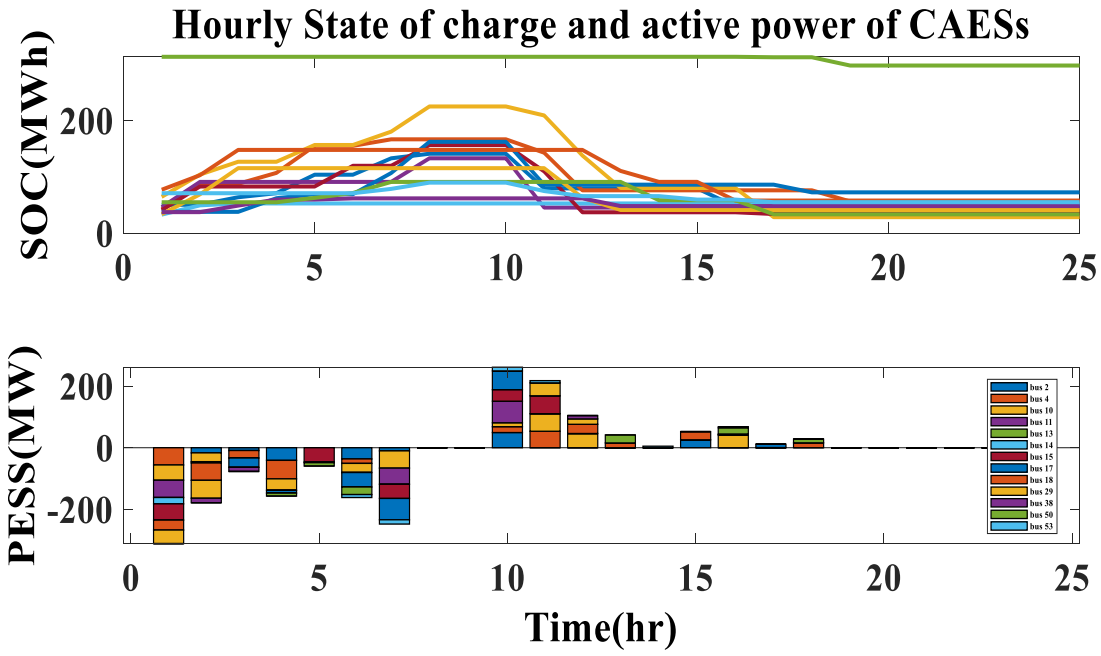

(c)

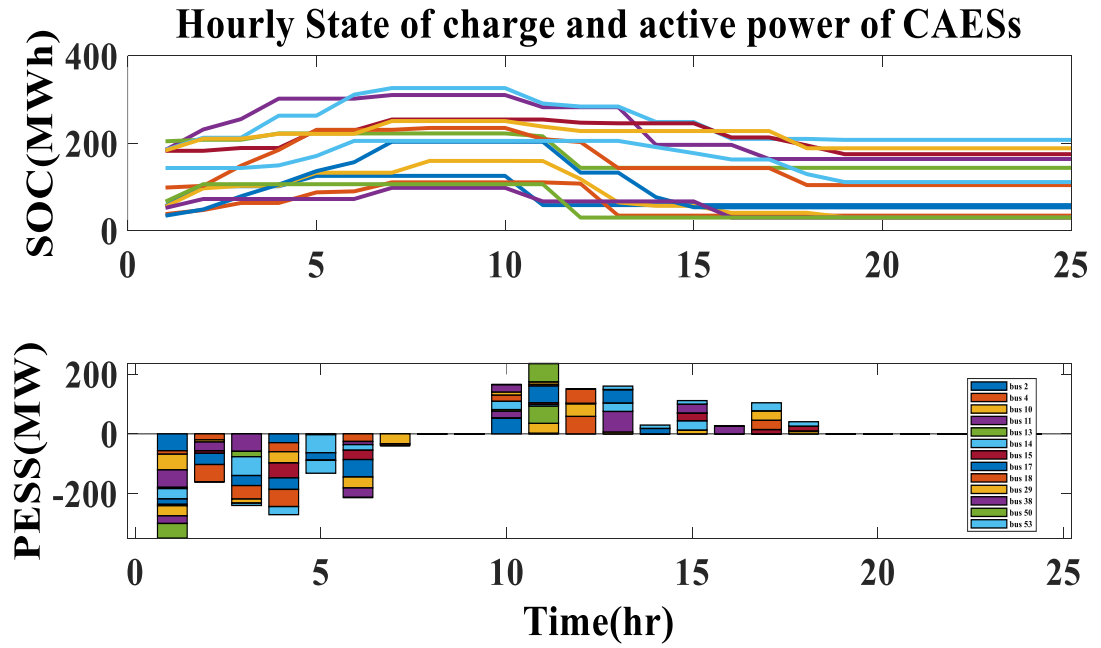

(d)

Figure 7.9: The hourly state of charge and active power of allocated CAESs considering independent wind farms and the operational strategy of ESSs: (a) in the 1st scenario, (b) in the 4th scenario, (c) in the 9th scenario and (d) in the 19th scenario

According to Figure 7.9 (a), (b), (c) and (d) and table 7.2, a maximum charging power of 233.1MW at t=6hr, 330.1MW at t=1hr, 311MW at t=1hr and 349.9MW at t=1hr occurs during scenarios s=1, s=4, s=9 and s=19. Because of the absence of wind power

in first scenario (0%), the total charging power of all allocated 13 CAESs is the lowest compared to other scenarios.

Table 7.2: Total charging and discharging power during certain periods for four different wind power scenarios considering independent wind farms with the operational strategy of ESS

Time (hour)	**Total PESS (MW)**			
	s=1	s=4	s=9	s=19
t=1	-143.3	-330.1	-311	-349.9
t=2	-216.7	-255.2	-178.4	-160.4
t=3	-214.2	-135.3	-76.95	-239.8
t=4	-155.3	-205.9	-156.8	-270.6
t=5	-68.29	-216.3	-59.44	-131.9
t=6	-233.1	-289.1	-161.6	-213
t=7	-135.1	-176.1	-247.6	-39.14
t=10	70.33	251	261.1	165
t=11	128.9	245.1	217.6	235.4
t=12	218.5	143.5	104.4	150.2
t=13	79.99	90.61	41.51	159.9
t=14	75.55	47.07	4.938	29.38
t=15	75.89	70.59	52.26	111.3
t=16	83.74	88.65	68.24	25.88
t=17	10.08	96.1	11.39	104
t=18	128.8	62.02	27.57	40.56

However, because of the high penetration level of wind power in s=19 and s=4, the total stored energy is the highest in these scenarios compared to the other two scenarios. Moreover, the stored energy during low load level in the previous hours is utilized very efficiently during the duration of range [10-13]hr in all scenarios especially in the 4th and 19th scenarios.

The adopted operational strategy of allocated CAESs considering independent wind farms would affect the load level especially the peak and valley load. According to Figure 7.10 (a), (b), (c) and (d), the base load, the load with CAESs and the total active power of all allocated CAESs during charging and discharging process considering

independent wind farms with and without including the peak shaving operational strategy are presented. During the charging mode which occurs in the duration of [1-8]hrs, the new total hourly load level in case 2 is the highest among base load and total load without considering the operational strategy. However, during the discharging mode which occurs in the duration of [10-18] hrs, the new total hourly load level in case 2 is the lowest among the base load and total load without considering the operational strategy. So, during all the selected scenarios with considering the operational strategy, the new total hourly load increased at the valley and low load points and decreased at the high and peak load points.

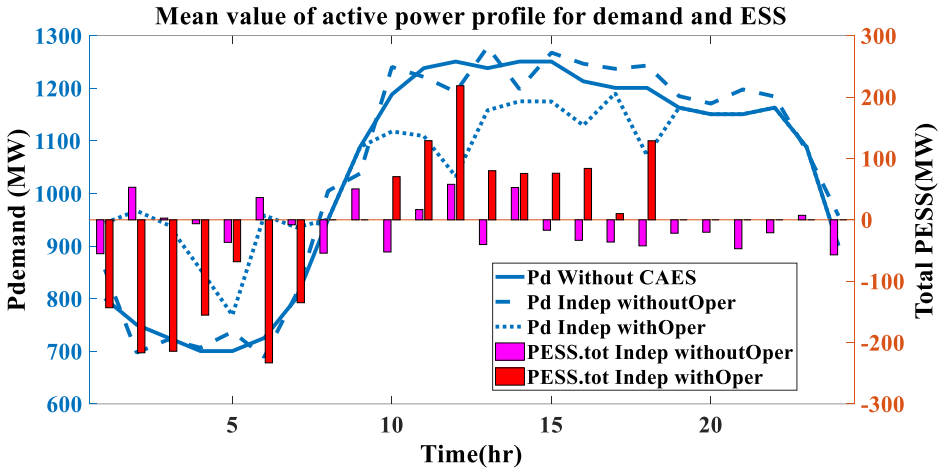

(a)

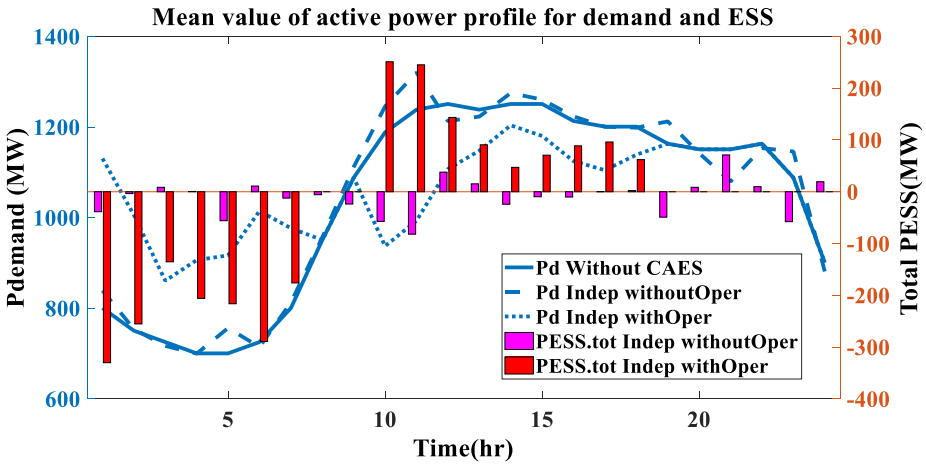

(b)

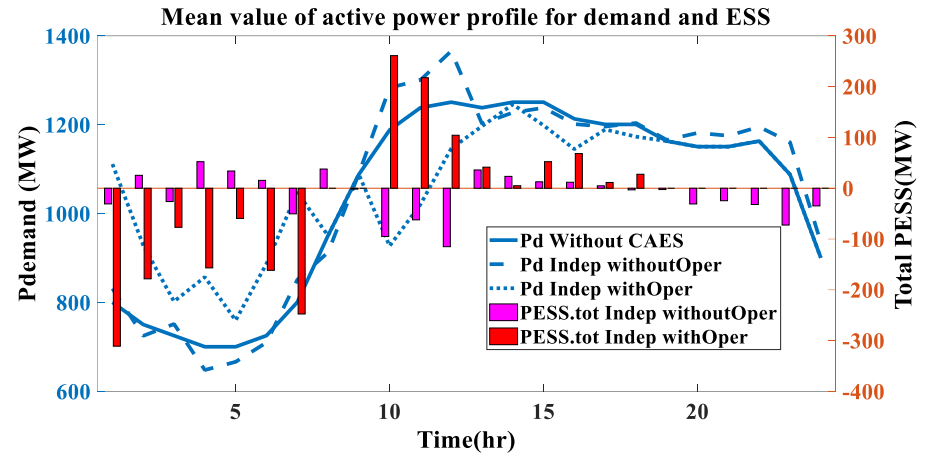

(c)

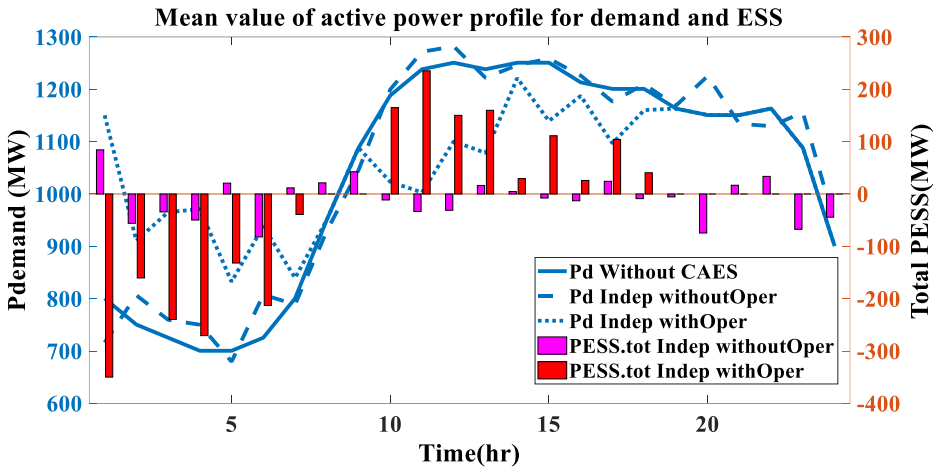

(d)

Figure 7.10: The total active load power and total active power of allocated CAESs considering independent wind farms and the two cases of with and without the operational strategy of ESSs: (a) in the 1st scenario, (b) in the 4th scenario, (c) in the 9th scenario and (d) in the 19th scenario

For example, according to Figure 7.10 (a), (b), (c) and (d) and table 7.3, during the 4th and 19th scenarios with wind power penetration level of 29.981% and 23.902%, the new total load at t=1hr scored its maximum percentage of rising equals to 41.24% and 43.71%. Also, during the highest wind power penetration level (s=4), the valley load point increased by 38.64% at t=4hr. Moreover, during discharging mode, the high and peak load points decreased to reach the maximum percentage of reduction equals to 19.80%, 17.58% and 19.01% at t=11hr (95% of peak load). However, in the case of without considering the peak shaving strategy, the total new load at some hours

decreased even lower than the valley point and increased even more than the peak point. For example, in Figure 7.10 (c), the valley load point at t=4hr decreased from 700.4MW to reach 648.2MW (7.453% reduction) and the peak load point at t=12hr increased from 1251MW to reach 1366MW (8.419% rising).

Table 7.3: Total hourly load for four different wind power scenarios considering independent wind farms with the operational strategy of ESS

Case 2										
Mode	Time (hour)	base load (MW)	New total load (MW)				Percentage of rising or reducing in new total load (%)			
			s=1	s=4	s=9	s=19	s=1	s=4	s=9	s=19
During charging	t=1	800.50	943.80	1130.60	1111.50	1150.40	17.90	41.24	38.85	43.71
	t=2	750.50	967.20	1005.70	928.90	910.90	28.87	34.00	23.77	21.37
	t=3	725.50	939.70	860.80	802.45	965.30	29.52	18.65	10.61	33.05
	t=4	700.40	855.70	906.30	857.20	971.00	**22.17**	**29.40**	**22.39**	**38.64**
	t=5	700.40	768.69	916.70	759.84	832.30	**9.75**	**30.88**	**8.49**	**18.83**
	t=6	725.50	958.60	1014.60	887.10	938.50	32.13	39.85	22.27	29.36
	t=7	808.60	943.70	984.70	1056.20	847.74	16.71	21.78	30.62	4.84
During discharging	t=10	1188.00	1117.67	937.00	926.90	1023.00	5.92	21.13	21.98	13.89
	t=11	1238.00	1109.10	992.90	1020.40	1002.60	**10.41**	**19.80**	**17.58**	**19.01**
	t=12	1251.00	1032.50	1107.50	1146.60	1100.80	**17.47**	**11.47**	**8.35**	**12.01**
	t=13	1238.00	1158.01	1147.39	1196.49	1078.10	**6.46**	**7.32**	**3.35**	**12.92**
	t=14	1251.00	1175.45	1203.93	1246.06	1221.62	**6.04**	**3.76**	**0.39**	**2.35**
	t=15	1251.00	1175.11	1180.41	1198.74	1139.70	**6.07**	**5.64**	**4.18**	**8.90**
	t=16	1213.00	1129.26	1124.35	1144.76	1187.12	6.90	7.31	5.63	2.13
	t=17	1201.00	1190.92	1104.90	1189.61	1097.00	0.84	8.00	0.95	8.66
	t=18	1201.00	1072.20	1138.98	1173.43	1160.44	10.72	5.16	2.30	3.38

As stated before and according to table 7.1, the daily expected thermal generation cost and emission in case 1 is more than case 2 by 7.38% and 14.76%. This can be proved according to Figure 7.11 (a), (b), (c) and (d). In the case of independent wind farms considering the peak shaving strategy, the total thermal generation power in all selected scenarios (s=1, s=4, s=9 and s=19) is higher in the first 8 hours or during charging mode and lower during high and peak load or discharging mode in the duration of range [9-18] hrs compared to case 1. For example, the total thermal generation power during discharging mode in the 1st, 4th, 9th and 19th scenarios at t=12hr, t=10hr, t=10hr and t=11hr equals to 1002MW, 594.8MW, 726.7MW and

718.5MW in case 2 and 1209MW, 924.4MW, 1226MW and 966.02MW in case 1. It is very clear that the system including all allocated CAESs is more dependent on thermal generators in case 1 compared to case 2 by a percentage reaches upto 17.12%, 35.65%, 40.73% and 25.62% in the 1st, 4th, 9th and 19th scenarios at t=12hr, t=10hr, t=10hr and t=11hr. The reason behind the higher dependency on thermal generators in case 1 during high and peak load points is because some of the three allocated CAESs are charging during this duration due to the lack of operational strategy. For instance, in Figure 7.11 (c) at t=10hr, 11hr and 12hr, the allocated CAESs are being charged with 95.08MW, 62.26MW and 115MW in case 1 using wind and thermal generators. However, during these durations, all 13 allocated CAESs in case 2 are discharging a total active power of 261.1MW, 217.6MW and 104.4MW into the system. Moreover, the required amount of power from thermal generators in case 2 equals to 1254MW at t=15hr, 867.7MW at t=15hr, 1107MW at t=15hr and 934.2MW at t=14hr during [10-18] hr. Comparing between these scenarios, it is very clear that during the 4th scenario the system is less dependent on thermal generators due to the highest penetration level of wind power equals to 30% approximately.

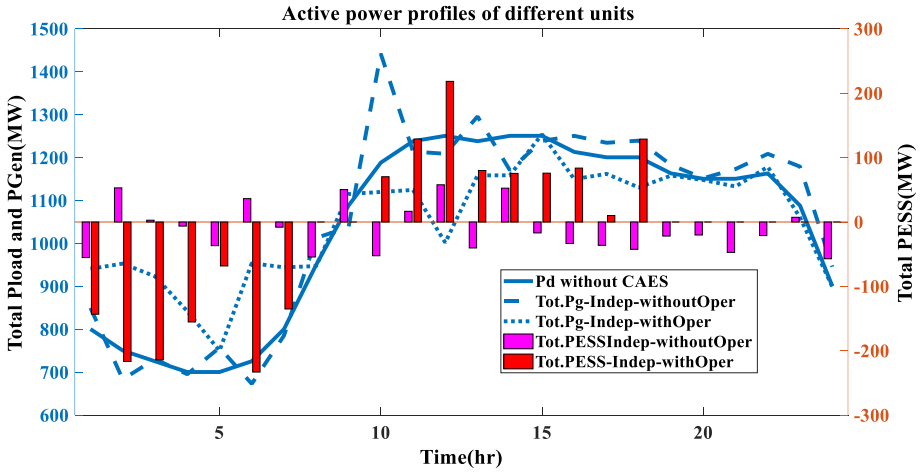

(a)

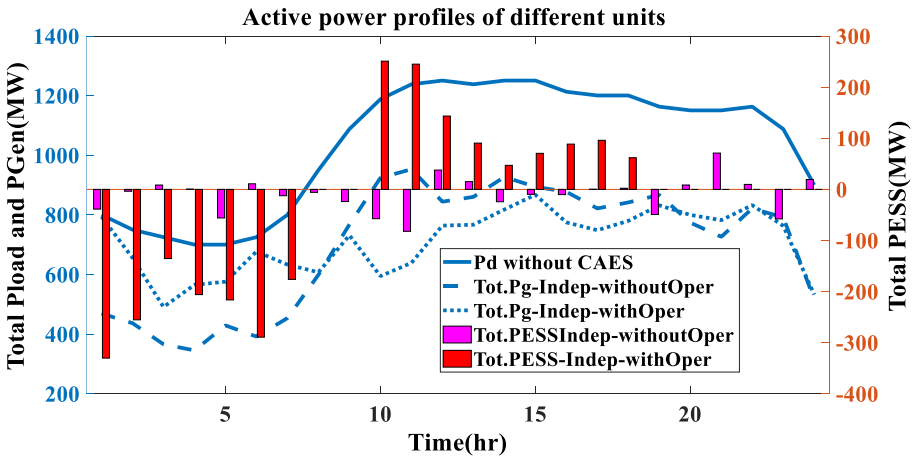

(b)

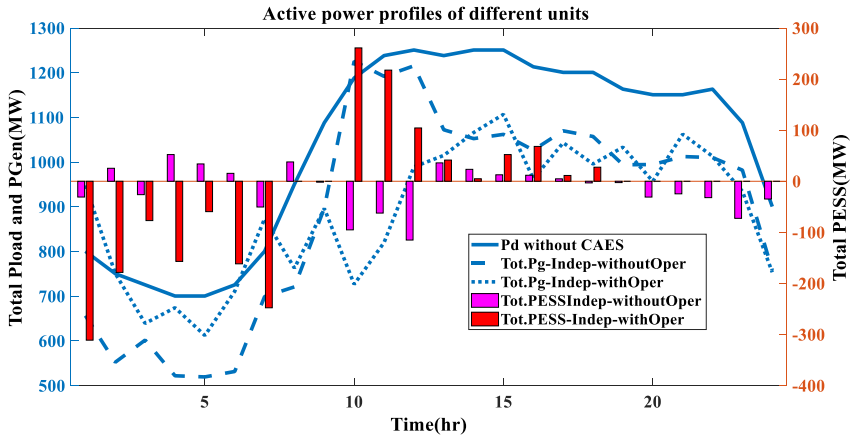

(c)

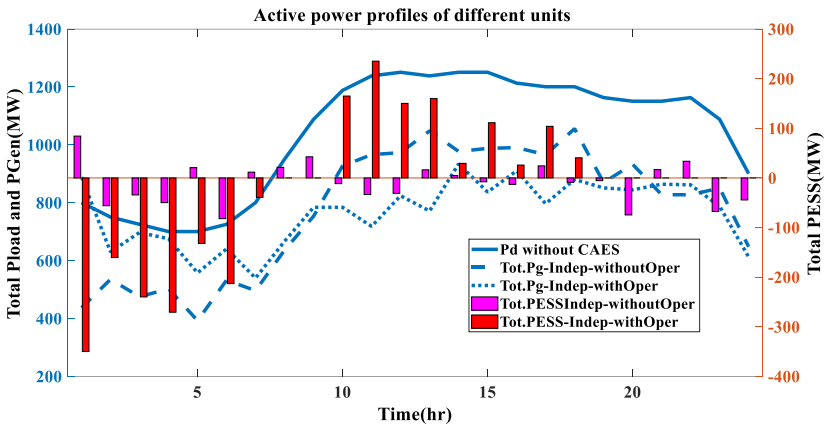

(d)

Figure 7.11:The total active load power, total active power of allocated CAESs and total active power of thermal generating units considering independent wind farms and the two cases of with and without the operational strategy of ESSs: (a) in the 1st scenario, (b) in the 4th scenario, (c) in the 9th scenario and (d) in the 19th scenario

Moreover, as stated before and according to table 7.1, the daily expected variable operation cost of all allocated CAESs in case 2 is more than case 1 by 41.3% because of the higher number of the optimally allocated CAESs. However, case 2 resulted in earning high daily expected arbitrage benefits because of the utilized peak shaving strategy and case 1 resulted in no any arbitrage benefits because of the absence of any operation strategy for the allocated CAESs. This can be proved according to Figure 7.12 (a), (b), (c) and (d). In the case of independent wind farms considering the peak shaving strategy, the total variable operation cost of all 13 allocated CAESs in all selected scenarios (s=1, s=4, s=9 and s=19) is higher than that of case 1 during the whole duration except during floating mode where the operation cost becomes zero. Also, in all selected scenarios, the arbitrage is negative during charging mode duration [1-8] hrs and has lower value compared to case 1 and highly positive during discharging mode [9-18] hrs and much higher value compared to case 1 and this is because of the adopted peak shaving strategy in case 2. Comparing the values of the arbitrage benefits in case 2 between the 1st and 4th scenarios according to Figure 7.12 (a) and (b), the minimum arbitrage values are -17340$ and -26410$ and the maximum arbitrage benefit values are 34960$ and 40160$. It is clear that more benefits can be earned in the 4th scenario compared to the 1st scenario and this is the logical manner because the maximum wind power penetration level (30%) occurs in the 4th scenario while the worst wind power scenario occurs in the 1st scenario (0% wind power).

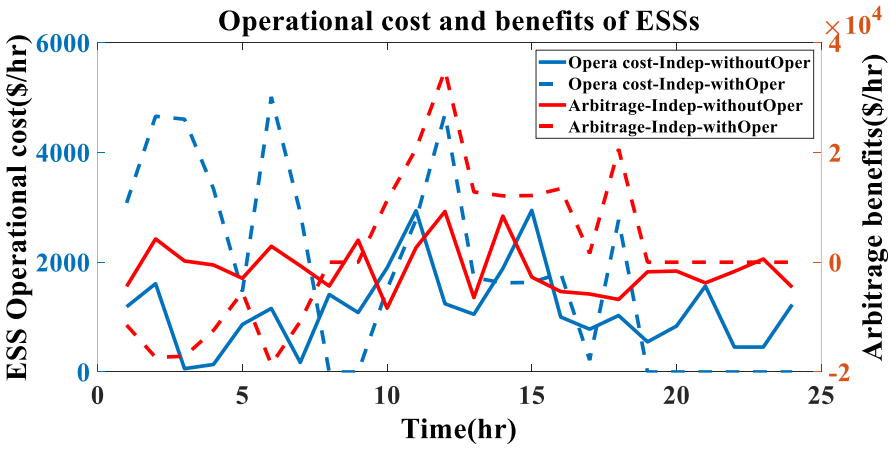
Operational cost and benefits of ESSs
Opera cost-Indep-withoutOper
Opera cost-Indep-withOper
Arbitrage-Indep-withoutOper
Arbitrage-Indep-withOper
ESS Operational cost($/hr)
Arbitrage benefits($/hr)
Time(hr)
×10^4

(a)

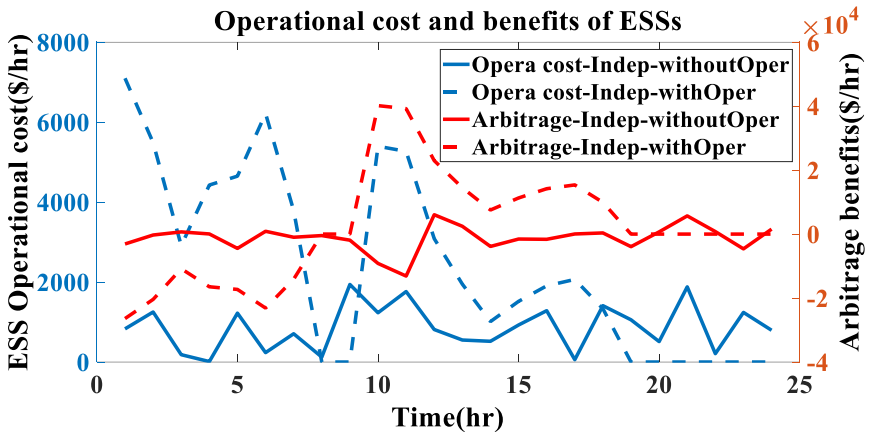
Operational cost and benefits of ESSs
Opera cost-Indep-withoutOper
Opera cost-Indep-withOper
Arbitrage-Indep-withoutOper
Arbitrage-Indep-withOper
ESS Operational cost($/hr)
Arbitrage benefits($/hr)
Time(hr)
×10^4

(b)

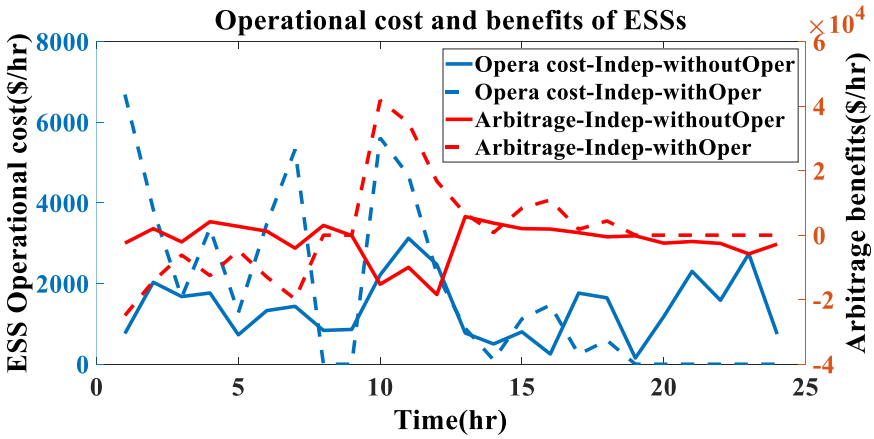
Operational cost and benefits of ESSs
Opera cost-Indep-withoutOper
Opera cost-Indep-withOper
Arbitrage-Indep-withoutOper
Arbitrage-Indep-withOper
ESS Operational cost($/hr)
Arbitrage benefits($/hr)
Time(hr)
×10^4

(c)

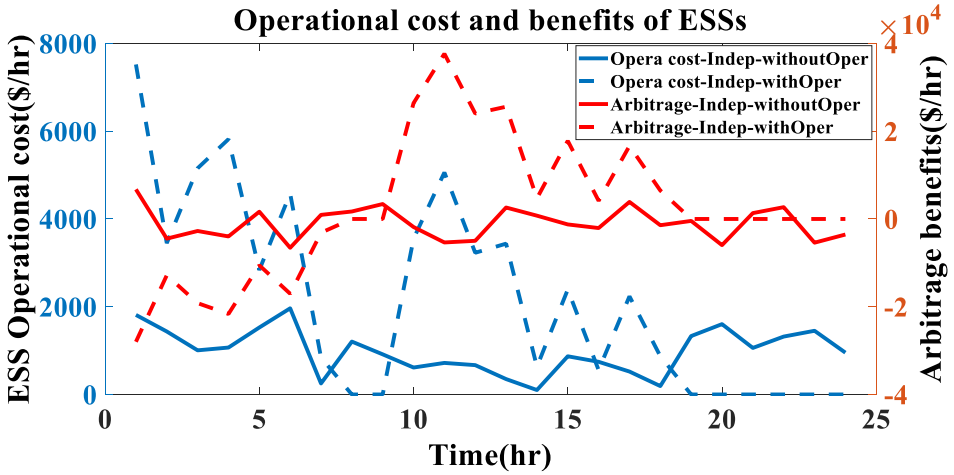

(d)

Figure 7.12:The total variable operational cost and arbitrage benefit of CAESs considering independent wind farms and the two cases of with and without the operational strategy of ESSs: (a) in the 1st scenario, (b) in the 4th scenario, (c) in the 9th scenario and (d) in the 19th scenario

Furthermore, as mentioned before in table 7.1, the maximum expected voltage deviation in the case of considering the peak shaving strategy would be less by 21%. According to the Figure 7.13 (a) and (b), the peak load points at t=15hr in the 1st and 4th scenarios are considered in order to compare the minimum and maximum per unit voltages at all buses in case 1 and case 2. During the peak load at t=15hr, the maximum voltage at all buses in both cases is less than the maximum allowed voltage limit as it can be seen in table 7.4 and Figure 7.13 (a) and (b) and the problem is in case 2 where the minimum voltage at bus 17 in the 1st scenario and bus 14 in the 4th scenario experienced a minimum voltage of 0.9263pu and 0.9286pu which is less than the allowed minimum voltage (0.94pu). So, the minimum bus voltages during peak load contributes in building the maximum expected voltage deviation to reach 4.417pu and 3.487pu in case 1 and case 2.

Table 7.4: Minimum and maximum voltages at peak load in the 1st and 4th scenario in case1 and case 2

Studied cases	**t=15hr**	
	s=1	s=4

	min.volt	max.volt	min.volt	max.volt
Case 1	Bus 3 (0.9437pu)	Bus 25 (1.04pu)	Bus 3 (0.9437pu)	Bus 25 (1.045pu)
Case 2	Bus 17 (0.9263pu)	Bus 18 (1.031pu)	Bus 14 (0.9286pu)	Bus 18 (1.032pu)

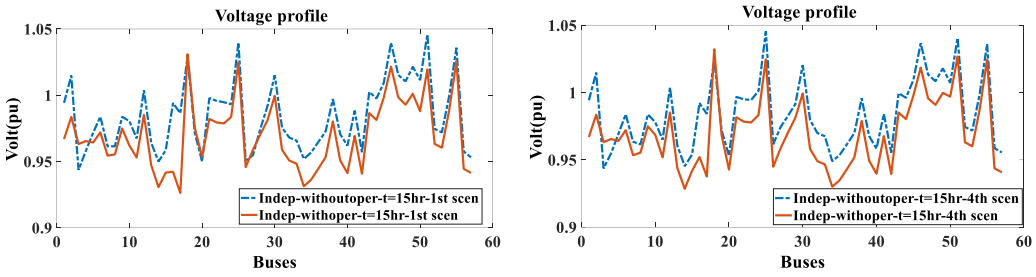

(a) (b)

Figure 7.13: Voltage profile considering independent wind farms in the cases of with and without the operational strategy of ESSs: (a) in the 1st scenario during the peak load at t=15hr and (b) in the 4th scenario during the peak load at t=15hr.

However, in the correlated case, the probability of having such penetration level is 0.045 which is much higher than that of independent case which equals to 0.028. The higher probability of having the maximum wind power penetration in correlated case could affect positively on the expected daily values.

Table 7.5:The obtained optimal values in case 2 and case 3

Optimal Values	**Studied Cases**	
	Case 2	Case 3
	Independent WFs With OPS	Correlated WFs With OPS
CAESs (bus, capacity, and power rating)	bus 2 (270MWh,60MW), bus 4 (270MWh,60MW), bus 10 (270.756MWh,60.168MW), bus 11 (352.141MWh,78.254MW), bus 13 (344.202MWh76.489MW), bus 14 (328.969MWh,73.104MW), bus 15 (270MWh,60MW), bus 17 (340.887MWh,75.753MW), bus 18 (270MWh,60MW), bus 29 (270MWh, 59.571MW), bus 38 (270MWh, 60MW), bus 50 (301.209MWh,66.935MW) and bus 53 (270MWh, 60MW)	bus 4 (270MWh,60MW), bus 5 (270MWh60MW), bus 7 (270MWh,60MW), bus 9 (317.184MWh,70.485MW), bus 11 (270MWh,60MW), bus 13 (270MWh,60MW), bus 27 (270MWh,60MW), bus 29 (270MWh,60MW), bus 38 (270MWh,60MW), bus 46 (293.231MWh,65.162MW), bus 47 (270.082MWh,60.018MW) and bus 53 (270MWh,60MW)

Life time (years)	All ESSs (41.096)	All ESSs (41.096)
CAES Investment Cost ($)	734217478.377	635247383.255
CAES Variable Operational Cost ($/day)	49556.775	39842.874
CAES Fixed Operational Cost ($/day)	5823.795	5038.807
CAES arbitrage ($/day)	46918.228	36544.984
Wind Gen Operational Cost ($/day)	191945.209	176667.023
Thermal Gen Operational Cost ($/day)	763445.149	805236.535
Total variable operational cost ($/day)	958028.904	985201.448
Finner ($/day)	716526.921	768691.551
F1 (Total daily cost) ($/day)	977147.980	991147.980
F2 (Total Emission) (Kg/day)	408603.077	424766.729
F3 (Max Volt.dev) (pu)	3.487	3.670

Moreover, in the 22th scenario, the wind power penetration level reached 25.217% and 23.485% in both independent and correlated cases with associated probabilities equal to 0.141 and 0.086. So, in this scenario, case 2 has higher wind power penetration as well as higher associated joint probability compared to case 3. This can affect more positively on the expected values in case 2 compared to case 3.

According to table 7.5, the three objective functions to be minimized F_1, F_2 and F_3 in case 2 are lower than that of case 3 by 1.413%, 3.805% and 5% to reach 977147.980$/day, 408603.077 kg/day and 3.487pu in case 2 and 991147.980 $/day, 424766.729kg/day and 3.670pu in case 3. Although, less ESS's investment cost by 13.48% with the same life time equals to 41.096 years are obtained in the correlated case, the independent case is better in achieving more economic, environmental and technical benefits. More economic benefits are achieved in case 2 because of the higher obtained daily expected arbitrage benefits and less daily expected thermal generation cost as it can be seen in table 7.5. Also, more environmental and technical benefits are achieved in case 2 because of the lower daily expected emission and maximum voltage deviation.

Chapter 8

CONCLUSIONS AND FUTURE WORK

8.1 Conclusions

This thesis was composed of two sections. In the first section of this thesis, the main objective was developing a hybrid probabilistic optimisation algorithm for optimal allocation of energy storage systems considering correlated wind farms. In the second section, an optimal planning and operational strategy of energy storage systems in power transmission networks has been proposed by relying on analysis of wind farms.

In the first section, bi-variate wind power distribution was modelled using clayton copulas and discretised by a developed mathematical discretization method based five-point estimation method. The joint wind power distribution was discretised into 25 scenarios in both independent and correlated wind farms. Moreover, three objective functions were minimized simultaneously, expected total cost, expected voltage deviation and expected emission. Simulation results proves the superiority of the hybrid NSGAII-MOPSO-PLF in minimizing the total expected cost and emission compare with NSGAII-PLF alone or MOPSO-PLF alone. For the first time, the results prove that considering the correlation among wind farms resulted in lower cost and emission compared to the case of independent wind farms at peak load.

In the second section, two-stage mixed integer non-linear optimisation problem is proposed to determine the optimal configuration (location, power ratings and capacity)

of a compressed air storage system, by considering the wind power uncertainties of independent and correlated wind farms as well as a peak shaving operational strategy. The generated 25 scenarios in the first section for two independent and correlated wind farms are utilized. The TS, PLF and OPS were utilised to minimise the difference between the total daily expected operational cost of conventional generators and energy arbitrage benefits obtained from ESSs in the lower-level optimisation problem. Conversely, the total daily expected planning and operational cost, total daily expected emission and maximum expected voltage deviation were minimised in the upper-level optimisation problem using the hybrid NSGAII–MOPSO algorithm which proved its superiority over NSGAII alone or MOPSO alone in the first section. The simulation results confirmed the advantage of considering the benefits of a peak shaving OPS from economic, technical and environmental points of view. Moreover, these benefits are superior in independent wind farms with OPS to those acquired from correlated wind farms with OPS for a duration of 24 hours.

8.2 Future work

Some suggestions and recommendations can be listed for future research on the optimal configuration of ESSs for power system planning and operation both in distribution and transmission system:

- All the research works mentioned in the literature solved the best configuration problem of ESSs based on a balanced power transmission system; therefore, the effect of unbalanced systems on the optimal configuration of ESSs could be investigated in future research.
- In the literature, the type of ESS was selected rather than optimised; therefore, more than one type of ESS should be considered as a decision variable for solving optimisation problems. An optimised type of ESS can positively affect

the studied objective functions; hence, optimising the type of ESS should be investigated in future research.

- Hybridisation of analytic methods, such as sensitivity approaches and meta-heuristic optimisation, can reduce search space and, hence, simulation time, but this combination was rarely utilised in the literature. Such hybrid methods could be used to obtain a solution very close to a global one with less computational effort.
- None of the mentioned research works considered coordination between ESSs and other devices. Such optimal coordination between storage and compensating devices in a hybrid power system could be investigated in future studies.
- None of the mentioned research works studied the optimal planning of ESS, DG and network reconfiguration considering protection coordination. So, future research work can be recommended entitled as ‘’ optimal planning of ESS, DG and network reconfiguration considering protection coordination, control strategy and uncertainties in distribution system.

REFERENCES

[1] Gaur, D., & Mathew, L. (2018, March). Optimal placement of FACTS devices using optimization techniques: A review. In *3rd International Conference on communication Systems, IOP Conference Series, Material Science and Engineering* (pp. 1-16).

[2] Root, C. E. (2006). The future beckons [electric power industry]. *IEEE Power and Energy Magazine*, 4(1), 24-31.

[3] Sirjani, R., & Jordehi, A. R. (2017). Optimal placement and sizing of distribution static compensator (D-STATCOM) in electric distribution networks: A review. *Renewable and Sustainable Energy Reviews*, 77, 688-694.

[4] Energy Information Administration, & Energy Department (Eds.). (2015). Annual energy outlook 2015: With projections to 2040. *Government Printing Office.*

[5] Sultana, U., Khairuddin, A. B., Aman, M. M., Mokhtar, A. S., & Zareen, N. (2016). A review of optimum DG placement based on minimization of power losses and voltage stability enhancement of distribution system. *Renewable and Sustainable Energy Reviews*, 63.

[6] U.S. Wind Energy Projects Wisconsin. (2019, January 30). Retrieved from https://cleangridalliance.org/our-work/projects?gp=wisconsin.

[7] Ahmad, A. A., Sirjani, R., & Daneshvar, S. (2020). New hybrid probabilistic optimisation algorithm for optimal allocation of energy storage systems considering correlated wind farms. *Journal of Energy Storage*, 29, 101335.

[8] Saboori, H., Hemmati, R., Ghiasi, S. M. S., & Dehghan, S. (2017). Energy storage planning in electric power distribution networks–A state-of-the-art review. *Renewable and sustainable energy reviews*, 79, 1108-1121.

[9] Das, C. K., Bass, O., Kothapalli, G., Mahmoud, T. S., & Habibi, D. (2018). Overview of energy storage systems in distribution networks: Placement, sizing, operation, and power quality. *Renewable and Sustainable Energy Reviews*, 91, 1205-1230.

[10] Wong, L. A., Ramachandaramurthy, V. K., Taylor, P., Ekanayake, J. B., Walker, S. L., & Padmanaban, S. (2019). Review on the optimal placement, sizing and control of an energy storage system in the distribution network. *Journal of Energy Storage*, 21, 489-5.

[11] Zhao, H., Wu, Q., Hu, S., Xu, H., & Rasmussen, C. N. (2015). Review of energy storage system for wind power integration support. *Applied energy*, 137, 545-553.

[12] Li, X., & Wang, S. (2019). A review on energy management, operation control and application methods for grid battery energy storage systems. *CSEE Journal of Power and Energy Systems.*

[13] Yang, Y., Bremner, S., Menictas, C., & Kay, M. (2018). Battery energy storage system size determination in renewable energy systems: A review. *Renewable and Sustainable Energy Reviews*, 91, 109-125.

[14] Sheibani, M. R., Yousefi, G. R., Latify, M. A., & Dolatabadi, S. H. (2018). Energy storage system expansion planning in power systems: a review. *IET Renewable Power Generation*, 12(11), 1203-1221.

[15] Hannan, M. A., Faisal, M., Ker, P. J., Begum, R. A., Dong, Z. Y., & Zhang, C. (2020). Review of optimal methods and algorithms for sizing energy storage systems to achieve decarbonization in microgrid applications. *Renewable and Sustainable Energy Reviews.*

[16] Energy Storage Statsitics and Facts. (2020, September 7). Retreived from https://www.statista.com/topics/4632/energy storage/#dossierSumary_chapter1.

[17] U.S. energy storage battery price development 2013-2022. (2021, January 29). Retreived from https://www.statista.com/statistics/860600/price-development-of-energy-storage-batteries-us/.

[18] Shaheen, A. M., Spea, S. R., Farrag, S. M., & Abido, M. A. (2018). A review of meta-heuristic algorithms for reactive power planning problem. *Ain Shams Engineering Journal*, 9(2), 215-231.

[19] Ahmad, A. A., & Sirjani, R. (2019). Optimal placement and sizing of multi-type FACTS devices in power systems using metaheuristic optimisation techniques: An updated review. *Ain Shams Engineering Journal.*

[20] Sedghi, M., Ahmadian, A., & Aliakbar-Golkar, M. (2015). Optimal storage planning in active distribution network considering uncertainty of wind power distributed generation. *IEEE Transactions on Power Systems*, 31(1), 304-316.

[21] Wen, S., Lan, H., Fu, Q., Yu, D., Hong, Y. Y., & Cheng, P. (2017). Optimal allocation of energy storage system considering multi-correlated wind farms. *Energies*, 10(5), 625.

[22] Díaz-González, F., Sumper, A., Gomis-Bellmunt, O., & Villafáfila-Robles, R. (2012). A review of energy storage technologies for wind power applications. *Renewable and sustainable energy reviews*, 16(4), 2154-2171.

[23] Sundararagavan, S., & Baker, E. (2012). Evaluating energy storage technologies for wind power integration. *Solar Energy*, 86(9), 2707-2717.

[24] Venkataramani, G., Parankusam, P., Ramalingam, V., & Wang, J. (2016). A review on compressed air energy storage–A pathway for smart grid and polygeneration. *Renewable and Sustainable Energy Reviews*, 62, 895-907.

[25] Schoenung, S. M., & Hassenzahl, W. V. (2003). Long-vs. short-term energy storage technologies analysis: a life-cycle cost study: a study for the DOE energy storage systems program (No. SAND2003-2783). *Sandia National Laboratories.*

[26] Park, H., & Baldick, R. (2017). Integration of compressed air energy storage systems co-located with wind resources in the ERCOT transmission system. *International Journal of Electrical Power & Energy Systems*, 90, 181-189.

[27] Ghofrani, M., Arabali, A., Etezadi-Amoli, M., & Fadali, M. S. (2013). A framework for optimal placement of energy storage units within a power system with high wind penetration. *IEEE Transactions on Sustainable Energy*, 4(2), 434-442.

[28] Castronuovo, E. D., & Lopes, J. P. (2004). On the optimization of the daily operation of a wind-hydro power plant. *IEEE Transactions on Power Systems*, 19(3), 1599-1606.

[29] Anagnostopoulos, J. S., & Papantonis, D. E. (2008). Simulation and size optimization of a pumped–storage power plant for the recovery of wind-farms rejected energy. *Renewable Energy*, 33(7), 1685-1694.

[30] Zafirakis, D., & Kaldellis, J. K. (2009). Economic evaluation of the dual mode CAES solution for increased wind energy contribution in autonomous island networks. *Energy policy*, 37(5), 1958-1969.

[31] Daneshi H, Daneshi A, Tabari NM, Jahromi AN. Security-constrained unitcommitment in a system with wind generation and compressed air energystorage. In: *6th international conference on the european energy market.*2009.

[32] Dursun, B., & Alboyaci, B. (2010). The contribution of wind-hydro pumped storage systems in meeting Turkey's electric energy demand. *Renewable and Sustainable Energy Reviews*, 14(7), 1979-1988.

[33] Wong, L. A., Ramachandaramurthy, V. K., Walker, S. L., Taylor, P., & Sanjari, M. J. (2019). Optimal placement and sizing of battery energy storage system for losses reduction using whale optimization algorithm. *Journal of Energy Storage*, 26, 100892.

[34] Yuan, Z., Wang, W., Wang, H., & Yildizbasi, A. (2020). A new methodology for optimal location and sizing of battery energy storage system in distribution networks for loss reduction. *Journal of Energy Storage*, 29, 101368.

[35] Khorramdel, H., Aghaei, J., Khorramdel, B., & Siano, P. (2015). Optimal battery sizing in microgrids using probabilistic unit commitment. *IEEE Transactions on Industrial Informatics*, 12(2), 834-843.

[36] Lazzeroni, P., & Repetto, M. (2019). Optimal planning of battery systems for power losses reduction in distribution grids. *Electric Power Systems Research*, 167, 94-112.

[37] Jiang, X., Jin, Y., Zheng, X., Hu, G., & Zeng, Q. (2020). Optimal configuration of grid-side battery energy storage system under power marketization. *Applied Energy*, 272, 115242.

[38] Awad, A. S., El-Fouly, T. H., & Salama, M. M. (2014). Optimal ESS allocation and load shedding for improving distribution system reliability. *IEEE Transactions on Smart Grid*, 5(5), 2339-2349.

[39] Mehrjerdi, H. (2019). Simultaneous load leveling and voltage profile improvement in distribution networks by optimal battery storage planning. *Energy*, 181, 916-926.

[40] Zheng, Y., Song, Y., Huang, A., & Hill, D. J. (2019). Hierarchical Optimal Allocation of Battery Energy Storage System for Multiple Services in Distribution Systems. *IEEE Transactions on Sustainable Energy*.

[41] Wen, S., Lan, H., Fu, Q., David, C. Y., & Zhang, L. (2014). Economic allocation for energy storage system considering wind power distribution. *IEEE Transactions on power Systems,* 30(2), 644-652.

[42] Jani, V., & Abdi, H. (2018). Optimal allocation of energy storage systems considering wind power uncertainty. *Journal of Energy Storage*, 20, 244-253.

[43] Saboori, H., Hemmati, R., & Jirdehi, M. A. (2015). Reliability improvement in radial electrical distribution network by optimal planning of energy storage systems. *Energy*, 93, 2299-2312.

[44] Karimi, A., Aminifar, F., Fereidunian, A., & Lesani, H. (2019). Energy storage allocation in wind integrated distribution networks: An MILP-Based approach. *Renewable energy*, 134, 1042-1055.

[45] Liu, W., Niu, S., & Xu, H. (2017). Optimal planning of battery energy storage considering reliability benefit and operation strategy in active distribution system. *Journal of Modern Power Systems and Clean Energy*, 5(2), 177-186.

[46] Miao, D., & Hossain, S. (2020). Improved gray wolf optimization algorithm for solving placement and sizing of electrical energy storage system in micro-grids. *ISA transactions.*

[47] Ahmad, A. K. A., & Sirjani, R. (2020, April). Optimal Allocation of Energy Storage System in Transmission System Considering Wind Power. In *2020 7th*

International Conference on Electrical and Electronics Engineering (ICEEE) (pp. 181-187). IEEE.

[48] Nick, M., Cherkaoui, R., & Paolone, M. (2014). Optimal allocation of dispersed energy storage systems in active distribution networks for energy balance and grid support. *IEEE Transactions on Power Systems,* 29(5), 2300-2310.

[49] Calero, I., Canizares, C. A., & Bhattacharya, K. (2019). Compressed air energy storage system modeling for power system studies. *IEEE Transactions on Power Systems,* 34(5), 3359-3371.

[50] Qu, L., & Qiao, W. (2010). Constant power control of DFIG wind turbines with supercapacitor energy storage. *IEEE Transactions on Industry Applications,* 47(1), 359-367.

[51] Ray, P. K., Mohanty, S. R., & Kishor, N. (2011). Proportional–integral controller based small-signal analysis of hybrid distributed generation systems. *Energy Conversion and Management,* 52(4), 1943-1954.

[52] Denholm, P., & Sioshansi, R. (2009). The value of compressed air energy storage with wind in transmission-constrained electric power systems. *Energy Policy,* 37(8), 3149-3158.

[53] Selim, A., Kamel, S., Jurado, F., Lopes, J. A. P., & Matos, M. (2020). Optimal setting of PV and battery energy storage in radial distribution systems using

multi-objective criteria with fuzzy logic decision-making. *IET Generation, Transmission & Distribu.*

[54] Singh, P., Meena, N. K., Slowik, A., & Bishnoi, S. K. (2020). Modified african buffalo optimization for strategic integration of battery energy storage in distribution networks. *IEEE Access*, 8, 14289-14301.

[55] Mottola, F., Proto, D., Varilone, P., & Verde, P. (2020). Planning of Distributed Energy Storage Systems inμ Grids Accounting for Voltage Dips. *Energies*, 13(2), 401.

[56] Trivedi, A., Aih, H. C., & Srinivasan, D. (2020). A stochastic cost–benefit analysis framework for allocating energy storage system in distribution network for load leveling. *Applied Energy*, 280, 115944.

[57] Liu, Y., Wu, X., Du, J., Song, Z., & Wu, G. (2020). Optimal sizing of a wind-energy storage system considering battery life. *Renewable Energy*, 147, 2470-2483.

[58] Li, J., Hu, D., Mu, G., Wang, S., Zhang, Z., Zhang, X., ... & Wang, J. (2020). Optimal control strategy for large-scale VRB energy storage auxiliary power system in peak shaving. *International Journal of Electrical Power & Energy Systems*, 120, 106007.

[59] Jin, R., Song, J., Liu, J., Li, W., & Lu, C. (2020). Location and Capacity Optimization of Distributed Energy Storage System in Peak-Shaving. *Energies*, 13(3), 513.

[60] AL Ahmad A, Sirjani R. (2021). Optimal planning and operational strategy ofenergy storage systems in power transmissionnetworks: An analysis of wind farms. *International Journal of Energy Resesarch.*

[61] Opathella, C., Elkasrawy, A., Mohamed, A. A., & Venkatesh, B. (2020). MILP formulation for generation and storage asset sizing and sitting for reliability constrained system planning. *International Journal of Electrical Power & Energy Systems*, 116, 105529.

[62] Lata, P., & Vadhera, S. (2020). TLBO-based approach to optimally place and sizing of energy storage system for reliability enhancement of radial distribution system. *International Transactions on Electrical Energy Systems,* 30(5), e12334.

[63] Gyuk, I. P., & Eckroad, S. (2004). Energy storage for grid connected wind generation applications. *US Department of Energy.*

[64] Kang, T., Yao, J., Duong, T., Yang, S., & Zhu, X. (2017). A hybrid approach for power system security enhancement via optimal installation of flexible AC transmission system (FACTS) devices. *Energies*, 10(9), 1305.

[65] Jordehi, A. R., Jasni, J., Abd Wahab, N., Kadir, M. Z., & Javadi, M. S. (2015). Enhanced leader PSO (ELPSO): a new algorithm for allocating distributed TCSC's in power systems. *International Journal of Electrical Power & Energy Systems*, 64, 771-784.

[66] Rezaee Jordehi, A., & Jasni, J. (2013). Parameter selection in particle swarm optimisation: a survey. *Journal of Experimental & Theoretical Artificial Intelligence*, 25(4), 527-542.

[67] Ai, X., Wen, J., Wu, T., & Lee, W. J. (2013). A discrete point estimate method for probabilistic load flow based on the measured data of wind power. *IEEE Transactions on Industry Applications,* 49(5), 2244-2252.

[68] Fu, Q., Yu, D., & Ghorai, J. (2011, July). Probabilistic load flow analysis for power systems with multi-correlated wind sources. In 2011 IEEE power and energy society general meeting (pp. 1-6). *IEEE.*

[69] Borkowska, B. (1974). Probabilistic load flow. *IEEE Transactions on Power Apparatus and Systems*, (3), 752-759.

[70] Morales, J. M., Baringo, L., Conejo, A. J., & Mínguez, R. (2010). Probabilistic power flow with correlated wind sources. *IET generation, transmission & distribution*, 4(5), 641-651.

[71] Ciapessoni, E., Cirio, D., Pitto, A., Massucco, S., & Silvestro, F. (2014, October). A novel approach to account for uncertainty and correlations in probabilistic power flow. *In IEEE PES Innovative Smart Grid Technologies, Europe* (pp. 1-6). IEEE.

[72] Usaola, J. (2010). Probabilistic load flow with correlated wind power injections. *Electric Power Systems Research*, 80(5), 528-536.

[73] Verbic, G., & Canizares, C. A. (2006). Probabilistic optimal power flow in electricity markets based on a two-point estimate method. *IEEE transactions on Power Systems*, 21(4), 1883-1893.

[74] Morales, J. M., & Perez-Ruiz, J. (2007). Point estimate schemes to solve the probabilistic power flow. *IEEE Transactions on power systems*, 22(4), 1594-1601.

[75] Li, Y., Li, W., Yan, W., Yu, J., & Zhao, X. (2014). Probabilistic optimal power flow considering correlations of wind speeds following different distributions. *IEEE Transactions on Power Systems*, 29(4), 1847-1854.

[76] Saunders, C. S. (2013). Point estimate method addressing correlated wind power for probabilistic optimal power flow. *IEEE Transactions on Power Systems*, 29(3), 1045-1054.

[77] Li, X., Cao, J., & Du, D. (2015). Probabilistic optimal power flow for power systems considering wind uncertainty and load correlation. *Neurocomputing*, 148, 240-247.

[78] Shargh, S., Mohammadi-Ivatloo, B., Seyedi, H., & Abapour, M. (2016). Probabilistic multi-objective optimal power flow considering correlated wind power and load uncertainties. *Renewable energy*, 94, 10-21.

[79] Gupta, N. (2016). Probabilistic load flow with detailed wind generator models considering correlated wind generation and correlated loads. *Renewable energy*, 94, 96-105.

[80] Bolinger, M., & Wiser, R. (2009). Wind power price trends in the United States: struggling to remain competitive in the face of strong growth. *Energy Policy*, 37(3), 1061-1071.

[81] Wiser, R. (2008). Annual report on US wind power installation, cost, and performance trends: 2007 (No. DOE/GO-102008-2590). *EERE Publication and Product Library*.

[82] Eyer, J., & Corey, G. (2010). Energy storage for the electricity grid: Benefits and market potential assessment guide. *Sandia National Laboratories*, 20(10), 5.

[83] Rezaeian Marjani, S., Talavat, V., & Galvani, S. (2019). Optimal allocation of D-STATCOM and reconfiguration in radial distribution network using MOPSO

algorithm in TOPSIS framework. *International Transactions on Electrical Energy Systems*, 29(2), e2723.

[84] Blagojevic, B., Athanassiadis, D., Spinelli, R., Raitila, J., & Vos, J. (2020). Determining the relative importance of factors affecting the success of innovations in forest technology using AHP. *Journal of Multi-Criteria Decision Analysis*, 27(1-2), 129-1.

[85] Yusoff, Y., Ngadiman, M. S., & Zain, A. M. (2011). Overview of NSGA-II for optimizing machining process parameters. *Procedia Engineering*, 15, 3978-3983.

[86] Deb, K., Agrawal, S., Pratap, A., & Meyarivan, T. (2000, September). A fast elitist non-dominated sorting genetic algorithm for multi-objective optimization: NSGA-II. In *International conference on parallel problem solving from nature* (pp. 849-858). Sprin.

[87] Wartana, I. M., Singh, J. G., Ongsakul, W., Buayai, K., & Sreedharan, S. (2011, September). Optimal placement of UPFC for maximizing system loadability and minimize active power losses by NSGA-II. In 2011 *International Conference & Utility Exhibition on P.*

[88] Pires, D. F., Antunes, C. H., & Martins, A. G. (2012). NSGA-II with local search for a multi-objective reactive power compensation problem. *International Journal of Electrical Power & Energy Systems*, 43(1), 313-324.

[89] Abdmouleh, Z., Gastli, A., Ben-Brahim, L., Haouari, M., & Al-Emadi, N. A. (2017). Review of optimization techniques applied for the integration of distributed generation from renewable energy sources. *Renewable Energy,* 113, 266-280.

[90] Gupta, A., Swarnkar, K. K., & Wadhwani, K. (2012). Combined economic emission dispatch problem using particle swarm optimization. *International Journal of Computer Applications*, 49(6), 7628-0695.

[91] Zeng, Y., & Sun, Y. (2014). Application of hybrid MOPSO algorithm to optimal reactive power dispatch problem considering voltage stability. *Journal of Electrical and Computer Engineering*, 2014, 10.

[92] Power data access viewer_Prediction of Worldwide Energy Resoruces.(2021, Febraury 20). Retrieved from https://power.larc.nasa.gov/data-access-viewer/.

[93] Eckroad, S., & Gyuk, I. (2003). EPRI-DOE handbook of energy storage for transmission & distribution applications. *Electric Power Research Institute*, Inc, 3-35.

[94] Cheng, T., Chen, M., Fleming, P. J., Yang, Z., & Gan, S. (2017). A novel hybrid teaching learning based multi-objective particle swarm optimization. *Neurocomputing*, 222, 11-25.

[95] Kaveh, A., & Laknejadi, K. (2011). A novel hybrid charge system search and particle swarm optimization method for multi-objective optimization. *Expert Systems with Applications*, 38(12), 15475-15488.

[96] Verma, A., & Kaushal, S. (2017). A hybrid multi-objective particle swarm optimization for scientific workflow scheduling. *Parallel Computing*, 62, 1-19.

[97] Salazar, D., Rocco, C. M., & Galván, B. J. (2006). Optimization of constrained multiple-objective reliability problems using evolutionary algorithms. *Reliability Engineering & System Safety*, 91(9), 1057-1070.

[98] Subcommittee, P. M. (1979). IEEE reliability test system. *IEEE Transactions on power apparatus and systems*, (6), 2047-2054.

APPENDICES

Appendix A: IEEE 30-bus system (BUS-DATA)

IEEE 30 BUS SYSTEM - BUS DATA						
Bus	type	Pd (MW)	Qd (MVAR)	Bs (MVAR)	Vmax (pu)	Vmin (pu)
1	3	0	0	0	1.05	0.95
2	1	21.7	12.7	0	1.1	0.95
3	1	2.4	1.2	0	1.05	0.95
4	1	7.6	1.6	0	1.05	0.95
5	1	0	0	19	1.05	0.95
6	1	0	0	0	1.05	0.95
7	1	22.8	10.9	0	1.05	0.95
8	1	30	30	0	1.05	0.95
9	1	0	0	0	1.05	0.95
10	1	5.8	2	0	1.05	0.95
11	1	0	0	0	1.05	0.95
12	1	11.2	7.5	0	1.05	0.95
13	2	0	0	0	1.1	0.95
14	1	6.2	1.6	0	1.05	0.95
15	1	8.2	2.5	0	1.05	0.95
16	1	3.5	1.8	0	1.05	0.95
17	1	9	5.8	0	1.05	0.95
18	1	3.2	0.9	0	1.05	0.95
19	1	9.5	3.4	0	1.05	0.95
20	1	2.2	0.7	0	1.05	0.95
21	1	17.5	11.2	0	1.05	0.95
22	2	0	0	0	1.1	0.95
23	2	3.2	1.6	0	1.1	0.95
24	1	8.7	6.7	4	1.05	0.95
25	1	0	0	0	1.05	0.95
26	1	3.5	2.3	0	1.05	0.95
27	2	0	0	0	1.1	0.95
28	1	0	0	0	1.05	0.95
29	1	2.4	0.9	0	1.05	0.95
30	1	10.6	1.9	0	1.05	0.95

Appendix B: IEEE 30-bus system (LINE-DATA)

IEEE 30 BUS SYSTEM - LINE DATA					
fbus	tbus	r (pu)	x (pu)	b/2 (pu)	Line capacity (MVA)
1	2	0.02	0.06	0.03	130
1	3	0.05	0.19	0.02	130
2	4	0.06	0.17	0.02	65
3	4	0.01	0.04	0	130
2	5	0.05	0.2	0.02	130
2	6	0.06	0.18	0.02	65
4	6	0.01	0.04	0	90
5	7	0.05	0.12	0.01	70
6	7	0.03	0.08	0.01	130
6	8	0.01	0.04	0	32
6	9	0	0.21	0	65
6	10	0	0.56	0	32
9	11	0	0.21	0	65
9	10	0	0.11	0	65
4	12	0	0.26	0	65
12	13	0	0.14	0	65
12	14	0.12	0.26	0	32
12	15	0.07	0.13	0	32
12	16	0.09	0.2	0	32
14	15	0.22	0.2	0	16
16	17	0.08	0.19	0	16
15	18	0.11	0.22	0	16
18	19	0.06	0.13	0	16
19	20	0.03	0.07	0	32
10	20	0.09	0.21	0	32
10	17	0.03	0.08	0	32
10	21	0.03	0.07	0	32
10	22	0.07	0.15	0	32
21	22	0.01	0.02	0	32
15	23	0.1	0.2	0	16
22	24	0.12	0.18	0	16
23	24	0.13	0.27	0	16
24	25	0.19	0.33	0	16
25	26	0.25	0.38	0	16
25	27	0.11	0.21	0	16
28	27	0	0.4	0	65
27	29	0.22	0.42	0	16
27	30	0.32	0.6	0	16
29	30	0.24	0.45	0	16
8	28	0.06	0.2	0.02	32
6	28	0.02	0.06	0.01	32

Appendix C: IEEE 57-bus system (BUS-DATA)

IEEE 57 BUS SYSTEM - BUS DATA						
Bus	type	Pd (MW)	Qd (MVAR)	Bs (MVAR)	Vmax (pu)	Vmin (pu)
1	3	55	17	0	1.06	0.94
2	1	3	88	0	1.06	0.94
3	2	41	21	0	1.06	0.94
4	1	0	0	0	1.06	0.94
5	1	13	4	0	1.06	0.94
6	2	75	2	0	1.06	0.94
7	1	0	0	0	1.06	0.94
8	1	150	22	0	1.06	0.94
9	2	121	26	0	1.06	0.94
10	1	5	2	0	1.06	0.94
11	1	0	0	0	1.06	0.94
12	2	377	24	0	1.06	0.94
13	1	18	2.3	0	1.06	0.94
14	1	10.5	5.3	0	1.06	0.94
15	1	22	5	0	1.06	0.94
16	1	43	3	0	1.06	0.94
17	1	42	8	0	1.06	0.94
18	1	27.2	9.8	10	1.06	0.94
19	1	3.3	0.6	0	1.06	0.94
20	1	2.3	1	0	1.06	0.94
21	1	0	0	0	1.06	0.94
22	1	0	0	0	1.06	0.94
23	1	6.3	2.1	0	1.06	0.94
24	1	0	0	0	1.06	0.94
25	1	6.3	3.2	5.9	1.06	0.94
26	1	0	0	0	1.06	0.94
27	1	9.3	0.5	0	1.06	0.94
28	1	4.6	2.3	0	1.06	0.94
29	1	17	2.6	0	1.06	0.94
30	1	3.6	1.8	0	1.06	0.94
31	1	5.8	2.9	0	1.06	0.94
32	1	1.6	0.8	0	1.06	0.94
33	1	3.8	1.9	0	1.06	0.94
34	1	0	0	0	1.06	0.94
35	1	6	3	0	1.06	0.94
36	1	0	0	0	1.06	0.94
37	1	0	0	0	1.06	0.94
38	1	14	7	0	1.06	0.94

39	1	0	0	0	1.06	0.94
40	1	0	0	0	1.06	0.94
41	1	6.3	3	0	1.06	0.94
42	1	7.1	4.4	0	1.06	0.94
43	1	2	1	0	1.06	0.94
44	1	12	1.8	0	1.06	0.94
45	1	0	0	0	1.06	0.94
46	1	0	0	0	1.06	0.94
47	1	29.7	11.6	0	1.06	0.94
48	1	0	0	0	1.06	0.94
49	1	18	8.5	0	1.06	0.94
50	1	21	10.5	0	1.06	0.94
51	1	18	5.3	0	1.06	0.94
52	1	4.9	2.2	0	1.06	0.94
53	1	20	10	6.3	1.06	0.94
54	1	4.1	1.4	0	1.06	0.94
55	1	6.8	3.4	0	1.06	0.94
56	1	7.6	2.2	0	1.06	0.94
57	1	6.7	2	0	1.06	0.94

Appendix D: IEEE 57-bus system (LINE-DATA)

IEEE 57-BUS SYSTEM - LINE DATA					
fbus	tbus	r (pu)	x (pu)	b/2 (pu)	Line Capacity (MVA)
1	2	0.0083	0.028	0.129	-
2	3	0.0298	0.085	0.0818	-
3	4	0.0112	0.0366	0.038	-
4	5	0.0625	0.132	0.0258	-
4	6	0.043	0.148	0.0348	-
6	7	0.02	0.102	0.0276	-
6	8	0.0339	0.173	0.047	-
8	9	0.0099	0.0505	0.0548	-
9	10	0.0369	0.1679	0.044	-
9	11	0.0258	0.0848	0.0218	-
9	12	0.0648	0.295	0.0772	-
9	13	0.0481	0.158	0.0406	-
13	14	0.0132	0.0434	0.011	-
13	15	0.0269	0.0869	0.023	-
1	15	0.0178	0.091	0.0988	-
1	16	0.0454	0.206	0.0546	-
1	17	0.0238	0.108	0.0286	-
3	15	0.0162	0.053	0.0544	-
4	18	0	0.555	0	-
4	18	0	0.43	0	-
5	6	0.0302	0.0641	0.0124	-
7	8	0.0139	0.0712	0.0194	-
10	12	0.0277	0.1262	0.0328	-
11	13	0.0223	0.0732	0.0188	-
12	13	0.0178	0.058	0.0604	-
12	16	0.018	0.0813	0.0216	-
12	17	0.0397	0.179	0.0476	-
14	15	0.0171	0.0547	0.0148	-
18	19	0.461	0.685	0	-
19	20	0.283	0.434	0	-
21	20	0	0.7767	0	-
21	22	0.0736	0.117	0	-
22	23	0.0099	0.0152	0	-
23	24	0.166	0.256	0.0084	-
24	25	0	1.182	0	-
24	25	0	1.23	0	-
24	26	0	0.0473	0	-
26	27	0.165	0.254	0	-

27	28	0.0618	0.0954	0	-
28	29	0.0418	0.0587	0	-
7	29	0	0.0648	0	-
25	30	0.135	0.202	0	-
30	31	0.326	0.497	0	-
31	32	0.507	0.755	0	-
32	33	0.0392	0.036	0	-
34	32	0	0.953	0	-
34	35	0.052	0.078	0.0032	-
35	36	0.043	0.0537	0.0016	-
36	37	0.029	0.0366	0	-
37	38	0.0651	0.1009	0.002	-
37	39	0.0239	0.0379	0	-
36	40	0.03	0.0466	0	-
22	38	0.0192	0.0295	0	-
11	41	0	0.749	0	-
41	42	0.207	0.352	0	-
41	43	0	0.412	0	-
38	44	0.0289	0.0585	0.002	-
15	45	0	0.1042	0	-
14	46	0	0.0735	0	-
46	47	0.023	0.068	0.0032	-
47	48	0.0182	0.0233	0	-
48	49	0.0834	0.129	0.0048	-
49	50	0.0801	0.128	0	-
50	51	0.1386	0.22	0	-
10	51	0	0.0712	0	-
13	49	0	0.191	0	-
29	52	0.1442	0.187	0	-
52	53	0.0762	0.0984	0	-
53	54	0.1878	0.232	0	-
54	55	0.1732	0.2265	0	-
11	43	0	0.153	0	-
44	45	0.0624	0.1242	0.004	-
40	56	0	1.195	0	-
56	41	0.553	0.549	0	-
56	42	0.2125	0.354	0	-
39	57	0	1.355	0	-
57	56	0.174	0.26	0	-
38	49	0.115	0.177	0.003	-
38	48	0.0312	0.0482	0	-
9	55	0	0.1205	0	-